Coarse-graining methods and polymer dynamics

Dissertation

zur Erlangung des Grades

„Doktor der Naturwissenschaften“

am Fachbereich Physik

der Johannes Gutenberg-Universität

in Mainz

Dominik Fritz

geb. in Stuttgart

Mainz, 2010

Datum der mündlichen Prüfung: 05. Mai 2010

Summary

This thesis studies molecular dynamics simulations on two levels of resolution: the detailed level of atomistic simulations, where the motion of explicit atoms in a many-particle system is considered, and the coarse-grained level, where the motion of "superatoms" composed of up to 10 atoms is modeled. While atomistic models are capable of describing material specific effects on small scales, the time and length scales they can cover are limited due to their computational costs. Polymer systems are typically characterized by effects on a broad range of length and time scales. Therefore it is often impossible to atomistically simulate processes, which determine macroscopic properties in polymer systems. Coarse-grained (CG) simulations extend the range of accessible time and length scales by three to four orders of magnitude. However, no standardized coarse-graining procedure has been established yet.

Following the ideas of structure-based coarse-graining, a coarse-grained model for polystyrene is presented. Structure-based methods parameterize CG models to reproduce static properties of atomistic melts such as radial distribution functions between superatoms or other probability distributions for coarse-grained degrees of freedom. Two enhancements of the coarse-graining methodology are suggested. Correlations between local degrees of freedom are implicitly taken into account by additional potentials acting between neighboring superatoms in the polymer chain. This improves the reproduction of local chain conformations and allows the study of different tacticities of polystyrene. It also gives better control of the chain stiffness, which agrees perfectly with the atomistic model, and leads to a reproduction of experimental results for overall chain dimensions, such as the characteristic ratio C_∞, for all different tacticities. The second new aspect is the computationally cheap development of nonbonded CG potentials based on the sampling of pairs of oligomers in vacuum. Static properties of polymer melts are obtained as predictions of the CG model in contrast to other structure-based CG models, which are iteratively refined to reproduce reference melt structures.

The dynamics of simulations at the two levels of resolution are compared. The time scales of dynamical processes in atomistic and coarse-grained simulations can be connected by a time scaling factor, which depends on several specific system properties as molecular weight, density, temperature, and other components in mixtures. In this thesis the influence of molecular weight in systems of oligomers and the situation in two-component mixtures is studied. For a system of small additives in a melt of long polymer chains the temperature dependence of the additive diffusion is predicted and compared to experiments.

Zusammenfassung

Die vorliegende Arbeit untersucht Molekulardynamik-Simulationen auf zwei Auflösungsebenen: detaillierte atomistische Simulationen, in denen die Bewegung einzelner Atome in einem Vielteilchensystem beleuchtet wird, und vergröberte Simulationen, in denen die Bewegung von „Superatomen“, die aus bis zu zehn Atomen bestehen, betrachtet wird. Während atomistische Modelle gut geeignet sind, materialspezifische Vorgänge auf kleinen Skalen zu beschreiben, sind Zeit- und Längenskalen, die sie abdecken können, begrenzt durch die hohe Rechenleistung, die sie erfordern. Polymersysteme sind typischerweise gekennzeichnet durch Effekte in einem weiten Bereich von Zeit- und Längenskalen. Daher ist es in Polymersystemen oft unmöglich, Vorgänge atomistisch zu simulieren, die relevant für makroskopische Eigenschaften sind. Vergröberte Modelle, auch als „Coarse-graining“-Modelle bezeichnet, erweitern den Bereich der simulierbaren Zeit- und Längenskalen um drei bis vier Größenordnungen. Bis jetzt hat sich jedoch keine Standardmethode des Coarse-graining durchgesetzt.

Ausgehend von der Methodik des strukturbasierten Coarse-graining wird ein vergröbertes Modell für Polystyrol vorgestellt. Strukturbasierte Methoden konstruieren Coarse-graining-Modelle mit dem Ziel, statische Eigenschaften von atomistischen Schmelzen nachzubilden, wie z.B. radiale Verteilungsfunktionen zwischen den Superatomen oder andere Wahrscheinlichkeitsverteilungen für vergröberte Freiheitsgrade. Zwei Verbesserungen der Coarse-graining-Methode werden vorgeschlagen. Durch zusätzliche Potentiale zwischen benachbarten Superatomen in der Polymerkette werden Korrelationen zwischen Freiheitsgraden miteinbezogen. Das verbessert die Nachbildung lokaler Konformationen und ermöglicht die Untersuchung von Polystyrol verschiedener Taktizität. Darüberhinaus lässt sich die Steifigkeit der Kette besser kontrollieren, die dadurch derjenigen im atomistischen Modell entspricht. Dies führt schließlich dazu, dass das Coarse-graining-Modell die Dimension gesamter Ketten in Polymerschmelzen, ausgedrückt durch das charakteristische Verhältnis C_∞, in Übereinstimmung mit experimentellen Daten für Polystyrol aller Taktizitäten beschreibt. Der zweite neue Aspekt betrifft die Entwicklung nichtgebundener Wechselwirkungspotentiale basierend auf dem Sampling eines Oligomerpaares im Vakuum. Statische Eigenschaften von Polymerschmelzen ergeben sich damit als Vorhersagen des Coarse-graining-Modells, im Gegensatz zu anderen strukturbasierten Methoden, die iterative Optimierungen nutzen, um die Struktur einer Referenzschmelze nachzubilden.

Die Dynamik von Simulationen auf den zwei Auflösungsebenen wird verglichen. Die Zeitskalen dynamischer Prozesse in atomistischen und vergröberten Simulationen können durch einen Skalierungsfaktor in Beziehung gesetzt werden, der von mehreren Systemeigenschaften wie Molekulargewicht, Dichte, Temperatur und zusätzlichen Komponenten in Mischungen abhängt. In dieser Arbeit wird der Einfluss von Molekulargewicht und Zwei-Komponenten-Mischungen auf Oligomersysteme betrachtet. Für ein weiteres System wird die Temperaturabhängigkeit der Diffusion von kleinen Molekülen in einer Schmelze langer Polymerketten untersucht und mit Experimenten verglichen.

Contents

Introduction **1**

1 Molecular dynamics simulations **5**
1.1 Periodic boundary conditions 5
1.2 Force fields 6
1.2.1 Atomistic force fields 6
1.2.2 Long-range dispersion interaction 11
1.2.3 Long-range Coulomb interaction 12
1.3 Equations of motion 14
1.3.1 Verlet methods 15
1.3.2 Constraints 16
1.3.3 Controlling the system 18

2 Coarse-graining methods **23**
2.1 General Coarse-Graining Procedure 24
2.1.1 Mapping scheme 25
2.1.2 Bonded potentials 26
2.1.3 Nonbonded potentials 28
2.1.4 Backmapping 30

3 Coarse-grained model for polystyrene **33**
3.1 Basic ideas 33
3.2 Tacticity of polystyrene 35
3.3 Mapping scheme 37
3.4 Bonded interactions 39
3.4.1 Interaction range along the chain 40
3.4.2 Correlations in single chains 44
3.4.3 Interactions for bonds, angles and dihedrals 47
3.4.4 Intrachain interactions between 1-5 neighbors 49
3.4.5 Chain stiffness and the range of bonded interactions 53
3.4.6 Combining different potentials: Atactic polystyrene 56
3.4.7 Correlations in coarse-grained chains 59
3.5 Nonbonded interactions 62

4 Melt simulations **69**
4.1 Conformations in melts 69

4.1.1 Local distributions . . . 69
4.1.2 Internal distances . . . 73
4.2 Packing and density in melts . . . 76
4.3 Temperature dependence and transferability . . . 78

5 Dynamics of multiscale polymer simulations 81
5.1 Time scales in atomistic and coarse-grained simulations . . . 81
5.1.1 Time mapping by matching mean square displacements . . . 83
5.1.2 Time mapping for oligomer systems . . . 84
5.1.3 Time mapping for mixtures of two components . . . 88
5.1.4 Mean square displacements in pure and mixed systems . . . 91
5.2 Dynamics of coarse-grained polystyrene melts . . . 96
5.3 Additive diffusion in polymer melts . . . 100

Conclusion 105

A Appendix 107
A.1 Simulation details of atomistic systems . . . 107
A.1.1 Sampling of isolated chains . . . 107
A.1.2 Sampling of isolated oligomer pairs . . . 108
A.1.3 10-mer melts . . . 108
A.1.4 Oligomer melts . . . 109
A.1.5 Oligomer mixtures . . . 110
A.1.6 PS melt, 10kDa . . . 111
A.1.7 EB/PS systems . . . 111
A.2 Simulation details of coarse-grained systems . . . 112
A.2.1 Sampling of isolated chains . . . 112
A.2.2 10-mer melts . . . 113
A.2.3 Oligomer melts . . . 113
A.2.4 Oligomer mixtures . . . 115
A.2.5 PS melt, 10kDa . . . 116
A.2.6 PS melt, 20kDa . . . 116
A.2.7 EB/PS systems . . . 117
A.3 Implementation of the coarse-grained topology . . . 118
A.3.1 Chain direction . . . 118
A.3.2 Dihedral orientation . . . 120
A.3.3 Bonded 1-5 interactions . . . 123
A.4 Parameters of the atomistic force field . . . 124

Acknowledgments 127

Bibliography 128

Introduction

Polymers form a broad class of materials. They are found in nature or are produced synthetically and appear all around us. In industrial plastic products like packaging foil, insulation of buildings, clothing fibers, laundry detergents, coatings, car tires and diapers; from food technology and high performance materials in medicine to many biological systems, including even DNA that stores the genome of all living organisms. The possible range of properties and applications of polymers is huge.

Polymers are organic chain molecules, which are characterized by the repetition of chemically equal or similar units called monomers. These monomers are typically connected by covalent chemical bonds to form polymers, in the simplest case linear chains of one type of repeat unit. Melts of these homopolymers show an interesting macroscopic behavior depending on the length of the chains. For short chain length they behave like liquids, but if the chain length is increased they show properties of rubber. The response to mechanical deformations may even depend on how fast the deformation is exerted and released, i.e. they are viscoelastic. Whereas they respond elastically like solids at high frequencies, they start to flow like viscous liquids under slow deformations.

This illustrates the wide range of time and length scales of phenomena occurring in polymer systems. The viscous behavior on large time scales is more than just the result of local molecular-scale processes. It reflects an important characteristic of polymers: They cannot cross each other, since this would break chemical bonds. To gain a general understanding of the properties of polymer systems, one has to know about the universal behavior of these chains and the topological constraints which evolve from their entanglements. To obtain properties of specific polymer systems, such universal behavior has to be linked to chemical details.

Computer simulations on an atomistic level have brought new insight into phenomena on the molecular scale, not only for melts of linear polymer chains, but for soft condensed matter and biomolecular systems as well. However, many processes in these complex systems occur on length and time scales that are beyond the reach of current detailed atomistic simulations.

One approach to overcome this limitation and to reach longer time and length scales in simulations is coarse-graining (CG). Coarse-grained models cluster groups of atoms together into CG “sites” or “superatoms”. The CG sites interact by effective interactions, which are designed to contain the averaged influence of “detailed” degrees of freedom. The reduced number of degrees of freedom is one reason why CG models are computationally faster than atomistic models. The second reason, in general, lies in the physically “faster” dynamics of the CG systems, see below. As a result of these different influencing factors the accessible time and length scales can be increased by three to four orders

of magnitude. By this the mesoscopic scale can be reached, where important phenomena emerge, e.g. self-assembly in biomolecular systems or diffusive chain motion in long polymer melts.

When CG models are developed, the general aim is to reduce the number of explicitly treated degrees of freedom in a way that keeps the accuracy of the global and long-time behavior as close as possible to the detailed system. For melts of linear polymer chains, the following properties should be reproduced by a CG model: The packing of the chains on a local level and the overall dimension of individual chains, i.e. if they are extended or coiled up. If the chains are more extended, they overlap more with other chains and are finally more entangled, which has a strong influence on macroscopic melt properties. The chain dimension is closely related to the stiffness of the polymer chain.

The first CG models used generic "bead-spring" models, in which chains cannot cross each other due to excluded volume and have a certain stiffness, imposed by angular potentials. These models are already capable of describing the universal behavior of polymers without any information about the specific chemical structure of the monomers. Since then, CG models for chemically specific systems became of interest, which keep certain specific properties linked to chemical details of the underlying polymer. This is also the scope of this thesis.

Coarse-graining methods face several challenges at the moment. Two of these aspects are closely linked to the studies presented in this thesis.

The first one is the degree of transferability of CG models between different systems and between different thermodynamic conditions. Even though one cannot expect that a CG model is *completely* transferable, because it is a simplified picture of a complex system and by reducing the number of degrees of freedom certain information has been effectively averaged away, the conditions at which the model is developed certainly influence the transferability. The question is how many specific properties of the atomistic reference system used to parameterize a CG model enter into the CG model and thereby cause deviations as soon as the CG model is simulated under varied conditions.

Among the CG methods which aim at close reproduction of the structure, CG interaction potentials are typically developed by iterative methods using an atomistic *melt* state as the reference system. The influence of the choice of the reference system can be illustrated by considering a CG potential between small molecules, which is parameterized on a liquid of these molecules as a reference system. If we assume that the molecules in a liquid are packed in such a way that each molecule is surrounded by several shells of neighbors (where the outer shells are more and more disordered), the effective CG potential (obtained from the liquid state) between the small molecules might have several minima, corresponding to the different shells of neighbors. Of course this CG model would reproduce the structure of the liquid, but it would possibly fail to describe the system under varied conditions. If for example a second component is added to the system and one would expect a different packing of the molecules in a homogeneous mixture, the previously considered CG potential might fail to describe this mixture. It might lead to the formation of clusters of molecules of one type only because their structure (having several shells of neighbors of the same type) would be more similar to the reference

structure, for which the model was developed, than the structure of a homogeneous mixture with different components. From these considerations the CG potentials in this work were developed from atomistic simulations of chain sequences in *vacuum*. Information on properties of the melt state have not been used to parameterize the model, but served rather as test cases to prove the predictions of the model.

The second important aspect of CG models is their time-dependent, dynamical behavior. CG dynamics are generally faster than the dynamics of the underlying atomistic systems. The averaging over detailed, local degrees of freedom leads to a smoother potential energy surface and consequently faster dynamics of CG models. This is a desirable feature of CG models, especially if statistical sampling is their primary goal. If the goal is to study the dynamics of CG models, the question is how is the intrinsic CG time scale linked to the time scale of the underlying model. A common approach to link the two time scales for a specific CG model is the comparison of a dynamical quantity in both, the CG and the atomistic system. This link allows quantitative predictions of the dynamics, e.g. of polymer systems, from CG dynamics. The influence of the specific CG and atomistic model used, molecular weight, density, temperature and of other components in mixed systems still remain open questions. Better knowledge of the link between the time scales and its dependence on varying conditions is also related to the aspect of transferability and in the end to the predictive capability of CG modeling.

This thesis is organized as follows. Chapter 1 gives a review of the basics of molecular dynamics simulations, which are relevant for the atomistic as well as for the CG simulations in this work. The general method of structure-based coarse-graining and common approaches to develop CG interaction potentials are discussed in chapter 2. The core of this thesis is the CG methodology, applied to the exemplary case of polystyrene. The development of the CG model and its new approaches are presented in chapter 3. In chapter 4 the CG model is applied to simulate polymer melts. The static properties of atactic, isotactic and syndiotactic polystyrene are compared to atomistic simulations and experimental data. In chapter 5 the dynamical aspects of CG simulations are discussed for several different systems.

1 Molecular dynamics simulations

In molecular dynamics (MD) simulations we deal with systems to which the laws of classical mechanics are applied. The main part of the system is the force field, which delivers a description of the potential energy surface on which the equations of motion are simulated. Given the positions of each atom in the system, the forces on each atom, as well as the total energy can be computed from this force field. Electronic motions are not considered.

The description of the force field takes into account the covalent structure of molecules. Therefore classical methods are not sufficient to describe chemical reactions, in which atoms change the environment which they are covalently bound to. In these cases quantum-chemical methods could be used. Even though classical methods are much faster than *ab initio* methods, of course the sizes of systems, which can be simulated are limited. The boundaries of the system need to follow certain boundary conditions. The simplest and most often applied conditions are *periodic boundary conditions*. They are described in the following section. Subsequently the typical form of force fields will be discussed, followed by the methods to solve the equations of motions numerically and by methods to control temperature and pressure of simulated systems.

1.1 Periodic boundary conditions

We are interested in studying bulk behavior of systems whose surface-to-volume ratio is sufficiently small to not significantly affect the observed properties. In simulations, the systems that we can afford to simulate are far away from a size at which effects at the surface could be possibly neglected. The way to overcome this problem is the use of periodic boundary conditions, where the system is exactly replicated in three dimensions. Therefore the simulated system is a unit cell of a periodic lattice. The unit cell can have an arbitrary triclinic shape, defined by three basis vectors with arbitrary angles.

For simulations of polymer melts usually a cubic box is employed. For other systems, notably proteins in solvent, the optimal unit cell has a minimal volume under the condition that there is a minimum distance between any atom of the protein and any atom of the neighboring image. In this case the amount of solvent in the unit cell is minimized and thus the computational time spent on the less interesting solvent. For spherical molecules the rhombic dodecahedron is the best choice. [1]

In periodic boundary conditions each atom interacts not only with atoms in the same unit cell, but also with the images of all the cells, including its own periodic images. While periodic boundary conditions avoid the perturbing influence of artificial boundaries like a vacuum or a reflective wall, they introduce the artefact of periodicity. They imply that the

potential functions are also periodic. Concerning the long-ranged Coulombic interactions this periodicity is taken into account by the use of lattice sums, which are described later. The other way to handle the effects of periodicity are modified interaction potentials that vanish for distances larger than half of the smallest length of the unit cell. In this way only interactions between nearest images occur. This modification of potentials, in turn, can cause its own artifacts. Jumps of the force appear at sudden cutoffs and cause additional noise, while smooth cutoffs can strongly modify the interaction. Methods to correct the influence of the cutoff are described later.

1.2 Force fields

The development of force fields can be based on different principles. Ideally, ab initio quantum calculations should provide descriptions for the interactions between atoms and molecules. Considering that the de Broglie wavelength $\Lambda = h/\sqrt{2\pi m k_\mathrm{B} T}$ for hydrogen at room temperature is around 10^{-10} m and therefore of the same order as the interatomic bond length, it is surprising that the classical treatment of these systems with molecular dynamics works. Quantum calculations on isolated molecules do often not suffice to obtain reliable force fields, as they are not accurate enough to produce overall accuracies better than $k_\mathrm{B}T$, which is required to yield accurate thermodynamic properties. In practice most force fields contain also parameters which are empirically adjusted to fit experimental data. This point is related to the degree of *transferability*. In an ideal force field the terms describing interactions between particles should be transferable between different molecules and conditions of the environment. This is often not the case. If force fields contain parameters adjusted to empirical observations, errors in one term may be compensated by changes in other terms, which, in turn, are inaccurate when they are used for other configurations and environments.

The aspect of transferability is not only important in the case of atomistic force fields, but also for the development of coarse-grained force fields. Whenever interaction potentials are developed under certain conditions, one has to check carefully to which extent these potentials can be used under varied conditions. On the other side one can try to find conditions for the development of interactions, which are as general as possible. This route was followed in this work for the development of a coarse-grained force field. The improvement of atomistic models was not the focus, but a given atomistic force field was used as the starting point and the basis to develop a coarse-grained model, which reproduces certain properties of the atomistic model.

1.2.1 Atomistic force fields

Atoms are the mass points that move in the force field. In all-atom (AA) models every atom is treated explicitly. Some atomistic models handle hydrogen atoms in a different way by treating them as spherical groups together with their heavier neighboring atoms, e.g. CH_2 or CH_3 groups. These groups act as a single mass point. These models are called united-atom (UA) models. [2] The incorporation of several atoms into one mass point can

already be seen as a first step of coarse-graining, since the method of coarse-graining that we are using in this work is the arrangement of several atoms in groups or *superatoms* that move in a coarse-grained force field.

As an example for a molecular force field this section describes typical terms, which are included in the atomistic model for polystyrene that was used for the simulations in this work. It is an all-atom model adapted by Müller-Plathe to describe benzene-polystyrene systems. [3, 4] The model contains previously developed parameters [5, 6] and an adapted potential to describe torsional rotations properly. This force field was also used as a basis for several CG polystyrene models. [7, 8, 9]

Atoms are the points on which the different terms of the force field are acting. This means that the force field describes all contributions to the forces as functions of the positions of the atoms. In this atomistic representation two groups of interactions are used. The first group are bonded interactions that act on pairs or groups of atoms, which are chemically connected by up to n bonds (usually $n = 3$). The second group are nonbonded interactions between atoms, based on their distance, which might change during the simulation. These pairs of atoms belong to different molecules or to the same molecule, provided the atoms are separated by at least n bonds (usually $n = 2$ or 3). [10] The difference between these two types also is a computational one: bonded interactions apply to atoms, which can be read from a fixed list, whereas pairs of atoms involved in nonbonded interactions change with time and have to be updated regularly.

In Figure 1.1 a schematic view of force field terms and an example for an atomistic molecule is given. In this work polymer systems of long linear chain molecules are simulated. In the case of polystyrene (the repeat unit is C_8H_8) the atomistic representation is branched due to side groups, whereas the coarse-grained model deals with a chain without side groups. The scheme of bonded and nonbonded interactions is in principle the same in both cases.

The bonded potentials can be distinguished by the number of neighboring atoms involved in the interaction:[1]

1. Interactions between two atoms connected by a chemical bond can be described by a harmonic potential of the form

$$V_b(r_{ij}) = \frac{1}{2} k_b (r_{ij} - b_0)^2 \tag{1.1}$$

where the force constant k_b and the bond length b_0 are parameters depending on the bond type. The fast bond oscillations, especially of the light hydrogen atoms, are often neither of special interest nor of crucial importance for the properties of the whole system, because the choice of a harmonic potential leads to an average bond length, which does not change with temperature, as it would be the case for an anharmonic potential. Therefore simulations are often performed with fixed bond lengths (see section 1.3.2). This allows for the use of longer timesteps.

[1] The potentials can also have different functional forms, depending on the specific system of interest.

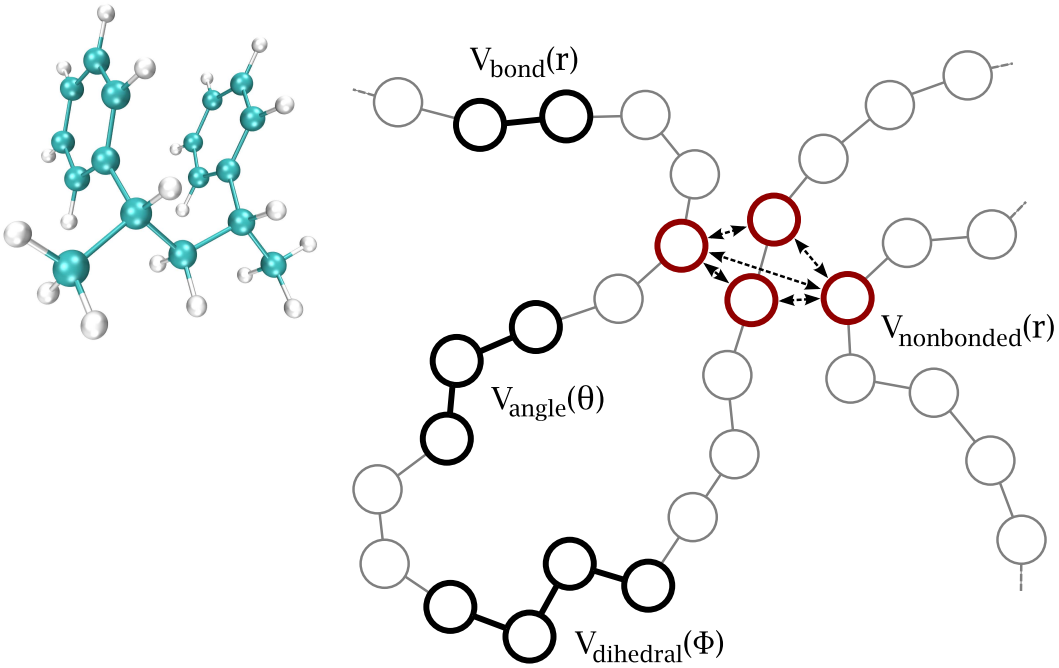

Figure 1.1: Schematic view of force field terms for a system of linear chain molecules (right): bonded potentials act on groups of two (bonds), three (angles) or four (dihedrals) neighbors connected by chemical bonds; nonbonded potentials act on particles, which are close to each other in space, but not involved in a joint bonded interaction. This scheme holds for coarse-grained force fields, which often consist of linear polymer chains, but also for atomistic force fields, where the molecules are typically branched or incorporate aromatic rings, see left side: an atomistic representation of a polystyrene dimer (left), where atoms are shown as beads (blue carbon and white hydrogen atoms) and bonds are given by lines.

2. Angular bending potentials describe interactions between three atoms which are connected by two consecutive bonds. In this case also a harmonic potential is used:

$$V_a(\theta_{ijk}) = \frac{1}{2} k_\theta (\theta_{ijk} - \theta_0)^2 \tag{1.2}$$

3. Proper dihedral angles are used to describe torsions around bonds. They involve four atoms i, j, k, l, connected by three consecutive bonds, and are periodic:

$$V_d(\phi_{ijkl}) = k_\phi (1 + \cos(n\phi - \phi_s)) \tag{1.3}$$

The dihedral angle ϕ is the angle between the ijk plane and the jkl plane, see Figure 1.2. In addition to this explicit form of the potential a steric contribution to the torsional barriers occurs in force fields, which include nonbonded interactions between the first and last atom belonging to the dihedral. This is also the case in the atomistic force field used in this work.

4. Improper dihedral angles are defined in the same wat as proper dihedrals and are used to keep groups of atoms planar, see Figure 1.2, or to prevent molecules from flipping over to mirror images:

$$V_{id}(\xi_{ijkl}) = \frac{1}{2} k_\xi (\xi_{ijkl} - \xi_0)^2 \tag{1.4}$$

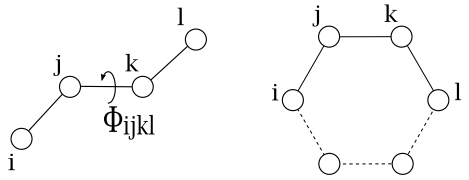

Figure 1.2: Dihedral angles: The proper dihedral angle ϕ (left) is the angle between the ijk plane and the jkl plane. According to the IUPAC/IUB convention zero corresponds to the *cis* configuration (i and l on the same side). Improper dihedrals are defined in the same way. To keep a ring planar improper dihedrals are applied to all groups of four subsequent atoms in the ring with a reference angle $\xi_0 = 0°$ between the planes ijk and jkl (right).

The nonbonded interactions are pairwise additive and a function of the distance r_{ij} between the two atoms of each pair. Pairs that are involved in bonded interactions are usually excluded from the nonbonded interactions. Depending on the dihedral functions used, 1-4 nonbonded interactions between atoms included in a bonded dihedral interaction (separated by $n = 3$ bonds) can also have a (possibly modified) nonbonded interaction. In the force field of this work the nonbonded interaction also acts on these 1-4 pairs. Nonbonded interactions are usually taken into account for pairs of atoms within a certain cutoff radius. In the case of periodic boundary conditions they can also be computed as full lattice sums over the periodic lattice. Two types of nonbonded interactions are used:

1. Short-ranged repulsion and longer-ranged dispersion between pairs of atoms belonging to different chains or to the same chain but separated by more than n bonds ($n = 2$ in this work). They are described by Lennard-Jones interactions:

$$V_{LJ}(r_{ij}) = 4\epsilon_{ij}\left[(\frac{\sigma_{ij}}{r_{ij}})^{12} - (\frac{\sigma_{ij}}{r_{ij}})^{6}\right] \tag{1.5}$$

   where ϵ and σ are specific parameters for each different type of atom. Or alternatively:

$$V_{LJ}(r_{ij}) = \frac{C_{ij}^{(12)}}{r_{ij}^{12}} - \frac{C_{ij}^{(6)}}{r_{ij}^{6}} \tag{1.6}$$

   Parameters between unlike atoms are determind by the Lorentz-Berthelot mixing rules: [11]

$$\sigma_{ij} = \frac{1}{2}(\sigma_{ii} + \sigma_{jj}), \quad \epsilon_{ij} = (\epsilon_{ii}\epsilon_{jj})^{1/2} \tag{1.7}$$

   The treatment of long-ranged contributions of the dispersion beyond the cutoff is discussed below in section 1.2.2.

2. Longer-ranged Coulomb interactions between charges or partial charges on atoms:

$$V_C(r_{ij}) = \frac{1}{4\pi\varepsilon_0}\frac{q_i q_j}{r_{ij}} \tag{1.8}$$

   The treatment of the long-ranged part is described below in section 1.2.3.

Virtual interaction sites

Virtual interaction sites are used by several force fields. Even though they are not part of the original atomistic force field used in this work they can be used to represent coarse-grained mapping points within an atomistic simulation and they allow for a convenient reintroduction of atomistic details into coarse-grained systems (see section 2.1.4).

Virtual sites have no mass and their position $\mathbf{r}_s$ is a function of the positions of other particles $\mathbf{r}_i$: $\mathbf{r}_s = f(\mathbf{r}_1, \mathbf{r}_2, \ldots, \mathbf{r}_n)$. In the context of coarse-graining they can be used in the backmapping procedure to restrain atomistic molecules in positions, in which their mapping points coincide with target positions given from CG simulations. This is realized in simulations by introducing a harmonic force acting between the virtual sites and their respective target position in space. The force acting on the virtual site must be redistributed over the particles with mass in a consistent way. We can write the potential energy as

$$V = V(\mathbf{r}_s, \mathbf{r}_1, \mathbf{r}_2, \ldots, \mathbf{r}_n) = V^*(\mathbf{r}_1, \mathbf{r}_2, \ldots, \mathbf{r}_n) \tag{1.9}$$

The force on particle i is then

$$\mathbf{F}_i = -\frac{\partial V^*}{\partial \mathbf{r}_i} = -\frac{\partial V}{\partial \mathbf{r}_i} - \frac{\partial \mathbf{r}_s}{\partial \mathbf{r}_i}\frac{\partial V}{\partial \mathbf{r}_s} = \mathbf{F}_i^{\text{direct}} + \mathbf{F}_i' \tag{1.10}$$

where $\mathbf{F}_i^{\text{direct}}$ is the normal force acting on particle i due to the other particles and $\mathbf{F}'_i$ is the part of the force acting on the virtual site, which is distributed to particle i. [12] The type of virtual site used in this work is the conceptually simple case of a linear combination

$$\mathbf{r}_s = \sum_{i=1}^{N} w_i \mathbf{r}_i \tag{1.11}$$

where the weights w_i are given from the relative weights a_i, which usually correspond to the masses of the atoms involved in the virtual sites.

$$w_i = a_i \left(\sum_{j=1}^{N} a_j \right)^{-1} \tag{1.12}$$

The force is redistributed using the same weights:

$$\mathbf{F}'_i = w_i \mathbf{F}_s \tag{1.13}$$

1.2.2 Long-range dispersion interaction

Nonbonded potentials are usually used with a cutoff distance, since the inclusion of all atom pairs in the system would scale with N^2, which gets computationally very expensive for large systems. The treatment of the interaction beyond the cutoff is done in a computationally less demanding way, which can be applied for the dispersion potential. The repulsive part is assumed to decrease fast enough to be neglected beyond the cutoff.

Using a simple cutoff for the potential induces an unphysical delta peak in the force at the cutoff distance. Another possibility is to shift the potential to zero at the cutoff, which leads just to a shift in the force at the cutoff distance. This jump can lead to artifacts when particles diffuse in or out from the cutoff. The sudden force causes additional noise, which leads to a heating of the system or to artifacts in the density distribution. Shifting the force itself to zero at the cutoff can avoid these artifacts, but at the same time it leads to a deviation of the potential. In practical simulations several kinds of switching functions are used to switch off the force smoothly at the cutoff distance.

The error due to the neglect of dispersion interactions beyond the cutoff can be calculated and taken into account in the computation of energy and pressure of the system. For the simple case of a truncated potential we have a dispersion interaction $V^{\text{disp}} = -C_6 r^{-6}$, which we set to zero for distances beyond the cutoff r_c. The average number density is ρ and the radial distribution function is $g(r)$. The correction of the potential energy and therefore of the internal energy u per particle is

$$\Delta u = \frac{1}{2}\rho \int_{r_c}^{\infty} V^{\text{disp}}(r) 4\pi r^2 g(r) dr \tag{1.14}$$

Assuming that $g(r) = 1$ for $r \geq r_c$ we get

$$\Delta u = -\frac{2\pi}{3}\rho C_6 r_c^{-3} \tag{1.15}$$

and in a similar way for the pressure correction using a plain cutoff [11]

$$\Delta p = -\frac{4\pi}{3}\rho^2 C_6 r_c^{-3} \tag{1.16}$$

Similar expressions exist for shifted potentials or potentials with shifted force. [1]

1.2.3 Long-range Coulomb interaction

We saw that for dispersion forces the contribution of a truncated tail to the potential energy can be estimated using eq. 1.14. This shows that the tail correction to the potential energy diverges, unless the potential energy function $\Delta V(r)$ decays faster than r^{-3}. This is why truncation of the potential and tail correction does not work for Coulombic interactions. On the other hand, even though Coulomb interactions are considerably longer-ranged than dispersion interactions, they tend to cancel at large distances because of overall charge neutrality.

Coulomb interactions can be cut off at a given distance, but this has to be done carefully. If full charges instead of dipoles are cut off, this will produce severe artifacts. One method to take into account effects beyond the cutoff is the introduction of a reaction field. [13] This incorporates a dielectric response of the medium beyond the cutoff to a total dipole moment of the charges within the cutoff radius. It is assumed that the medium outside the cutoff r_c has a relative dielectric constant ε_{RF}. Here we are considering a system without explicit ions and a truncation on a neutral-group basis.[2] In this system any charge q_i interacts directly with all other charges q_j within the cutoff radius r_c. The interaction with induced dipoles outside the cutoff is taken into account by the reaction field. The total dipole moment $\mathbf{M}$ in the sphere centered around i is defined as

$$\mathbf{M} = \sum_{j;r_{ij}\leq r_c} q_j \left(\mathbf{r}_j - \mathbf{r}_i\right) \tag{1.17}$$

The sum includes all j, whose distance r_{ij} from i is within the radius r_c. The reaction field

[2] The truncation on a neutral-group basis means that groups of charges (which are spatially close and have a neutral net charge) are included or excluded from the cutoff sphere together. Not the individual distance between two charges r_{ij} is evaluated in comparison to the cutoff distance r_c but the distance R_{ij} between reporter positions of the neutral groups to which i and j belong.

at position $\mathbf{r}_i$ is then given by

$$\mathbf{E}_{RF}(\mathbf{r}_i) = \frac{1}{4\pi\varepsilon_0 r_c^3} f(\varepsilon_{RF}) \sum_{j;r_{ij}\leq r_c} q_j \left(\mathbf{r}_j - \mathbf{r}_i\right), \tag{1.18}$$

$$f(\varepsilon_{RF}) = \frac{2\,(\varepsilon_{RF} - 1)}{(2\varepsilon_{RF} + 1)} \tag{1.19}$$

This contribution is taken into account in the calculation of the forces on particle i, given by

$$\mathbf{F}_i = \frac{q_i}{4\pi\varepsilon_0} \left[\sum_{\substack{j;r_{ij}\leq r_c \\ (i,j)\notin \texttt{exclst}}} q_j \frac{\mathbf{r}_{ij}}{r_{ij}^3} - \sum_{j;r_{ij}\leq r_c} q_j f(\varepsilon_{RF}) \frac{\mathbf{r}_{ij}}{r_c^3} \right] \tag{1.20}$$

where $\mathbf{r}_{ij} = \mathbf{r}_i - \mathbf{r}_j$ and the first term with the sum over the direct Coulombic interactions does not take into account pairs that belong to an exclusion list `exclst`, because their interactions are already accounted for in other bonded force field terms. The potential energy function that generates these forces is obtained by integration

$$V(\mathbf{r}) = \frac{1}{4\pi\varepsilon_0} \sum_i q_i \left[\sum_{\substack{j>i;r_{ij}\leq r_c \\ (i,j)\notin \texttt{exclst}}} q_j \left(r_{ij}^{-1} - r_c^{-1}\right) + \sum_{j\geq i;r_{ij}\leq r_c} q_j \frac{f(\varepsilon_{RF})}{2r_c^3} \left(r_{ij}^2 - r_c^2\right) \right] \tag{1.21}$$

and is zero at the cutoff. [1]

To treat inhomogeneous systems or systems containing explicit ions, reaction field methods are not satisfactory. One way to treat these systems are methods which do not use a simple cutoff, but sum over the lattice of all periodic images. The Ewald summation method, first introduced to calculate long-range interactions of periodic images in crystals, [14] treats a system of point charges by splitting it in two sums: A first sum contains the point-like charges which are superimposed by spherical Gaussian charge distributions of opposite charge and thereby effectively neutralized for large distances. This sum is solved in real space within a limited range. The second term sums over the charge distributions that were superimposed in real space, now with the same charges as the original point charges. The long-ranged potential of these Gaussians can be evaluated by solving Poisson's equation, which is done in reciprocal space using Fourier transforms.

The computational effort of Ewald summations is of the order N^2. For large systems with a big number of charges N this becomes prohibitively large. Alternatives are particle-mesh methods that scale as $N \log N$, e.g. the particle-mesh Ewald (PME) method. [15, 16] Instead of summing wave vectors directly, the charges are assigned to a grid, which is then Fourier transformed using fast Fourier transforms (FFT).

1.3 Equations of motion

Having a force field as discussed before, which describes a potential V, we can now consider a system of N particles interacting via this potential. The classical equations of motion for this system can be written in various ways. [17] In the Lagrangian formulation the trajectory is described by N second-order differential equations.

$$\frac{d}{dt}\left(\frac{\partial L}{\partial \dot{q}_k}\right) - \frac{\partial L}{\partial q_k} = 0 \tag{1.22}$$

where L is the Lagrangian, defined in terms of kinetic energy T and potential energy V as $L = L(q, \dot{q}) = T - V$, and q_k and $\dot{q}_k$ are the generalized coordinates and their time derivatives, respectively. The generalized momenta p_k are defined as

$$p_k = \frac{\partial L}{\partial \dot{q}_k} \tag{1.23}$$

With the alternative formulation using the Hamiltonian

$$H(q, p) = \sum_k \dot{q}_k p_k - L(q, \dot{q}) \tag{1.24}$$

we get $2N$ first-order equations

$$\dot{q}_k = \frac{\partial H}{\partial p_k}, \quad \dot{p}_k = -\frac{\partial H}{\partial q_k} \tag{1.25}$$

If the potential V is independent of velocities and time, the Hamiltonian is the total energy of the system:

$$H = T + V = E \tag{1.26}$$

In cartesian coordinates the equations of motion then read as

$$\mathbf{r}_i = \frac{\mathbf{p}_i}{m_i}, \quad \dot{\mathbf{p}}_i = -\frac{\partial V}{\partial \mathbf{r}_i} = \mathbf{F}_i \tag{1.27}$$

or

$$m_i \ddot{\mathbf{r}}_i = \mathbf{F}_i \tag{1.28}$$

where $\mathbf{F}_i$ is the force acting on particle i. If we assume that T and V do not depend on time explicitly then $\frac{dH}{dt} = 0$ and the total energy of the system is constant. Properly solving the equations of motion for a system without time- or velocity-dependent forces will therefore produce a microcanonical or NVE ensemble. In practical simulations there will be errors that cause deviations from the ideal behavior: integration errors due to the use of a finite timestep and also due to the finite numerical precision will not conserve the total energy exactly and errors in the forces due to truncation can cause energy drifts. To obtain long, stable trajectories in simulations there are always modifications of the pure equations of motion needed.

Although no algorithm can provide an exact solution for long times and simulated trajectories will exponentially diverge from the "true" trajectory compatible with the same initial conditions, it turns out not to be a serious problem. In MD simulations we are not interested in what exactly will happen to a system that has been prepared in a precisely known initial state. We are interested in statistical predictions, in the average behavior of a system that has been prepared in an initial state about which we know something (e.g. the total energy). [18]

There are different methods to solve the equations of motion. The following criteria influence the choice of the algorithm:

1. The algorithm should be reversible in time, since this is an inherent property of the equations of motion. If we change the signs of all velocities, all particles will move back along their previous trajectories. In practice also time-reversible algorithms might deviate depending on the implementation and the numerical precision.

2. Generated trajectories should conserve volume in phase space, i.e. the algorithm should be symplectic. [1]

3. To keep the computational effort as small as possible, it is preferable to use only one force evaluation per timestep, because the calculation of the forces is the most expensive part in each integration step.

In the following the simple and robust Verlet or leap-frog algorithm is presented.

1.3.1 Verlet methods

This family of algorithms is simple, robust, time-reversible and symplectic. These methods are widely used to integrate the classical equations of motion. The original Verlet algorithm [19] can be derived from a Taylor expansion at time $t + \Delta t$ and $t - \Delta t$ [18]

$$r(t + \Delta t) = r(t) + v(t)\Delta t + \frac{F(t)}{2m}\Delta t^2 + \frac{\dddot{r}(t)}{6}\Delta t^3 + O(\Delta t^4)$$

and

$$r(t - \Delta t) = r(t) - v(t)\Delta t + \frac{F(t)}{2m}\Delta t^2 - \frac{\dddot{r}(t)}{6}\Delta t^3 + O(\Delta t^4)$$

Summing these two equations , we obtain

$$r(t + \Delta t) + r(t - \Delta t) = 2r(t) + \frac{F(t)}{m}\Delta t^2 + O(\Delta t^4)$$

or

$$r(t + \Delta t) \approx 2r(t) - r(t - \Delta t) + \frac{F(t)}{m}\Delta t^2 \tag{1.29}$$

The Verlet algorithm does not use the velocities to calculate the new positions. The velocity is found in retrospect from

$$v(t) = \frac{r(t+\Delta t) - r(t-\Delta t)}{2\Delta t} + O(\Delta t^2) \tag{1.30}$$

Several algorithms are equivalent to the Verlet scheme. One is the leap-frog algorithm [20, 21], which uses the velocities halfway between time steps and uses these velocities to compute the the new positions

$$r(t+\Delta t) = r(t) + v(t+\frac{\Delta t}{2})\Delta t \tag{1.31}$$

$$v(t+\frac{\Delta t}{2}) = v(t-\frac{\Delta t}{2}) + \frac{F(t)}{m}\Delta t \tag{1.32}$$

In comparison to the Verlet algorithm, the leap-frog algorithm has the advantage that the velocities explicitly appear in the integration scheme, which allows for a coupling of the system to a thermal bath. This algorithm was used also for the simulations presented in this work. Another widely used algorithm is the velocity-Verlet algorithm [22], which uses velocities and positions at the same time and is also equivalent to the original Verlet scheme.

$$r(t+\Delta t) = r(t) + v(t)\Delta t + \frac{F(t)}{2m}\Delta t^2 \tag{1.33}$$

$$v(t+\Delta t) = v(t) + \frac{F(t+\Delta t) + F(t)}{2m}\Delta t \tag{1.34}$$

All the previously mentioned algorithms can be derived with the Reference System Propagator Algorithms (RESPA) method, which uses the Liouville formulation of classical mechanics and simple operator algebra. [23, 24] It is also possible to derive multiple time step versions, in which two different time steps are used for integrating the equations of motion: a shorter time step for rapidly changing short-range forces and a longer time step for slowly changing long-range forces.

Also higher-order algorithms have been used in MD simulations, in particular the predictor-corrector algorithms. They predict positions and a number of derivatives based on a Taylor expansion of previous values. Calculating the forces at the predicted positions, the deviations from the predicted accelerations are evaluated and the predicted positions and derivatives are corrected. These methods are quite accurate for small time steps but unstable for longer time steps. They are neither time-reversible nor symplectic, require more storage and have been pushed aside by the previously presented Verlet algorithms.

1.3.2 Constraints

As mentioned before, constraining the bond length of atomistic bonds can increase the speed of simulations. The time step in the integration of the equations of motion is chosen to be shorter than the shortest relevant time scale in a system. To describe these fastest

oscillations properly, one oscillation period should correspond to several time steps (typically of order 50 [10]). In typical atomistic simulations with a force field as described before, the intramolecular vibrations represent the motion with the highest frequency. If this high-frequency vibration of bonds is not of special interest, constraining these bonds allows for the use of a longer time step and faster simulations.

Including constraints in a simulation changes the equations of motion. Fixing bond length introduces holonomic constraints (they only depend on coordinates), which can be described by constraint equations $\sigma_s(r) = 0$ that should be satisfied at all times. We then can write a new Lagrangian that contains all the constraints

$$L' = L - \sum_s \lambda_s \sigma_s(r) \tag{1.35}$$

where λ_s denotes a set of Lagrange multipliers. The new equations of motion are

$$m_i \ddot{\mathbf{r}}_i = \mathbf{F}_i - \sum_s \lambda_s \frac{\partial \sigma_s}{\partial \mathbf{r}_i} \tag{1.36}$$

The second right term describes the constraint forces. To integrate these equations it is necessary to find a proper set of Lagrange multipliers λ_s. Two common methods are described in the following.

SHAKE

This method resets the coordinates after an unconstrained time step to satisfy the constraints within a given precision. First the new positions $\mathbf{r'}_i$ disregarding the constraints are computed

$$\mathbf{r'}_i = 2\mathbf{r}_i(t) - \mathbf{r}_i(t + \Delta t) + \frac{\Delta t^2}{m_i}\mathbf{F}_i^u(t) \tag{1.37}$$

and then the positions are corrected with $\Delta\mathbf{r}$ such that

$$\sigma_s(\mathbf{r'}_i + \Delta\mathbf{r}) = 0, \quad s = 1, \ldots, m \tag{1.38}$$

where

$$\Delta\mathbf{r}_i = \frac{\Delta t^2}{m_i} \sum_s \lambda_s(t) \frac{\partial \sigma_s(\mathbf{r}(t))}{\partial \mathbf{r}_i} \tag{1.39}$$

This set of m (generally non-linear) coupled equations for the m λ's is then solved sequentially for the constraints and the procedure is iterated to convergence. [25]

LINCS

This method rewrites the equations of motion to include the constraints. The λ's are solved from the fact that the σ's are zero at all times and therefore also their time derivatives.

First, we write eq. 1.36 in matrix notation as

$$\mathbf{M}\ddot{\mathbf{r}} = \mathbf{f} + \mathbf{C}^{\mathbf{T}}\boldsymbol{\lambda} \tag{1.40}$$

where $\mathbf{r}$ and $\mathbf{f}$ are $3N \times 1$ matrices containing coordinates and unconstraint forces, $\mathbf{M}$ is the $3N \times 3N$ diagonal matrix of masses, and the constraint matrix $\mathbf{C}$ that is defined by

$$C_{si} = \frac{\partial \sigma_s}{\partial r_i} \tag{1.41}$$

Because the constraint equations are zero, the first and second derivatives of the constraints are also zero and the following relation is found

$$\mathbf{C}\ddot{\mathbf{r}} = -\dot{\mathbf{C}}\dot{\mathbf{r}} \tag{1.42}$$

By left-multiplying eq. 1.40 by $\mathbf{CM^{-1}}$ and using relation 1.42 we obtain

$$\boldsymbol{\lambda} = -(\mathbf{CM^{-1}C^{T}})^{-1}(\mathbf{CM^{-1}f} + \dot{\mathbf{C}}\dot{\mathbf{r}}) \tag{1.43}$$

The matrix $\mathbf{CM^{-1}C^{T}}$ is non-singular and can be inverted, if the constraints are independent. [26] Substituting this expression for $\boldsymbol{\lambda}$ in eq. 1.40 we obtain the equations of motion

$$\ddot{\mathbf{r}} = (\mathbf{1} - \mathbf{TC})\mathbf{M^{-1}f} - \mathbf{T}\dot{\mathbf{C}}\dot{\mathbf{r}} \tag{1.44}$$

where $\mathbf{T}$ is defined as

$$\mathbf{T} = \mathbf{M^{-1}C^{T}}(\mathbf{CM^{-1}C^{T}})^{-1} \tag{1.45}$$

The matrix $\mathbf{1} - \mathbf{TC}$ is a projection matrix that projects the accelerations due to the unconstrained forces onto the constrained hypersurface. The first term of eq. 1.44 contains the constraint accelerations due to the systematic forces and the other term the constraint accelerations due to centripetal forces. Details about the implementation can be found in ref. 27.

1.3.3 Controlling the system

Applying the equations of motion (eq. 1.27) in a simulation of a system without time- or velocity-dependent forces will produce a microcanonical or NVE ensemble. As discussed before, while integrating the equations in practical simulations we always introduce errors due to the finite time step and due to numerical accuracy. The simulated Hamiltonian systems do ideally conserve their initial distribution in phase space, but there is no restoring force inherent in the dynamics that would correct for deviations that might slowly develop and accumulate.

Introducing an external influence that drives the system to a given distribution, provides this restoring force, which will be small, if the Hamiltonian dynamics of the system is accurate. In that way it is possible to simulate at constant temperature and to generate a canonical NVT ensemble or an isothermal-isobaric NpT ensemble. These ensembles

are often favorable in simulations since they describe conditions, which come closer to experimental ones than the NVE ensemble.

There are several methods to control temperature and pressure in the system. Some of them do not generate well-defined ensembles, but are still of practical use. The choice of the method depends on the purpose of the simulation and if only average equilibrium quantities, properties of fluctuations or dynamical quantities are of interest.

Stochastic methods

One method to control control the temperature and to obtain a canonical ensemble is the stochastic dynamics (SD) Langevin thermostat. [28] In Langevin dynamics a frictional force, which is proportional to the velocity, is added to the conservative force. This friction force removes kinetic energy from the system. At the same time a random force adds kinetic energy to the system. To generate a canonical ensemble these two contributions have to obey the fluctuation-dissipation theorem. The equations of motion have the following form:

$$\dot{p}_i = F_i - \xi_i p_i + R_i(t) \tag{1.46}$$

where $R_i(t)$ is a zero-average noise process with

$$\langle R_i(0) R_i(t) \rangle = 2 m_i \xi_i k_B T \delta(t) \tag{1.47}$$

When $1/\xi_i$ is large compared to the time scales present in the system, Langevin dynamics can be seen as molecular dynamics with a stochastic thermostat. On the other hand, if $1/\xi_i$ is small, the dynamics of the system will be completely different from molecular dynamics, but since the ensemble is canonical, the sampling is still correct.

An advantage of this thermostat is that it acts on a local scale. Particles which are too "cold" gain more energy by the noise term, while too "hot" particles are slowed down by the friction. This keeps numerical instabilities, which usually arise from inaccurate calculation of a local collisionlike process, effectively under control and prevents them from propagating. A disadvantage of this thermostat is that it is not momentum conserving, which is one of the conditions to treat hydrodynamics correctly.

This can be circumvented by using the method of dissipative particle dynamics (DPD) as a thermostat. [29, 30] As the SD thermostat it also uses friction and noise on a local scale, but those are applied to pairs of particles. The friction scales the relative velocities between pairs of nearby particles and the noise acts on pairs of particles, such that Newton's third law is strictly fulfilled and the momentum of the system is conserved. Therefore this method reproduces hydrodynamic behavior on large length and time scales. [31]

Weak-coupling methods

Weak-coupling methods can be used to control temperature and pressure. [32] They are also known as Berendsen thermostat and barostat. To control temperature the velocities

are rescaled in each step. This is done by forcing the system to obey the rate equation

$$\frac{dT}{dt} = \frac{T_0 - T}{\tau} \tag{1.48}$$

which lets the temperature T of the system decay exponentially to the desired temperature T_0 with a time constant τ. This is achieved by scaling the velocities in each step with a scaling factor λ,

$$\lambda^2 = 1 + \frac{\Delta t}{\tau}\left(\frac{T_0}{T} - 1\right) \tag{1.49}$$

where T is given by the kinetic energy after updating the velocities in a normal (unscaled) time step.

This thermostat is not acting locally but on a global scale, since only the kinetic energy of the whole systems is monitored and all particle velocities are scaled by the same factor. This can lead to severe artifacts, e.g. for systems of big proteins in water, where the temperatures for the protein and the solvent can differ strongly while the "average" temperature of the system is correct. In this case both groups can be controlled separately by two independent thermostats.

The smallest possible value of the time constant $\tau = \Delta t$ corresponds to the strong-coupling Gauss isokinetic thermostat [33, 34], which produces a canonical ensemble. For increasing τ the kinetic energy starts to fluctuate at the expense of fluctuations of the potentials energy. Fluctuations become equal for τ around the intrinsic relaxation time for the exchange between kinetic and potential energy. For much longer τ the scaling has no effect and a microcanonical ensemble is obtained. The generated ensemble is therefore between microcanonical and canonical for temperature scaling. [1]

In practice it seems safe to obtain ensemble averages with this method but not fluctuations in order to determine thermodynamic quantities, but caution is advised due to the above described artifacts.

Pressure is controlled in a similar manner using

$$\frac{dp}{dt} = \frac{p_0 - p}{\tau_p} \tag{1.50}$$

Assuming a known isothermal compressibility, $\beta_T = -(1/V)\,\partial V/\partial T$, coordinates and volume are scaled with

$$\mathbf{r}' = \chi\mathbf{r}, \quad V' = \chi^3 V \tag{1.51}$$

every time step with a scaling factor χ, given by

$$\chi^3 = 1 - \beta_T \frac{\Delta t}{\tau_p}(p_0 - p) \tag{1.52}$$

As in the case of the temperature coupling the generated ensemble is not known exactly and fluctuations cannot be used.

Extended system dynamics

Nosé introduced the idea to extend the system with an extra degree of freedom that can be used to control a variable in the system. [35] In a modified form by Hoover [36] this scheme is known as the Nosé-Hoover thermostat. The extra degree of freedom is a variable η, which is a scaling factor for the velocities. It has an associated "momentum" $p_\eta = Q\dot{\eta}$ with a "mass" Q. The number of degrees of freedom is $n = 3N - n_c$, for a system with N particles and n_c constraints. The new equations of motion are

$$\dot{q}_i = \frac{p_i}{m_i} \tag{1.53}$$

$$\dot{p}_i = F(q) - p_i \frac{p_\eta}{Q} \tag{1.54}$$

$$\dot{p}_\eta = \sum_i \frac{p_i^2}{2m_i} - nk_BT \tag{1.55}$$

In this scheme the temperature difference to the desired temperature acts on the time derivative of the velocity scaling factor and not on the scaling factor itself, as in the Berendsen thermostat. In contrast to the latter, the temperature is approaching equilibrium oscillatory and not in a smooth exponential decay. Since its distribution in phase space is canonical, it is more reliable to use the Nosé-Hoover thermostat in already equilibrated systems, but not for equilibration.

Canonical sampling through velocity rescaling

A thermostat that was recently proposed by Bussi et al. [37] uses velocity rescaling to obtain a canonical ensemble. The velocity rescaling method consists in multiplying the velocities of all particles by the same factor α, which forces the total kinetic energy K to be equal to the average kinetic energy at the target temperature, $\overline{K} = 1/2nk_BT$, where n is the number of degrees of freedom. The rescaling factor α then is

$$\alpha = \sqrt{\frac{\overline{K}}{K}} \tag{1.56}$$

The proposed modification to calculate the scaling factor enforces a canonical distribution for the kinetic energy. Instead of forcing the kinetic energy to be exactly equal to $\overline{K}$, the target value K_t is selected using a stochastic procedure aimed at obtaining the desired ensemble. The velocities then are rescaled by the factor

$$\alpha = \sqrt{\frac{K_t}{K}} \tag{1.57}$$

and K_t is drawn from the canonical equilibrium distribution for the kinetic energy

$$\overline{P}(K_t)dK_t \propto K_t^{(n/2-1)} e^{-\beta K_t} dK_t \tag{1.58}$$

Between rescalings the system is evolved by a fixed or randomly varied number of time steps. This is the simplest formulation of this method, which disturbs the velocities of the particles considerably. In a smoother approach the rescaling procedure is distributed among a number of time steps and the choice of K_t is based on the previous value of K, but still the canonical ensemble is obtained. This thermostat was tested with respect to dynamic properties of liquids, where it showed to be applicable and consistent with diffusion coefficients extracted from microcanonical simulations.

2 Coarse-graining methods

Soft matter systems show properties and a behavior that is determined by effects and processes that span a wide range of time- and length scales. Interesting time scales and system sizes are often beyond reach by detailed molecular dynamics simulations. To answer questions related to long time scales and large systems sizes it is desirable to have methods simplifying the system. These methods should reproduce the "interesting" behavior in dynamical simulations in a more efficient way, while "uninteresting" details might be neglected. The aim is to reduce the number of explicitly treated degrees of freedom in a way that keeps the accuracy of global and long-time behavior as close as possible to the detailed system. These types of approaches are often described with the word "coarse-graining", even though this term is often used in a more specific sense for models that cluster groups of atoms together into CG "sites" or "superatoms". The CG model which is presented in this work also belongs to the group of CG models that average over local details.

The first choice for a CG model is to distinguish between the relevant degrees of freedom and the irrelevant degrees of freedom, for which a detailed knowledge of the behavior is not required. This choice depends on the system, the properties of interest and the required accuracy and is also arbitrary to some extent. It is desirable to choose the CG degrees of freedom in such a way, that the irrelevant degrees of freedom equilibrate much faster than the relevant CG degrees of freedom, because on the time scale where these two overlap, the predictions of dynamic details are inaccurate.

Long linear polymer chains are a good example for a system, where the distinction between relevant and irrelevant degrees of freedom offers advantages. The relevant degrees of freedom are the centers of mass of a number of consecutive atoms along the chain. This description is beneficial, because polymers show a universal behavior where macroscopic properties scale in a regular manner with the length of the chain (or the number of repeat units) independent from the specific chemical structure of the chain. This behavior is achieved already in simple coarse-grained models which include chain connectivity, excluded volume and a few basic types of interactions. If the parameters are chosen in way that prevents chains from cutting through each other, already static and dynamic scaling properties of polymeric systems (as the change from Rouse to reptation dynamics for entangled systems) can be investigated. [38]

By averaging over degrees of freedom we decrease the level of resolution at which we are looking at our systems. We proceed from the microscopic level of atomistic detail to the mesoscopic scale, where we still look at particles. By decreasing the resolution further we leave the particle-based models and describe more macroscopic properties. The development of particle-based coarse-grained models connects different levels of resolution

systematically. Therefore, simulations using CG models are often referred to as "multi-scale" methods. The link between scales can be realized in different ways: In the simplest case the simulations on different levels are performed sequentially and only information about structures or energies is passed between the two levels. In other cases the different resolutions are present simultaneously. They require models which are adjusted to be as consistent as possible, since they require direct interactions between the different levels. In dual-scale methods the representation of individual molecules stays unchanged during the simulation, [39, 40, 41] whereas the molecules in adaptive methods can change their representation on the fly, e.g. when they diffuse in or out of a region of special interest. [42, 43]

The systematic link between the atomistic level and the coarse-grained level requires the definition or choice of properties that are used as a measure, how consistent the models are. Three common choices are thermodynamic properties, spatial structures or forces:

- Experimental thermodynamic properties such as free energies are used to parameterize CG models. These models are developed to reproduce e.g. partitioning free energies and are used to describe a variety of biomolecules in the fluid phase. [44, 45] The structure of the system is not necessarily reproduced with these energy-based approaches.

- Achieving a good agreement between coarse-grained and detailed atomistic structure can be also an aim of coarse-graining approaches. This agreement is especially desirable in cases where atomistic details are reintroduced into the coarser systems. Therefore, structure-based coarse-graining methods represent another group of approaches. [46, 47, 48] They often use radial distribution functions as target functions, which they aim to reproduce in the CG simulations. In these cases it is not immediately obvious to which extent thermodynamic properties of the system are reproduced.

- Another method related to the structure-based ones is the force-matching method. [49, 50] This method constructs the CG potential energy landscape in such a way that the CG forces reproduce the atomistic forces in the underlying systems and has been used in particular for biomolecular systems. [51]

2.1 General Coarse-Graining Procedure

In the following we describe the typical approach to develop structure-based coarse-grained models for polymer chains. Typical examples are polycarbonates, [52, 53] for which this procedure was used first, and polystyrene, [54, 55] which is the system that is investigated more closely in this work.

The aim of structure-based coarse-graining is to reproduce the structure that a detailed atomistic model exhibits. Coarse-grained models are constructed in such a way that they reproduce distributions of conformational degrees of freedom (e.g. angles between three neighboring CG beads) or of distances between groups of atoms.

In many coarse-graining approaches the set of coarse-grained interactions is separated in two parts. The underlying assumption is that the total potential energy, U^{CG}, can be separated in a bonded part, $U^{\mathrm{CG}}_{\mathrm{bonded}}$, and in a nonbonded part, $U^{\mathrm{CG}}_{\mathrm{nonbonded}}$.

$$U^{\mathrm{CG}} = \sum U^{\mathrm{CG}}_{\mathrm{bonded}} + \sum U^{\mathrm{CG}}_{\mathrm{nonbonded}} \tag{2.1}$$

This distinction is similar to atomistic force fields. The CG intramolecular, bonded interactions act on groups of neighboring beads in a chain, which are usually connected by covalent bonds in the detailed atomistic representation. The CG intra- and intermolecular, nonbonded interactions act between pairs of beads within a certain cutoff distance. The beads can belong to different chains or to the same chain. Beads in the same chain are excluded from the nonbonded interaction, if they are already taken into account by a CG bonded interaction.

Following the ansatz of separating these two types of interactions, they can be developed independently. This is an important aspect in terms of transferability of CG models. Separating the development of intramolecular bonded interactions from the nonbonded interactions, the bonded interactions should be independent from the specific surroundings in a CG system. The development of bonded and nonbonded interaction potentials is described in the following after a preceding discussion of CG mapping schemes.

2.1.1 Mapping scheme

The first step in developing a coarse-grained model is the choice of a mapping scheme. It defines how atoms are grouped together and represented by “superatoms”, which are also called CG “beads”. Even though the rules for the mapping are usually simple, the question which mapping scheme is optimal is anything but trivial. Possible aspects that influence the quality of a mapping scheme are the following:

- The number of beads that are used to describe one repeat unit of the polymer. This is called the “degree of coarse-graining”. To model local conformations in more detail, a higher number of beads is necessary. On the other hand, the speed-up of the CG model increases, if the number of beads per volume (and therefore the number of interacting pairs of particles within a given cutoff distance) is lower.

- Coarse-grained degrees of freedom could be correlated, i.e. certain values for one degree of freedom could only occur in combination with another value for another degree of freedom. Treating these correlations in multi-parameter potentials would be computationally inefficient. A method to compare the correlations that are introduced by different mapping schemes has been presented recently by Poma and delle Site. [56]
  Correlations typically disappear when the degree of coarse-graining is high and CG beads are averaging over many detailed atoms. If local conformations are supposed to be modeled correctly, correlations can be unavoidable. A method to deal with those correlations is presented and discussed in this work (in section 3.4.2).

- Stiff atomistic groups, e.g. benzene rings, can be often treated as one group.
- Atomistic torsions that lead to big conformational changes of the molecule, should also be represented by CG degrees of freedom.
- The exact coordinates of the CG beads can be chosen in different ways, e.g. as the center of mass or the geometrical center of the underlying atoms or they can coincide with the coordinates of one selected atom (compare section 3.3). This choice might change the distributions for the CG degrees of freedom and may provide advantages for the re-introduction of atomistic details.
- Groups of atoms, which are symmetrical or have a spherical shape, seem to offer advantages, since the nonbonded interactions are pair potentials, which do not depend on the orientation of the CG beads but just on the distance of their centers. If a group of atoms has more symmetries, the nonbonded interaction between two of these groups is expected to be less dependent on the relative orientation of the two groups.
- The ratio of sizes and masses between different groups. Having big differences in the masses requires a smaller integration time step (for the smallest mass). Running the system in these cases with the same masses for all beads, still offers the use of a longer time step, but the dynamics of the system might be disturbed. In a similar manner, the spatial size of different groups might require a smaller time step, because the CG repulsive potential becomes softer for bigger groups. The time step is then limited by the more repulsive potential of the smallest group.

2.1.2 Bonded potentials

CG bonded interaction potentials are obtained by sampling distributions for CG conformational degrees of freedom based on a detailed atomistic simulation of a molecule in vacuum. The conformational degrees of freedom are expressed in terms of CG bond lengths r between neighboring beads, bond angles θ between three subsequent neighbors, and torsions or dihedral angles ϕ between four subsequent neighbors. The sampling of the isolated chain can be done by using Monte Carlo simulations or molecular dynamics with a stochastic thermostat (see Langevin thermostat, section 1.3.3). Long-range nonbonded intrachain interactions are excluded in the sampling of the atomistic isolated chain. Only atoms belonging to CG beads that are involved in a common CG bonded interaction, are interacting. For example, if CG torsion potentials are used, atoms interact with neighbors separated by up to three CG bonds.

The sampled chains are random walks, because they have only local interactions, but no excluded volume interactions for parts of the chain separated by several CG bonds. These long-range interactions are lateron treated by the same nonbonded potentials that are used for interchain interactions.

After sampling a sufficiently large number of independent conformations of the random walks at a given temperature T, probability distribution functions $P^{\mathrm{CG}}(r, \theta, \phi, T)$ are

obtained, which are, in general, unknown functions of the CG bond length r, bending angles θ and dihedral angles ϕ. The standard way to proceed in order to calculate the CG force field parameters, is to assume that $P^{\mathrm{CG}}(r,\theta,\phi,T)$ factorizes as

$$P^{\mathrm{CG}}(r,\theta,\phi,T) = P^{\mathrm{CG}}(r,T)\, P^{\mathrm{CG}}(\theta,T)\, P^{\mathrm{CG}}(\phi,T) \tag{2.2}$$

This assumption is only valid if the internal CG degrees of freedom are uncorrelated. In the next chapter (see section 3.4.2) we will discuss the case that we find correlations between CG degrees of freedom. There we present a method, how by carefully choosing beyond which distance to cut off local interactions along the backbone in the atomistic sampling and choosing a suitable set of bonded interactions, the CG model can be able to preserve correlations that the atomistic model shows. This enables us to proceed with the methodology presented here.

Having the probability distribution functions, the CG bonded potentials are given from the inverse Boltzmann relations

$$U^{\mathrm{CG}}(r,T) = -k_B T \ln\left(P^{\mathrm{CG}}(r,T)/r^2\right) \tag{2.3}$$

$$U^{\mathrm{CG}}(\theta,T) = -k_B T \ln\left(P^{\mathrm{CG}}(\theta,T)/\sin\theta\right) \tag{2.4}$$

$$U^{\mathrm{CG}}(\phi,T) = -k_B T \ln P^{\mathrm{CG}}(\phi,T) \tag{2.5}$$

In the above expressions the probability distribution functions for bond length and bending angle are normalized by taking into account the corresponding volume elements r^2 and $\sin\theta$. These potentials are potentials of mean force and therefore free energies. Consequently they are temperature dependent, not only due to the prefactor $-k_B T$ but also due to the temperature dependent distribution functions P. In practice, one has to test the temperature range in which a CG model is applicable (usually ± 10-20%) and where a reparameterization is required.

It is also possible to develop the bonded potentials based on simulations of atomistic polymer melts, rather than of isolated chains. [46] In this case the clear separation between bonded and nonbonded interactions is not longer given, since bonded and nonbonded interactions are developed simultaneously and are potentially interdependent. The derivation of bonded potentials from a single molecule in vacuum, however, can be only successful in two cases: If the conformations in vacuum and in the bulk (or in solution) are not substantially different or, secondly, if the CG nonbonded interaction potentials impose the same change on local conformations as the atomistic environment. This can be difficult to obtain in biomolecular systems, where molecules are typically solvated in water. The presence of hydrogen bonds in these systems can change local conformations strongly. In these cases it can be useful to sample molecules in aqueous solution and to include solvent effects implicitly in the CG bonded potentials. [57, 58]

2.1.3 Nonbonded potentials

Nonbonded interactions can be developed in different ways. Following the general strategy of structure-based coarse-graining, the aim is to find nonbonded interaction potentials that reproduce the structure of the systems of interest. The measures, which are sensitive to these potentials, are usually radial distribution functions (RDF). To avoid computationally expensive multi-body interactions, only pair potentials are used to describe nonbonded interactions. It can be shown that a pair potential, which exactly reproduces a given radial distribution function, is a unique solution up to a constant factor. [59] In practical applications it turns out that several different potentials can reproduce a given structure with very small errors.

Analytical potentials with adjusted parameters

For amorphous polymers with a melt density known from experiments or atomistic simulations it can be sufficient to introduce a purely repulsive excluded volume interaction. This approach has used for the systems mentioned above. The functional form was either a repulsive Lennard-Jones form [52, 54], in which only the radii σ of the CG beads are adjusted,

$$U^{\text{CG, LJ}}_{\text{nonbonded}}(r) = \begin{cases} 4\epsilon\left[\left(\frac{\sigma}{r}\right)^{12} - \left(\frac{\sigma}{r}\right)^{6} + \frac{1}{4}\right], & r \leq 2^{1/6}\sigma \\ 0, & r > 2^{1/6}\sigma \end{cases} \tag{2.6}$$

or a repulsive Lennard-Jones type with modified exponents [55],

$$U^{\text{CG, LJ-type}}_{\text{nonbonded}}(r) = \begin{cases} 4\epsilon\left[\left(\frac{\sigma}{r}\right)^{n} - \left(\frac{\sigma}{r}\right)^{m} + c\right], & r \leq \frac{n}{m}^{\frac{1}{n-m}}\sigma \\ 0, & r > \frac{n}{m}^{\frac{1}{n-m}}\sigma \end{cases} \tag{2.7}$$

which in addition to the bead size modifies the “softness” of the potential (values used in ref. 55 are between 7-6 and 7-4). In this case the parameters are adjusted by comparing RDFs of CG and atomistic melts of short chains. The softer potentials, besides the better agreement in the RDF, allows the use of a longer timestep in the integration of the equations of motion.

Iterative Boltzmann inversion

Another approach to develop CG nonbonded interactions is the iterative Boltzmann inversion method. [47, 60] It uses numerically generated tabulated potentials that are not limited by the choice of a functional form and can reproduce a given RDF precisely. The method starts from an initial guess for the nonbonded potential $U^{\text{CG}}_{\text{nonbonded,0}}$. Often the Boltzmann inverse of the RDF $g^{\text{target}}(r)$ is used as an initial guess.

$$U^{\text{CG}}_{\text{nonbonded,0}} = -k_B T \ln g^{\text{target}}(r) \tag{2.8}$$

This is not the potential which would reproduce the RDF in a real liquid system, but only in the limit of infinitely dilute systems, because many-body interactions are not taken

directly into account. The first guessed potential $U^{\mathrm{CG}}_{\mathrm{nonbonded},0}$ is used in a CG simulation of a liquid and yields a distribution $g_0(r)$, which is different from the target $g^{\mathrm{target}}(r)$. The potential is then modified by a correction term $k_BT \ln\left(\frac{g_i(r)}{g^{\mathrm{target}}(r)}\right)$:

$$U^{\mathrm{CG}}_{\mathrm{nonbonded},i+1} = U^{\mathrm{CG}}_{\mathrm{nonbonded},i} + k_BT \ln\left(\frac{g_i(r)}{g^{\mathrm{target}}(r)}\right) \tag{2.9}$$

This corrected potential is again used in a CG simulation of a liquid and the resulting distribution $g_i(r)$ is compared to the target. This process is iterated until $g^{\mathrm{target}}(r)$ is reproduced. To achieve a faster convergence one can modify the correction term by a (possibly distance dependent) prefactor.

A very similar method is the Inverse Monte Carlo (IMC) method, [48, 61] which obtains the corrections for the potential in a different way using rigorous thermodynamic arguments.

It has been mentioned above that in practice a given RDF can be reproduced within hardly noticeable errors by several different pair potentials. This property allows to impose further constraints to the iterative Boltzmann inversion method in order to reproduce thermodynamic quantities without disturbing the local structure severely, e.g. pressure or compressibility. [62] The question to what extent structure-based CG models are able to reproduce several thermodynamic properties is still open, as well as the question for the optimal strategy to develop these models. Pursuing a high accuracy in one physical property could lead to a less accurate rendering of others. Finding an optimal choice for a CG potential may necessitate loosening some constraints in such a way that the correct physics that one is attempting to study is properly included. [63]

If systems of complex molecules with increasing numbers of different CG bead types are studied, it becomes difficult to develop the large number of different pair interactions simultaneously. A possible strategy in these cases is to split the target molecules into fragments to determine the interactions between different bead types based on the structure of mixtures of these fragments using the methods described above. [58] Using fragments of molecules can introduce an error, if in the liquid of fragments different conformations or relative orientations between molecules contribute differently to the structure than in the liquid of the complete target molecules. This is also a problem, if the potential of mean force between two molecules is determined directly, e.g. by the method of McCoy and Curro, which is described in the following.

Methods sampling molecular pairs

The method of McCoy and Curro does not use the structure of a liquid but an atomistic sampling of two fragments, whose mapping points are held at fixed distances. [64] They consider two molecules in a configuration Γ, where the distance between the the centers of mass of the molecules is R and $U^{\mathrm{at}}_{\mathrm{nb}}(\Gamma, R)$ is the sum of all nonbonded interactions. The effective potential between the molecules is provided by the potential of mean force

along R,

$$U_{\mathrm{nb}}^{\mathrm{CG}}(R,T) = -\frac{1}{\beta}\ln\left\langle \exp\left[-\beta U_{\mathrm{nb}}^{\mathrm{at}}(\Gamma,R)\right]\right\rangle_R \tag{2.10}$$

where $\beta = \frac{1}{k_B T}$ and $\langle\cdots\rangle_R$ denotes an average over all angular orientations of an isolated pair of molecules separated by R.

For polymers, where the configurations for two beads at short distances are strongly constrained by indirect interactions via the neighboring chain segments, a similar scheme has been presented by Fukunaga, Takimoto and Doi. [65] They extend the McCoy-Curro scheme with an additional potential for short distances R.

$$U_{\mathrm{nb}}^{\mathrm{CG}}(R,T) = -\frac{1}{\beta}\ln P_{\mathrm{nb}}^{\mathrm{at}}(R,T)\Theta(R^* - R) - \frac{1}{\beta}\ln\left\langle \exp\left[-\beta U_{\mathrm{nb}}^{\mathrm{at}}(\Gamma,R)\right]\right\rangle_R \tag{2.11}$$

where $P_{\mathrm{nb}}^{\mathrm{at}}(R,T)$ is the radial distribution function of the mapping points, $\Theta(R^* - R)$ is the Heaviside unit step function, and R^* is an empirical cutoff that is adjusted in order to reproduce the target RDF of the atomistic model. The additional term in this model takes into account an entropic contribution that represents a strong repulsive interaction for segments in close distance, while the second term represents the attractive interaction at longer distances

A similar approach to develop nonbonded potentials based on pairs of molecules instead of atomistic melts has been used in this work as well. The idea is to determine potentials of mean force between two short oligomers in vacuum. By using oligomers and not isolated beads, we obtain a sampling of relative orientations of the distance-constrained groups that takes into account the most important indirect constraint for these pairs of beads, namely being part of a polymer.

2.1.4 Backmapping

Backmapping or “inverse mapping” is the term used to describe the reintroduction of atomistic detail into a given CG structure. There is no unique solution to the problem of finding a set of atomistic coordinates, whose mapping points coincide with the CG target structure, because each CG structure corresponds to many underlying atomistic configurations. Thus, the detailed structures should have the correct statistical weight of those degrees of freedom that are not resolved in the CG description.

For polymer melts it is possible to obtain backmapped atomistic structures by fitting rigid, atomistic fragments onto the coordinates of CG chain segments. These atomistic fragments can be taken from a pool of atomistically sampled structures that show the correct statistical weights for the detailed degrees of freedom. [66, 67] If the detailed degrees of freedom can be equilibrated already in a short equilibration run, it is sufficient to construct the initial backmapped coordinates by simple geometrical rules. [54, 68] This works especially for CG models with a low degree of coarse-graining, i.e. for CG models that still include information about local torsional degrees of freedom or positions of side groups, because these degrees of freedom do not equilibrate fast enough during a short equilibration run. In all the previously mentioned methods the nonbonded interactions

between the different chains are switched on in an equilibration run, during which the chain segments can move without constraints to their initial CG mapping point. The displacements of chains segments that occur during this procedure are very small on the time scale that is necessary to equilibrate the local configurations.

If the CG polymer chains have very flexible units or if the CG structure includes small molecules, the atomistic structures diffuse away from the CG target coordinates already during short equilibration runs. The strategy in these cases is to constrain the atomistic coordinates in a way that they always satisfy the CG mapping scheme. Not the single atoms are constrained, but groups of atoms that define a CG mapping point together. [69, 70] This method also allows to insert the flexible chain units at random initial atomistic positions. The resulting structures are relaxed, while they are restrained to the CG mapping points, and can be perfectly equilibrated.

Combining CG simulations with an efficient backmapping procedure is a powerful tool to simulate soft matter processes on long time- and large length scales. For example, using the backmapping procedure for several snapshots of a CG trajectory delivers a trajectory in atomistic detail, which would be beyond reach with purely atomistic simulations and which reaches relevant timescales of NMR experiments. [67] The reintroduction of atomistic detail is also necessary to compare simulations to experimental results of neutron scattering or X-ray diffraction measurements. [67, 54]

Another aspect is the use of backmapped structures in further atomistic simulations. In these cases the coarse-grained simulations are used to deliver equilibrated melt structures. The backmapped structures can be used to insert small molecules in order to get solubilities or to study permeabilities. [71, 72, 73] In this work backmapped melts of polystyrene chains were used to study the diffusion of ethylbenzene in this matrix of long chains, see section 5.3.

3 Coarse-grained model for polystyrene

3.1 Basic ideas

This chapter presents a coarse-grained model for polystyrene (PS), which was developed during the course of this work. [74] The chemical structure of PS is shown in Figure 3.1. The development follows the method that was presented in the previous chapter and extends it at certain points. After choosing a mapping scheme, bonded and nonbonded interaction potentials are derived separately. For bonded interactions the approach is based on sampling distribution functions from atomistic simulations of isolated random walks, for nonbonded interactions the approach is based on sampling potentials of mean force between two short oligomers in vacuum. The method is extended and varied at two aspects: The concept of bonded interactions is not only used for bonds, angles and torsions within a chain, but also for interactions between beads connected by four or more subsequent CG bonds. This leads to an increased stiffness of the CG chains and to a better reproduction of local chain conformations. The other new approach is employed for the development of nonbonded interactions. No atomistic simulations of the condensed, melt state are used to develop the CG force field, but pairs of short oligomers are simulated in vacuum. Hence this approach is conceptually different from CG methods that use condensed phase structures as a prerequisite input for the parameterization of the model.

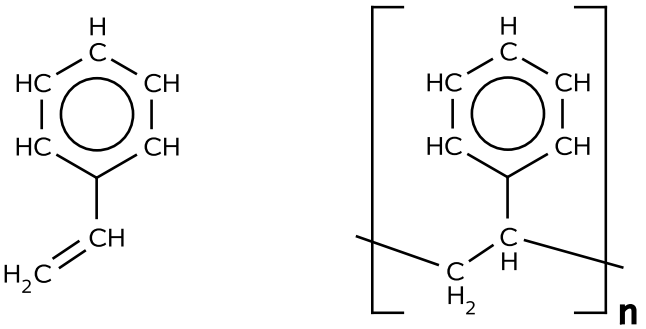

Figure 3.1: Chemical structure of styrene (left) and of polystyrene (right), which is obtained by polymerization of styrene monomers. The brackets indicate that the monomer unit is repeated *n* times to form chains of polystyrene.

The detailed atomistic model, on which the development of the CG model is based, is an all-atom (AA) model. The other option would be a united-atom (UA) model. The

reason for this choice depends on the aim and the systems that the CG model should describe. In the case of this work, one aim of the CG model is to compare dynamical properties of atomistic and CG simulations. The dynamics of CG models is in general much faster than the dynamics of detailed atomistic models. But already the dynamics of united-atom simulations is significantly increased compared to all-atom simulations. This can be understood by the fact that a UA model already represents a first step from detailed AA models towards more coarser models. Therefore the presented CG model has been based on a detailed all-atom description. A coarse-grained model based on a UA model for polystyrene already exists. [54, 55] The mapping scheme of the presented CG model was chosen in an analogous way to this already existing model. This allows a comparison of dynamical properties also between two CG models that are based on different detailed models. Still, the development of the CG model in this work is not only a repetition of a previously developed model, just using another detailed atomistic model, but it introduces new concepts in the development and the final form of the CG model, which reaches a higher agreement with the detailed atomistic model than previous CG models for polystyrene.

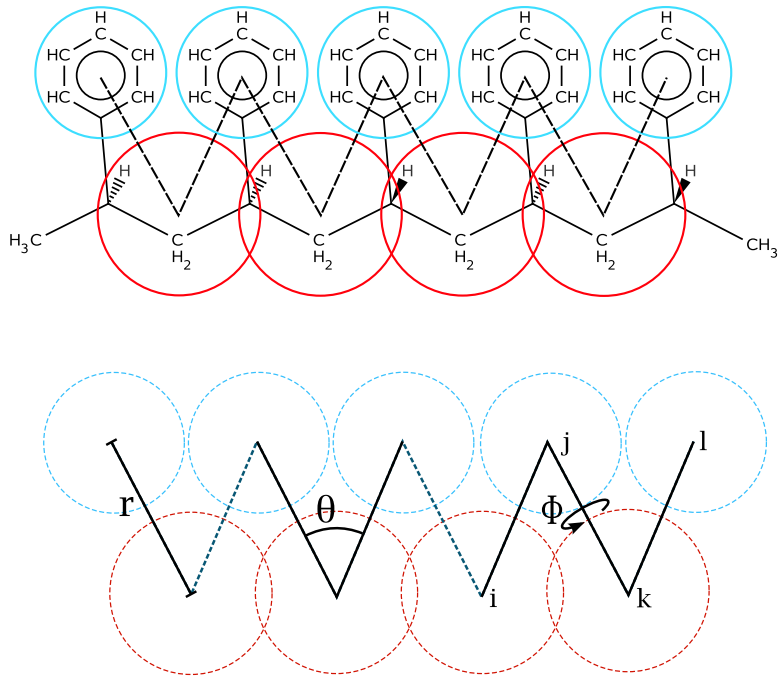

Figure 3.2: Coarse-graining: Groups of atoms are represented by CG beads or superatoms, according to a mapping scheme (top) that groups detailed atoms together and defines the locations of CG beads (as a function of the positions of the detailed atoms). The CG (bonded) degrees of freedom (bottom) are bond lengths r, angles θ between two neighboring bonds and torsion angles ϕ between three CG bonds (ϕ is the angle between the two planes defined by the beads ijk and jkl).

The idea of the CG model can be explained at Figure 3.2. The CG mapping scheme assigns groups of detailed atoms to one CG bead (described in section 3.3). Neighboring

CG beads interact along the CG bonds, expressed by potentials for bond length r, angles θ between three subsequent beads and torsions ϕ between four subsequent beads. The potentials for these CG degrees of freedom are developed in such a way that the distributions they generate in a CG simulation reproduce the corresponding distributions of an atomistic chain. The method to sample these distributions and the development of the CG potentials is investigated in section 3.4. In this work, the concept of bonded interactions is extended to intrachain pairs of beads connected by four CG bonds, see Figure 3.3. These interactions improve the quality of the CG model and a method to obtain them is presented in section 3.4.4. Finally the CG model is completed with the development of nonbonded interactions, which is done separately from the bonded potentials and is described in section 3.5.

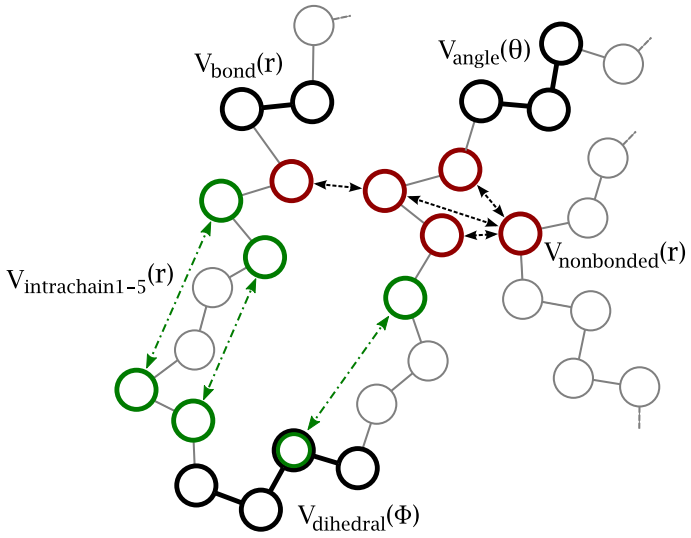

Figure 3.3: Schematic view of force field terms of the CG model for linear chain molecules: bonded potentials act on groups of two (bonds), three (angles) or four (dihedrals) neighbors connected by chemical bonds; in addition, bonded interactions between 1-5 neighbors (connected by four CG bonds) are introduced, which can be even extended to pairs of 1-6 and 1-7 neighbors. Nonbonded potentials act on particles, which are close to each other in space, but not involved in a joint bonded interaction.

3.2 Tacticity of polystyrene

One aim of the presented model is to reproduce distributions for the CG degrees of freedom as close as possible. To that end one has to distinguish between different local configurations of the side groups of the chain (compare Figure 3.4). The phenyl rings in a polystyrene chain are attached together with a hydrogen atom to a carbon atom, which is located in the backbone of the chain. The backbone carbon atom is connected to four atoms in a tetrahedral configuration (two carbon atoms in the backbone, one carbon atom

in the phenyl ring and one hydrogen atom). The phenyl group and the adjacent hydrogen atom cannot swap their positions, neither in real systems nor in atomistic simulations, due to steric hindrance. Because the local configuration of the phenyl groups does not change, also the relative orientation of two neighboring rings remains unchanged. Pairs of neighbors are called “diads” and one can distinguish two types, see Figure 3.4. In a *meso* diad both phenyl rings are pointing to the same side (assuming all-trans configuration of the backbone, i.e. all torsion angles along the backbone are fixed at 180 degree). A chain consisting only of meso diads is *isotactic*. In *racemo* diads the phenyl rings point to opposite sides. A chain consisting only of racemo diads is *syndiotactic*, having the phenyl rings along the chain pointing to alternating sides. In atactic chains the types of diads are randomly distributed. The types of diads influence the experimental properties of polystyrene melts strongly. Therefore, to describe PS of different tacticities in a CG model these two different types of diads have to be taken into account.

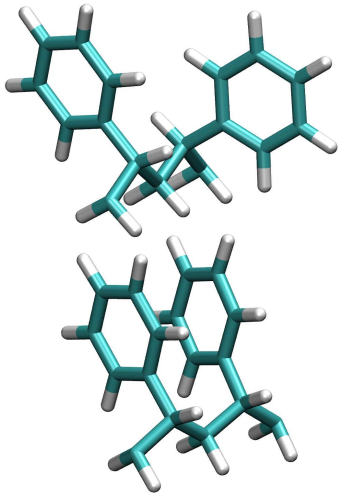

Figure 3.4: Diads in Polystyrene: In racemo diads (top) the phenyl rings point to different sides, in meso diads (bottom) they point to the same side (assuming an all-trans conformation of the backbone).

The distributions for local degrees of freedom as bonds, angles and torsions are mainly affected by the type of diad, to which these degrees of freedom belong. For example, an angle between three subsequent beads, consisting of two beads representing phenyl groups and one bead representing the intermediate part of the backbone, shows very different distributions for racemo and meso diads (compare Figure 3.4 and 3.10). An assumption in the following development of the CG model is that only the type of diad, to which a CG degree of freedom belongs, is defining the type of potential, which is used for this degree of freedom. The influence of neighboring diads can be neglected. This assumption was tested and confirmed (see section 3.4.6). It allows a strategy to develop bonded potentials for meso and racemo diads separately by using purely isotactic chains (only consisting of meso diads) and purely syndiotactic chains (only consisting of racemo

diads). Lateron these potentials are combined to describe chains of arbitrary tacticity. Also in this case of atactic polystyrene the model keeps information about the type of each diad in the chain and does not use any averaged potentials for “atactic diads”, which do not exist in the detailed model as well.

3.3 Mapping scheme

The mapping scheme used in this work is a 2:1 mapping, i.e. each monomer is represented by two CG superatoms. It was already used for a previous model for polystyrene. [55] The monomers in the CG model consist of two coarse-grained, spherical beads of different types, see Figure 3.5:

- **Bead A** contains carbon atoms in the backbone connecting two subsequent phenyl rings and hydrogen atoms attached to these carbon atoms. The CH-groups in the backbone to which the phenyl rings are attached, belong to two neighboring A beads. The center of bead A is the center of mass of the CH_2-group and the two CH-groups, that are taken with half of their masses.

- **Bead B** contains the atoms of the phenyl group. The center of bead B is mapped onto the center of mass.

The beads are connected by CG bonds A-B between the alternating types of beads. This leads to a chain without side groups. There are no bonds A-A or B-B between neighboring beads of the same type. The degrees of freedom in a CG chain are shown in Figure 3.2(bottom).

It is an important point that the CG model represents PS by a linear chain, while the detailed AA model has side groups. The close connection between the A beads (see Figure 3.5, bottom) due to the polymer backbone in the underlying atomistic model is not reproduced directly by a CG bond A-A between these beads, but indirectly by the angular potentials θ_{ABA} connecting these beads. These potentials θ_{ABA} are more narrow than the potentials θ_{BAB}, which rule indirectly the more variable distance between neighboring B beads. In the following, the CG degrees of freedom are mostly referred to by directly naming the involved bead types, e.g. as “ABA angle” for θ_{ABA} or “ABAB dihedral angle” for ϕ_{ABAB}.

The fact that the presented CG model is supposed to describe different tacticities of polystyrene is also reflected in the choice of the mapping scheme. Including the phenyl rings as a separate bead makes it possible to observe changes in the local conformations, depending on the tacticity, and to study aspects of local packing in more detail than a coarser scheme would allow for.

As mentioned before, the choice of the mapping scheme is not unique and depends on the questions and properties of interest. Comparing the mapping scheme used here to other coarse-grained models for polystyrene shows a variety of different choices. One model of Harmandaris et al. [55] uses the same scheme and has been compared to another model, where the mapping scheme is similar, but the group representing the B bead is

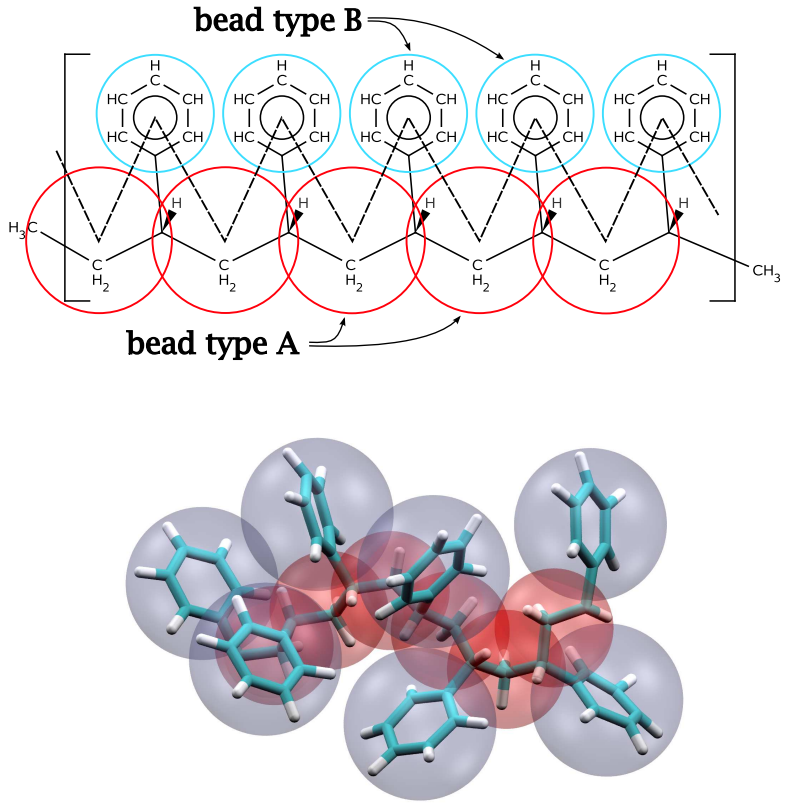

Figure 3.5: Mapping scheme: Each monomer is mapped onto two coarse-grained beads. Bead A is the center of mass of the CH_2-group and the two CH-groups, weighted with half of their masses. Bead B is the center of mass of the phenyl group. In the schematic picture (top), the proportion of chemical bond lengths is not correctly represented. Correct proportions are illustrated in the second picture (bottom), which is an actual snapshot of a short chain segment, taken from an atomistic MD simulation. The lower Figure was created with VMD, as well as the other simulation snapshots in this work. [75]

bigger, since it also includes the adjacent backbone carbon group, whereas the A bead on the backbone is reduced to only one CH_2-group. This size- and mass difference between the two beads causes some difficulties and the more balanced model has turned out to perform better.

Several other models use a 1:1 mapping scheme, but different choices were taken, see also Figure 3.6: Milano and Müller-Plathe [7] center the superatoms on methylene carbons and distinguish between two types of beads according to the diad they belong to. This model is able to keep information about the chain stereosequences, but torsional potentials are averaged over all the possible combinations of diads. Therefore the local distributions of torsional angles in CG simulations will deviate from the distributions in atomistic simulations.The model was refined by Spyriouni and coworkers. [76] The model of Qian and coworkers [9] places the superatoms on the center of mass of the monomers. Two different bead types represent the orientations of the side groups and

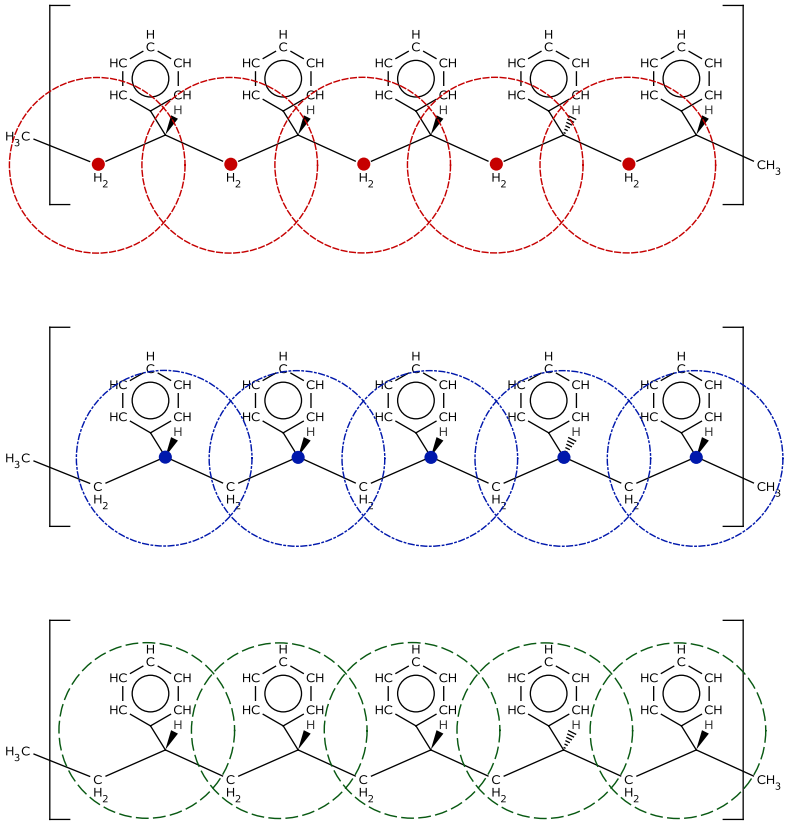

Figure 3.6: Alternative 1:1 mapping schemes for polystyrene, used by other CG models: CG beads are located on the methylene carbons by Milano and Müller-Plathe (top), CG beads are located on the backbone carbon to which the phenyl rings are attached by Sun and Faller (middle), or CG beads are placed on the center of mass of the monomers by Qian and coworkers (bottom). [7, 8, 9]

keep information about the chain stereosequences. As in the previous model torsional potentials are averaged. It has been also used to describe mixtures of PS and ethylbenzene. It should be noted that this mapping scheme is not symmetric and could define an artificial direction of the chain. Sun and Faller [8, 77] center the superatoms on the backbone carbons to which the phenyl rings are attached. They use a single type of bead and therefore the model only describes atactic PS without detailed information about chain stereosequences. This short overview already shows that the choice of suitable mapping scheme is not trivial and clear criteria to find an optimal scheme are not available.

3.4 Bonded interactions

Bonded interactions act on pairs or groups of CG beads that are connected by one or a few chemical bonds. They are developed separately from the nonbonded interactions that act on pairs of CG beads, which are spatially close, but not directly connected by a bonded

interaction. Furthermore, the bonded potentials depend on the tacticity of the chain and are developed separately for isotactic and syndiotactic chains.

Potentials for bonded degrees of freedom of the CG model are obtained by direct Boltzman-inversion (see eq. 2.3-2.5) of distributions obtained from all-atom simulations of single chains in vacuum using stochastic dynamics, for details see appendix A.1.1. All single chain sampling runs were performed with 25-mers at a temperature of 503 K using the all-atom force field adapted by Müller-Plathe to describe benzene-polystyrene systems. [3, 4] The model contains previously developed parameters [5, 6] and an adapted potential to describe torsional rotations properly. The functional form of the potentials has been described in section 1.2.1; parameters of the model can be found in the appendix A.4. This force field was also used as a basis for several CG polystyrene models, discussed in the previous section 3.3. [7, 8, 9]

The development follows the method described before (chapter 2) to factorize the distribution functions, but the influence of the "interaction range" during the sampling of the atomistic chain is analyzed in detail and leads to changes of the method, as described in the following. Since the distribution functions of the bonded degrees of freedom are determined by interactions along the chain at a short range only, we exclude long-range interactions and effectively sample random walks. The range of the atomistic potential used in this sampling procedure critically determines the ability of the CG model to reproduce "local conformations" at the level of a few neighboring repeat units.

3.4.1 Interaction range along the chain

In the previous CG model of Harmandaris et al. [55] bonded interactions up to torsions (acting on 1-4 neighbors and the intermediate beads) were taken into account. All longer ranged CG interactions starting from 1-5 upwards were modeled by repulsive nonbonded interactions, which were chosen the same as those used to describe interchain nonbonded interactions between CG beads in the melt. To develop the bonded potentials of the CG model, an all-atom model of the chain was sampled in vacuum with an atomistic force field that excludes all atom-atom nonbonded pair interactions along the chain falling outside the "1-4 range" of the CG chain description. This is shown in Fig. 3.7. We investigated the influence of the "interaction range" applied in the sampling of the single chains closer by repeating the sampling for all different interaction ranges between 1-2 and 1-8.

The influence of the interactions that we include in the sampling on the local distributions is shown in Figure 3.8, 3.9, 3.10 and 3.11 for all distributions of bond lengths, angles and dihedral angles in fully isotactic and syndiotactic chains. We see that in all cases the form of the distribution changes for each added interaction in a range up to 1-5 and stays almost the same if we add atomistic interactions corresponding to the 1-6 CG level or beyond. The interactions in the 1-6 range and beyond do not change the peak positions anymore; they do only change the peak heights slightly. By including the interaction range 1-5 we take into account the pentane effect between the backbone atoms in the A beads and we avoid an overlap of the phenyl groups of the B beads in the 1-5 range.

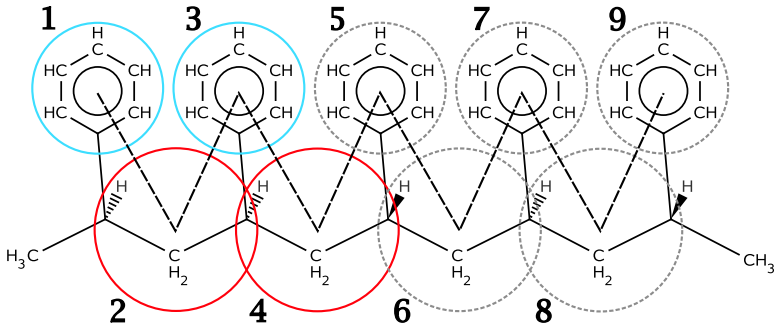

Figure 3.7: Definition of the interaction range: The atomistic polymer chain is sampled in vacuum. The atoms in each group interact with all atoms within a range of neighboring groups. In this example of the 1-4 interaction range the atoms in group 1 interact with the atoms in group 2, 3 and 4, but not with groups at larger distances. The atoms in group 4 interact not only with the atoms in group 3, 2 and 1, but also with the symmetrically located groups 5, 6 and 7. If groups along the backbone are involved (bead A), the CH groups that contribute with half of their masses to the mapping are fully taken into account.

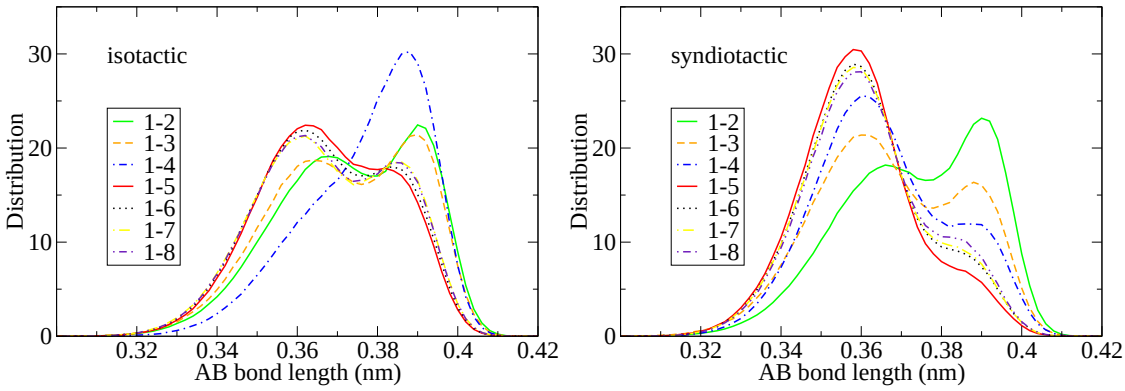

Figure 3.8: Distributions of AB bond lengths in fully isotactic (left) and fully syndiotactic (right) single chains in vacuum; the interaction range in these all-atom (AA) simulations was varied to correspond with CG interactions in a range from 1-2 to 1-8; for 1-5 and above the peak positions stay the same. All distributions in this figure as well as all following distributions for CG degrees of freedom in this work are normalized.

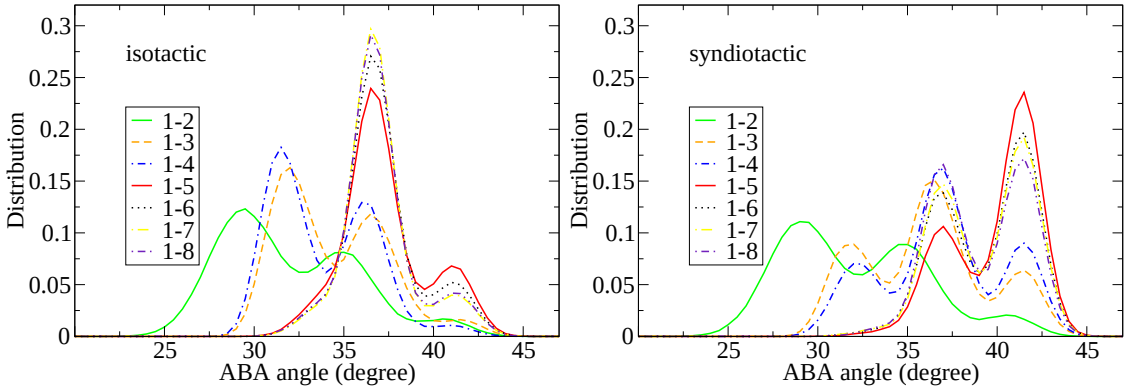

Figure 3.9: Distributions of ABA angles in fully isotactic (left) and fully syndiotactic (right) single chains in vacuum; all-atom runs with varied interaction range from 1-2 to 1-8.

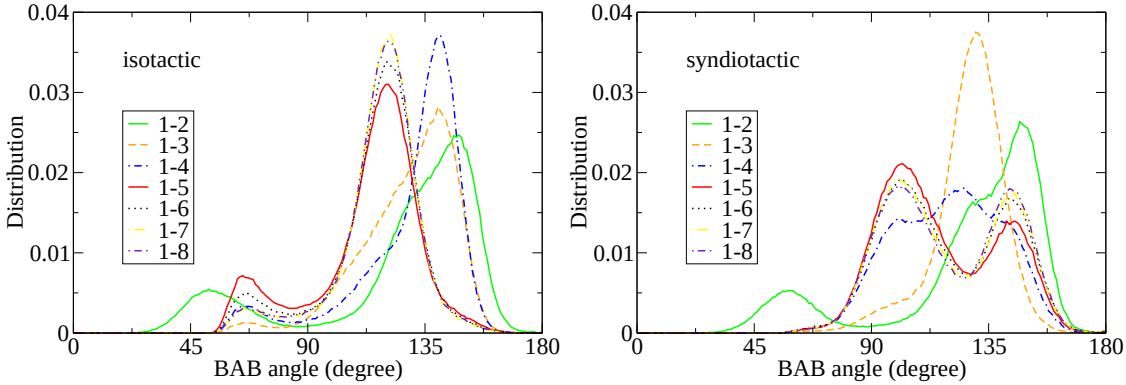

Figure 3.10: Distributions of BAB angles in fully isotactic (left) and fully syndiotactic (right) single chains in vacuum; all-atom runs with varied interaction range from 1-2 to 1-8.

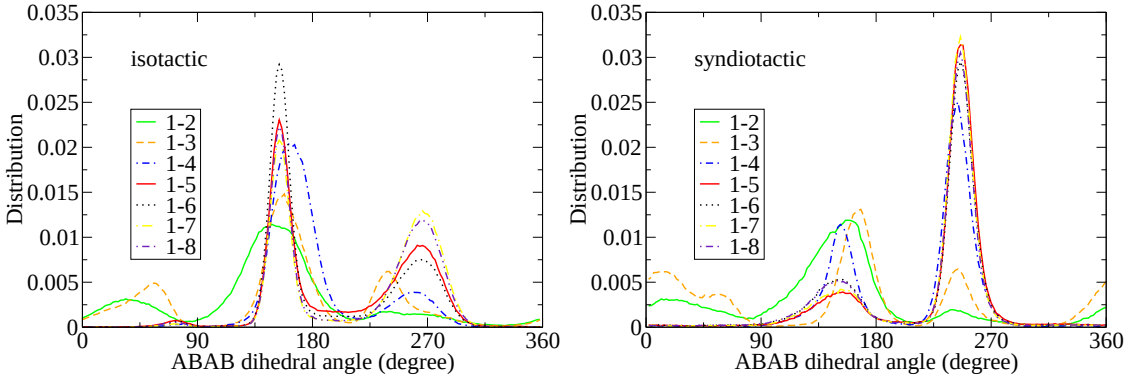

Figure 3.11: Distributions of ABAB dihedral angles in fully isotactic (left) and fully syndiotactic (right) single chains in vacuum; all-atom runs with varied interaction range from 1-2 to 1-8. For better visibility the dihedral values in the range from -180 to 0 are shifted to the range from 180 to 360.

Double counting

The reason for the use of a limited interaction range in the sampling of isolated chains lies in the idea that bonded and nonbonded interactions should be developed strictly separated. In a final CG model that would follow the previously described CG scheme (chapter 2), the 1-5 neighbors in the chain have the same interaction as any other pair of nonbonded beads. Therefore, including these 1-5 interactions in the interaction range of the sampling (that delivers bonded potentials) *and* applying the CG nonbonded interaction between these 1-5 pairs can be seen as "double counting" the influence of these interactions onto the final CG model.

But are these two influences the same? Does the use of CG nonbonded interactions between 1-5 neighbors change the CG bonded distributions in the same way as the extension of the interaction range from 1-4 to 1-5 in the atomistic sampling? The comparison of these two effects on the distributions of BAB angles is shown in Figure 3.12. The bonded potentials of the CG model are obtained by Boltzmann-inversion of the distributions sampled with the 1-4 interaction range. The CG nonbonded interactions are the ones described later in this work (see section 3.5). They act on the CG 1-5 neighbors (the effect from neighbors beyond 1-5 is not significant here). One can see clearly that the nonbonded potentials have a strong influence on the distributions,[1] but they do not change the distributions in a way corresponding to the extension of the interaction range.

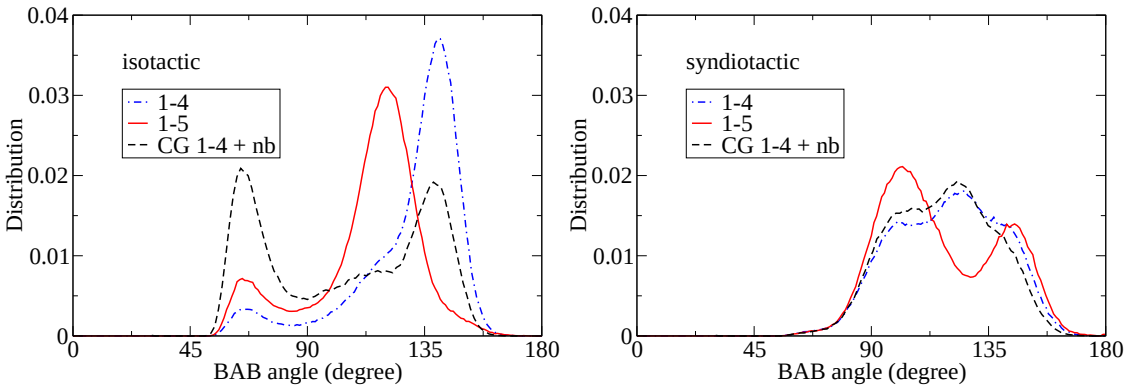

Figure 3.12: Distributions of BAB angles in fully isotactic (left) and fully syndiotactic (right) single chains; comparison between all-atom runs with interaction ranges of 1-4 and 1-5 and a CG run with bonded potentials (obtained from the sampling with 1-4 interaction range) and nonbonded interactions.

This example suggests to extend the interaction range in the sampling of the isolated atomistic chains. The argument of double counting is not applying directly here, because two different effects are counted. Nevertheless, the extension of the interaction range does not answer the question, if the nonbonded interaction should be used for 1-5 neighbors

[1] If the CG model would be used without the nonbonded interactions, it would exactly reproduce the atomistic distribution of the 1-4 interaction range, based on which it has been developed.

or if a modified bonded 1-5 interaction is a better choice. This question is studied in the following after a discussion of the changes with increasing interaction range.

3.4.2 Correlations in single chains

The reason why the distributions of CG angles and dihedral angles do not change their general form when the interaction range is extended beyond 1-5 becomes clear, if combinations of two neighboring dihedral angles in Figure 3.13 and 3.14 are studied. These plots show the combinations of two subsequent CG dihedral angles, obtained by sampling a single atomistic chain in vacuum and analyzing it in the CG description. In both figures the interaction range is varied from 1-3 to 1-6, in Figure 3.13 for an isotactic chain and in Figure 3.14 a syndiotactic chain.

The longer we choose the range of interactions to include, the more combinations of dihedral angles are suppressed in the sampling of the local distributions. But as soon as the 1-5 interactions are included, we sample always the same combinations, even if we include additional longer ranged interactions. This means that the interactions up to 1-5 determine correlations between local degrees of freedom in single chains and thereby also local conformations, as seen before. Interactions between 1-6 neighbors and above might slightly influence the peak heights but not the peak positions. Beyond 1-5 the additional interactions mainly contribute to excluded volume effects. These excluded volume interactions are described separately by nonbonded potentials (see section 3.5).

Based on the previous investigation of the interaction range and its influence on distributions of CG degrees of freedom and their correlations it seems reasonable to include interactions at least up to 1-5 in the sampling of the single chains from which the CG bonded potentials are obtained. By that we extend the path that was followed before [54, 55] to include only interactions up to 1-4 in the atomistic single-chain sampling.

A detail that can be noted here is the different axis of symmetry for the dihedral combinations in isotactic and syndiotactic chains. This gives a hint that the dihedral angles can have different orientations, i.e. the dihedral potentials in the CG model (which are periodic and range from -180 to 180) have to be mirrored (around 0 degree) in certain situations, depending on the tacticity of the chains.[2] Details on how the orientation of the dihedrals is taken into account in the implementation of the CG model can be found in the appendix A.3.

[2] If the direction along the chain, in which the dihedrals are evaluated, is changed, the orientation of meso diads is mirrored, whereas the one of racemo diads stays the same. This can be visualized in Figure 3.4: while a rotation of 180 degrees around the z-axis (pointing upwards) of the diads leads to an identical situation for the racemo diad, the meso diad is mirrored in this case.

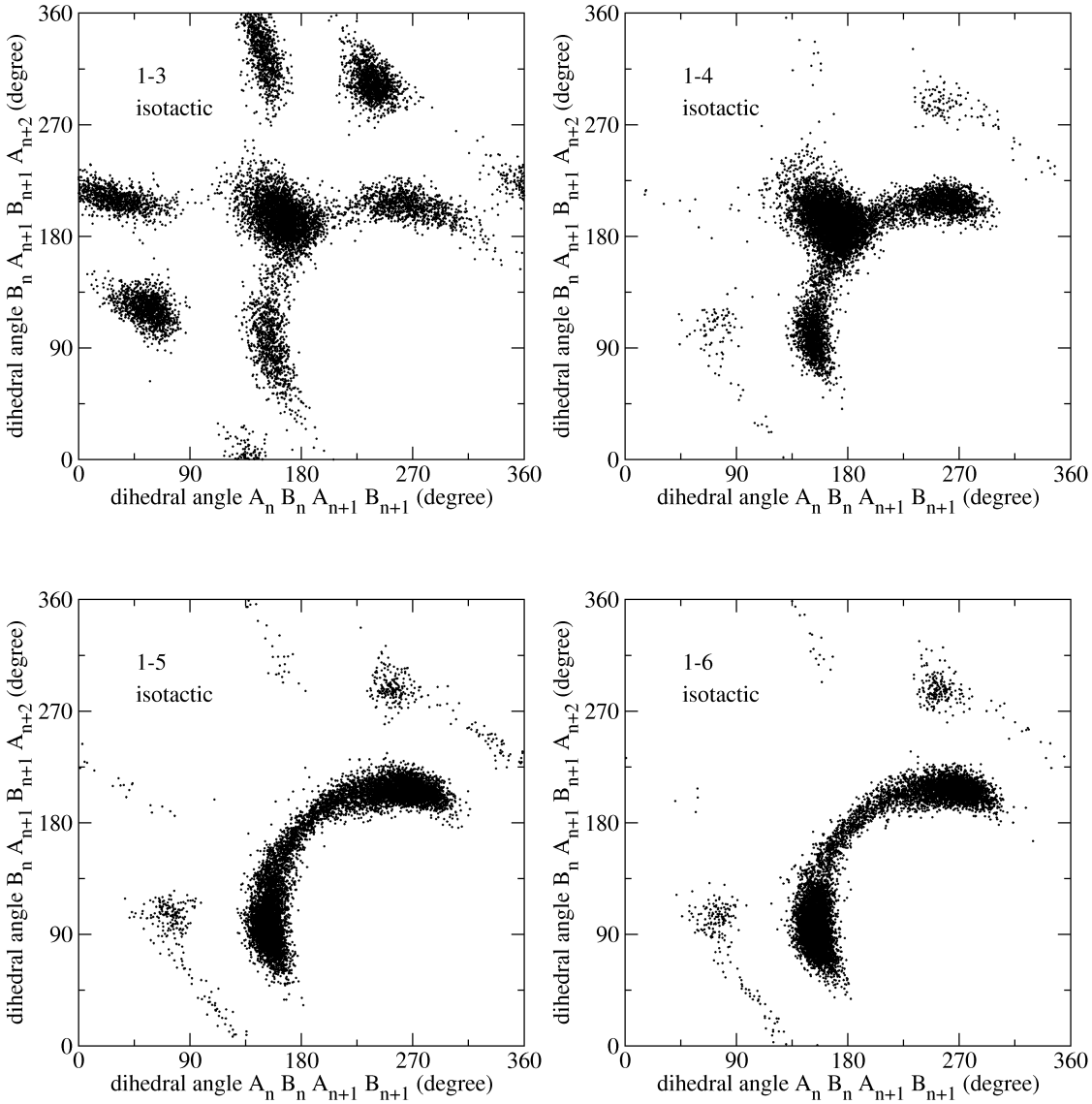

Figure 3.13: Combinations of two subsequent CG dihedral angles, obtained from the sampling of a single, isotactic chain in an atomistic simulation. The two dihedrals share three beads that form an angle BAB and include as fourth bead the A beads next to this BAB angle. Shown are the combinations of dihedral angles from four different atomistic simulations with varied range of interactions along the chain. The range of interactions is inceased from 1-3 interactions (upper panel, left), 1-4 interactions (upper panel, right), 1-5 interactions (lower panel, left) up to 1-6 interactions (lower panel, right). By including the interactions 1-4 and 1-5 several combinations are suppressed. For better visibility the dihedral values in the range from -180 to 0 are shifted to the range from 180 to 360.

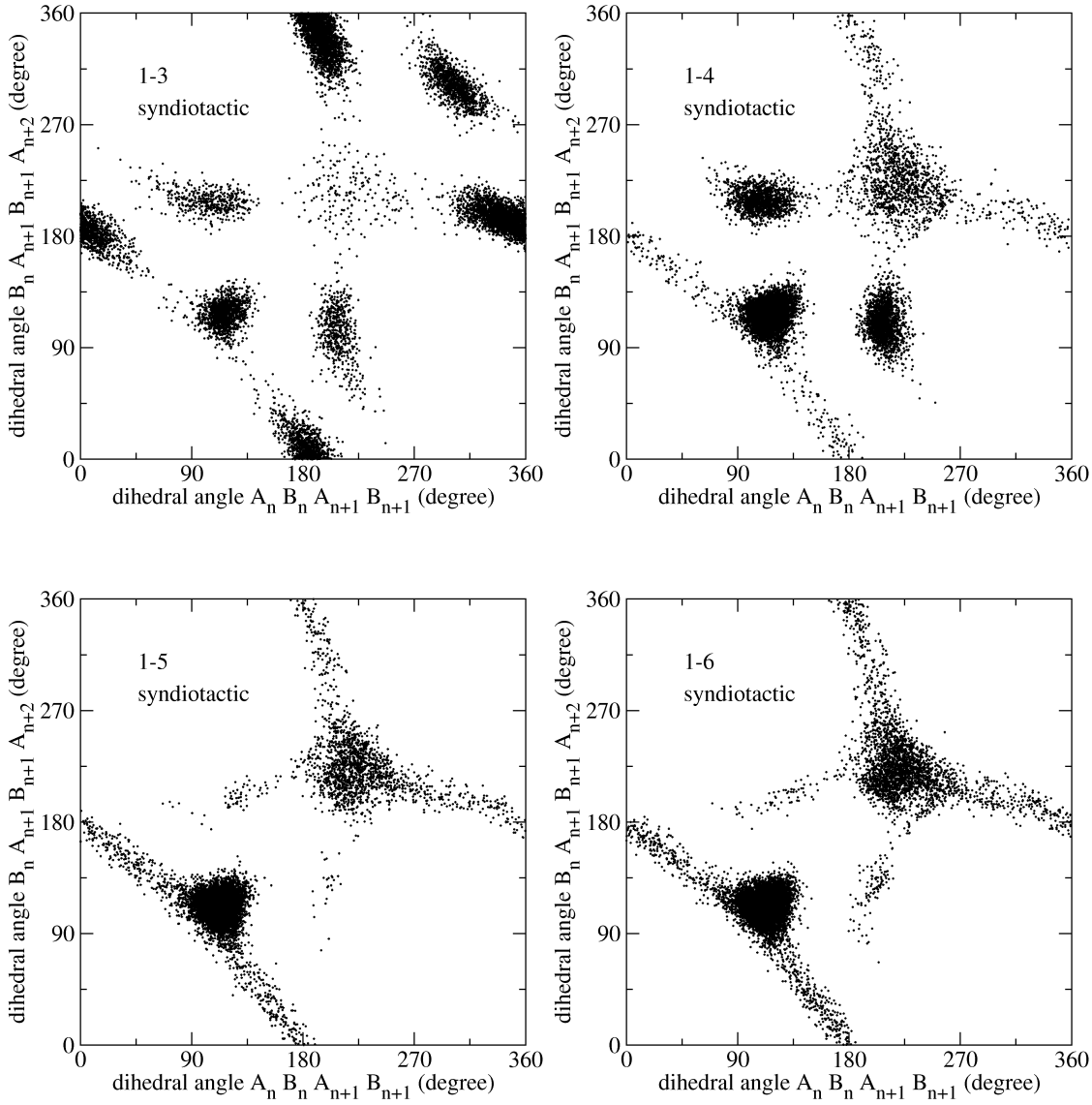

Figure 3.14: Combinations of two subsequent CG dihedral angles, obtained from the sampling of a single, syndiotactic chain in an atomistic simulation. The two dihedrals share three beads that form an angle BAB and include as fourth bead the A beads next to this BAB angle. Shown are the combinations of dihedral angles from four different atomistic simulations with varied range of interactions along the chain. The range of interactions is inceased from 1-3 interactions (upper panel, left), 1-4 interactions (upper panel, right), 1-5 interactions (lower panel, left) up to 1-6 interactions (lower panel, right). By including the interactions 1-4 and 1-5 several combinations are suppressed. For better visibility the dihedral values in the range from -180 to 0 are shifted to the range from 180 to 360.

3.4.3 Interactions for bonds, angles and dihedrals

Previously we discussed the influence of the interaction range on local conformations and correlations. We showed before that a sampling of atomistic chains with a short interaction range leads to an incomplete consideration of correlations between local degrees of freedom and to deviating distributions. These deviations can be only to a small extent corrected by the nonbonded interactions in the CG model. It is therefore favorable to take into account all local correlations in the atomistic sampling (based on which the CG bonded potentials are obtained) by choosing the interaction range sufficiently large. Following this path the distributions for the CG bonded degrees of freedom agree with the corresponding distributions in atomistic chains and also with distributions in atomistic melt simulations, which should be reproduced by the final CG model. Even though distributions in atomistic single chains and melts are not necessarily the same, due to the influence of other surrounding chains, the intrachain correlations are always present in the melt and in the presented case of polystyrene they are dominating the shape of the distributions (the peak positions). Nonbonded interactions with surrounding chains mostly influence the relative height of the peaks in atomistic melts and this effect can be captured in CG simulations as well.

We performed the atomistic sampling of single chains in vacuum with all interactions included up the the 1-6 CG level in the derivation of the CG bond, angle and torsion potentials. These potentials are shown in Figure 3.15 and 3.16.

The question of how to incorporate CG intrachain interactions that correspond to the extension of the interaction range (in our case the 1-5 and 1-6 interactions) into a CG model is not yet answered. Two options are possible:

- Using the regular nonbonded interactions between these 1-5 and 1-6 neighbors: In this case it is unclear, if we double count these interactions, because they influence the bonded distributions during the atomistic sampling *and* during the CG simulation. This effect, however, is not necessarily strong and a CG model using this method can be already superior to a CG model obtained from an atomistic sampling with a shorter interaction range that ignores certain correlations. On the other hand the atomistic sampling with an extended interaction range includes information about the 1-5 and 1-6 distributions, which can be used to reproduce these distributions.

- Using special interactions for intrachain 1-5 or 1-6 neighbors: Since the atomistic sampling delivers distributions for the distances between these neighbors, they can be used as a target that the CG model should reproduce. This approach was used in this work and the development of the intrachain interactions is described in the following section 3.4.4.

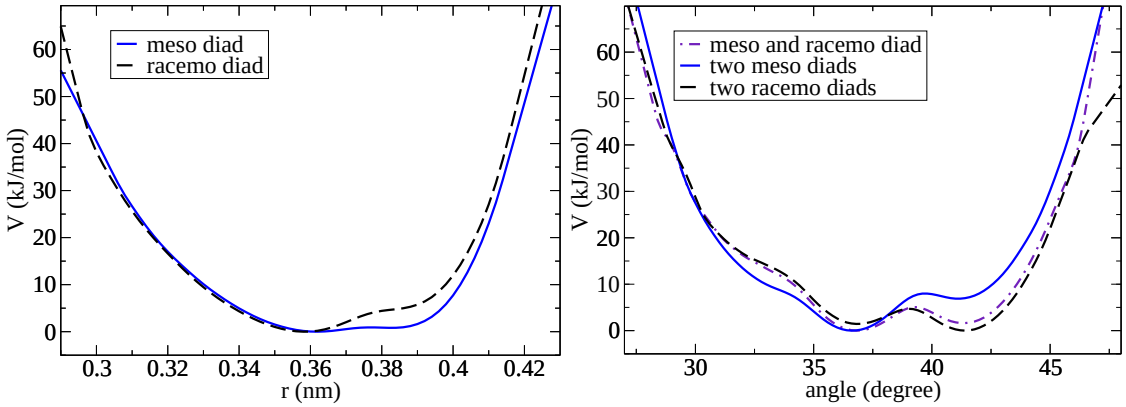

Figure 3.15: CG potentials for AB bond length (left) and ABA angles (right) for the different diads to which the involved CG beads belong to ($k_B T = 4.2$ kJ/mol at 503 K). For ABA angles two subsequent diads define the type of potentials and therefore three different combinations can occur. The case of one meso and one racemo diad does not occur in purely isotactic or syndiotactic chains; this potential was obtained by a chain using an alternating sequence of meso and racemo diads, referred to as "block tacticity" in this work, see section 3.4.6.

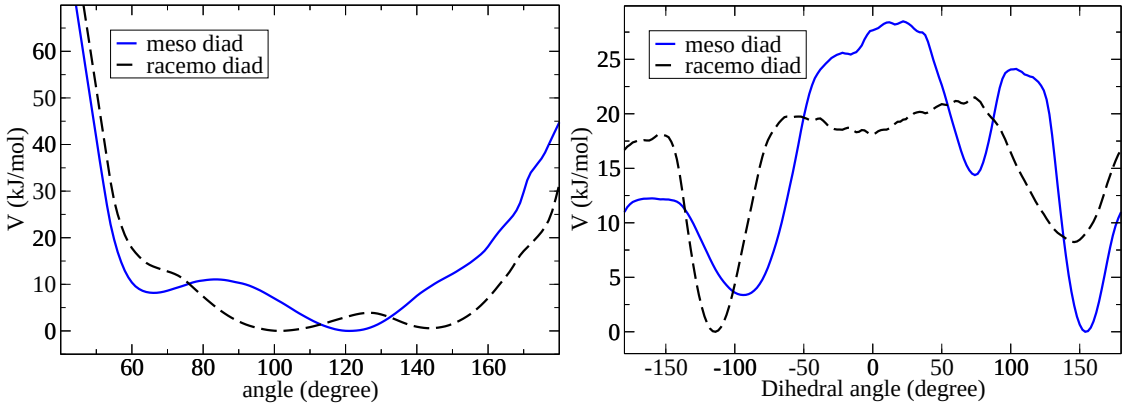

Figure 3.16: CG potentials for BAB angles (left) and dihedral angles (right) for the different diads to which the involved CG beads belong to.

3.4.4 Intrachain interactions between 1-5 neighbors

By extending the interaction range in the sampling of the atomistic chains we get information about distances between 1-5 and 1-6 neighbors. Here we present a method to obtain CG bonded potentials in a range beyond 1-4 that reproduces distance distributions between 1-5 neighbors very well without disturbing other bonded degrees of freedom strongly.

These bonded potentials are distance dependent *pair* potentials, contrary to angular and torsional potentials, which act on groups of three or four CG beads. The difference between the 1-5 interactions and the shorter bonded interactions is that by construction they are not completely decoupled, which was one of the basic assumptions before. Given a certain set of values for intermediate bonds, angles and dihedral angles, the distance between two 1-5 neighbors in the chain is completely determined. On the other hand, a certain 1-5 distance can be realized with several combinations of intermediate bonds, angles and dihedrals.

The fact that 1-5 distances and shorter bonded interactions are not decoupled can be seen as well, if we look at a single CG chain in vacuum, which has only bonded potentials for CG bonds, angles and dihedral angles and no bonded or nonbonded interactions with a longer range. If for one degree of freedom, say an angle, we switch off the potential, the sampling of the CG chain will show a uniform distribution for this degree of freedom (after normalizing with $\sin\theta$). The sampled distribution of 1-5 distances, however, will not be uniform, although there is no direct interaction present between the two beads. This influence of the intermediate interactions up to 1-4 has to be taken into account, when we develop the 1-5 CG potentials.

Isotactic chains

In Figure 3.17 these distributions are shown for A-A and B-B 1-5 distances in an isotactic CG chain, having only bonded interactions up to 1-4 (dashed-dotted line), denoted by $P^{\text{1-5,A-A}}_{\text{correcting}}(r,T)$ for the A-A case. If we only Boltzmann-invert the 1-5 distributions (dashed lines) from the sampling of an atomistic chain including the 1-5 range, denoted by $P^{\text{1-5,A-A}}_{\text{target}}(r,T)$, we would double count the contribution of the CG bonded interactions up to 1-4 (dashed-dotted line). Therefore we Boltzmann-invert the 1-5 distance distribution from a single all-atom chain, which is our target distribution, and subtract the Boltzmann-inverted 1-5 distribution of a CG chain having only bonded interactions up to 1-4:

$$U^{\text{CG}}(r,T) = -k_B T \left[\ln P^{\text{1-5,A-A}}_{\text{target}}(r,T) - \ln P^{\text{1-5,A-A}}_{\text{correcting}}(r,T)\right] \tag{3.1}$$

The CG bonded 1-5 potentials obtained in this way are shown in Figure 3.17 for the isotactic case. This plot shows also the CG nonbonded interactions that would be used for the interaction between these neighbors otherwise. The difference between the two potentials is large, hence the introduction of CG bonded potentials beyond 1-4 improves the model and will probably lead to a better reproduction of local conformations. This difference can be expected, since neighboring beads belonging to the same chain will have a different

average orientation towards each other than two close beads belonging to different chains, which is the situation in which the CG nonbonded potentials are developed.

With these CG bonded potentials we can sample 1-5 distributions in CG chains, which are in very good agreement with the distributions of the all-atom chain (continuous line in Figure 3.17, top panel). The effect of the 1-5 bonded interactions on the intermediate bonded distributions of angles and dihedral angles is shown in Figure 3.18. We can see that the distributions do not deviate strongly.

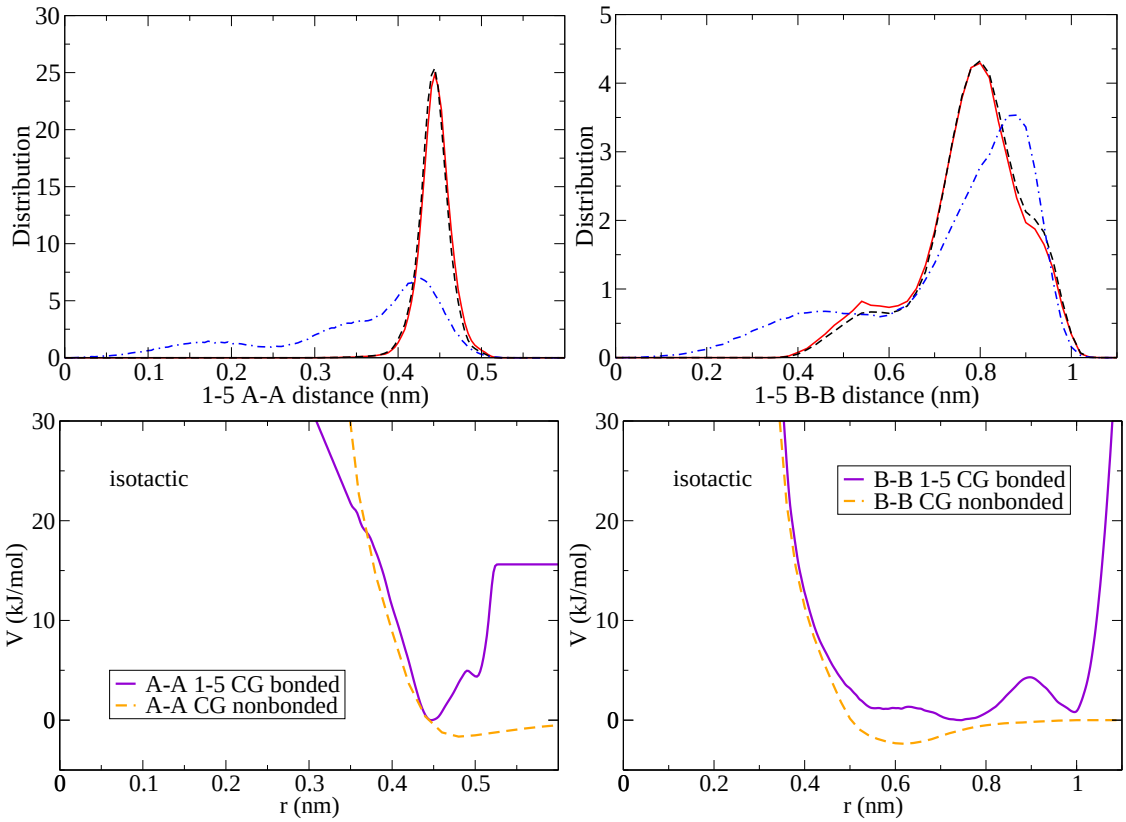

Figure 3.17: Distributions of 1-5 distances in isotactic chains for A-A and B-B beads (top): The target distribution from an all-atom single chain (dashed), the correcting distribution from a CG chain with bonded interactions up to 1-4 (dashed-dotted) and the final CG distribution of a CG chain with the additional bonded 1-5 potentials (continuous). The CG potentials for 1-5 distances in isotactic chains (bottom) for A-A (left) and B-B (right) beads: Bonded 1-5 (continuous) and nonbonded (dashed) potentials in comparison ($k_B T = 4.2$ kJ/mol at 503 K).

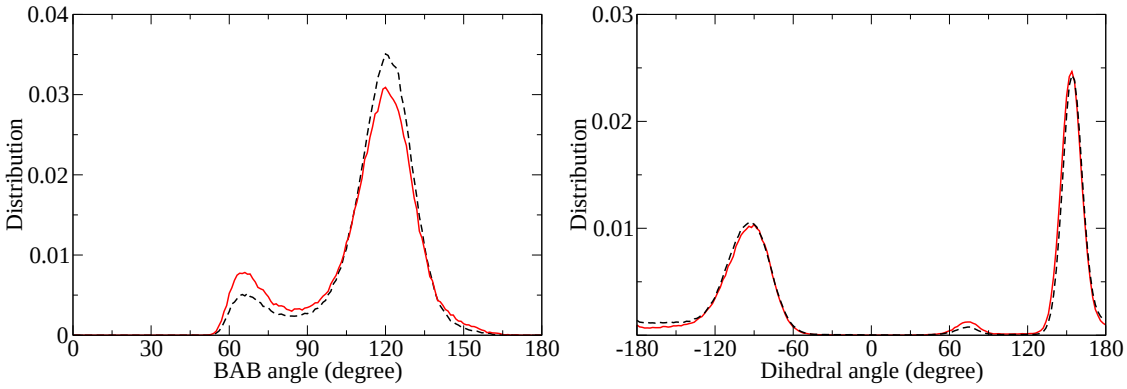

Figure 3.18: Distributions for angles (left) and dihedral angles (right) in isotactic chains in comparison for all-atom single chains (dashed) and CG chains with bonded 1-5 interactions (continuous).

Syndiotactic chains

Since we have to types of 1-5 interactions, A-A and B-B, they also may influence each other. For the isotactic case, presented before, this is a minor effect. For the syndiotactic case the correcting potential $P^{\text{1-5,B-B}}_{\text{correcting}}(r, T)$ has to be sampled from a CG chain including bonded potentials up to 1-4 and the 1-5 A-A potential and vice versa. This process of correcting the potentials can be done iteratively. For the syndiotactic case it is sufficient to do three steps:

- get the first A-A 1-5 potential by correcting with the distribution from a CG chain including only bonded interactions up to 1-4
- get the B-B 1-5 potential by correcting with the distribution from a CG chain with bonded interactions up to 1-4 and A-A 1-5 (from previous step)
- get a second corrected A-A 1-5 potential by correcting with the distribution from a CG chain with bonded interactions up to 1-4 and B-B 1-5

The corrected potentials and the distributions that we obtain by using these corrected potentials are shown in Figure 3.19. The influence on angles and dihedrals is shown in 3.20. We see that the distributions are not disturbed strongly in the syndiotactic case as well.

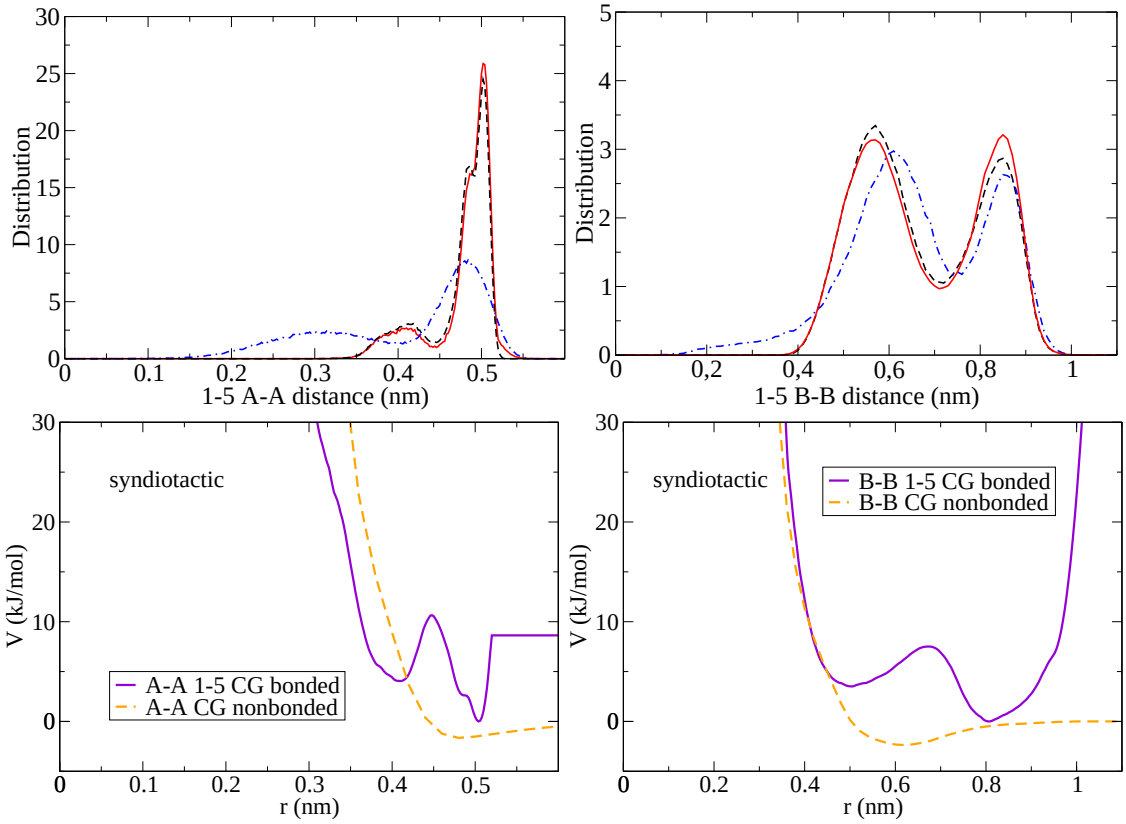

Figure 3.19: Distributions of 1-5 distances in syndiotactic chains for A-A and B-B beads (top): The target distribution from an all-atom single chain (dashed), the correcting distribution from a CG chain with bonded interactions up to 1-4 (dashed-dotted) and the final CG distribution of a CG chain with the additional bonded 1-5 potentials (continuous). The CG potentials for 1-5 distances in syndiotactic chains (bottom) for A-A (left) and B-B (right) beads: Bonded 1-5 (continuous) and nonbonded (dashed) potentials in comparison (k_BT = 4.2 kJ/mol at 503 K).

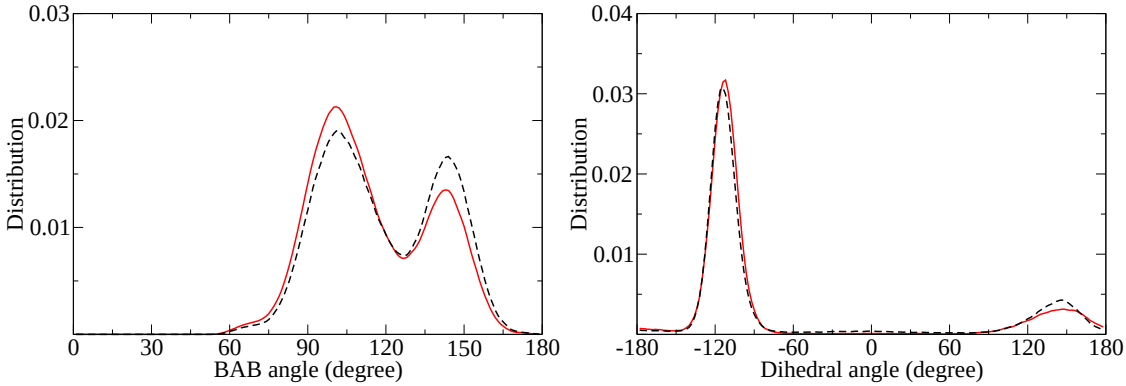

Figure 3.20: Distributions for angles (left) and dihedral angles (right) in syndiotactic chains for all-atom single chains (dashed) and CG chains with bonded 1-5 interactions (continuous).

3.4.5 Chain stiffness and the range of bonded interactions

Extending the previously discussed scheme to 1-6 interactions or above is straightforward. The Boltzmann-inverted distribution for the 1-6 distance from a single all-atom chain is corrected by the Boltzmann-inverted distribution of a CG chain, which includes only interactions up to 1-5, and so on. For atactic chains it is sufficient to use bonded 1-5 potentials. For fully isotactic and syndiotactic chains we use bonded interactions up to 1-7. Choosing such a range of bonded interactions the CG model reproduces the chain stiffness of atomistic systems.

To get information about the chain stiffness we extract the characteristic ratio, also referred to as "internal distances", from simulations of isolated chains. The characteristic ratio $C_n = \langle R^2(n)\rangle/(nl^2)$, where $\langle R^2(n)\rangle$ is the mean square distance between two repeat units, separated by n carbon-carbon bonds (two per monomer) of length l along the backbone. For CG systems we have as well two CG bonds per repeat unit and use the atomistic bond length $l = 0.153\,\text{nm}$. For atomistic systems we apply the mapping scheme and evaluate the internal distances between the mapping points. Therefore we can compare the internal distances for atomistic and CG systems directly.

For long polymer chains in melts the characteristic ratio reaches a plateau value of C_∞. The plateau is reached for a certain number of CG bonds along the chain. If two CG bonds are separated by this number of bonds, the vectors indicating their direction (or, in a coarser picture, the vectors along the chain contour) are uncorrelated. If two bonds are connected by a smaller number of bonds along the chain, they are correlated. This correlations are closely linked to the chain stiffness.

The question how many neighboring beads should be treated with a CG bonded interaction can be difficult and requires a closer look at local properties of the chain. Since the alternative to a bonded interaction is a regular nonbonded interaction, it is reasonable to compare chains that include these nonbonded interactions and do not have any long ranged exclusions. The situation of simulating such an isolated chain in vacuum is of course different from a chain in a polymer melt, because the chain will coil up. The internal distances for large n (distances between beads separated by n bonds) of these chains will be smaller than in a melt, but the slope for low n (between 6-12 for isotactic chains) still gives a measure for the chain stiffness.

In Figure 3.21 internal distances for isotactic chains are shown. In this case the use of 1-6 and 1-7 A-A bonded potentials increases the slope for low n and therefore the chain stiffness directly and leads to a good agreement with the atomistic reference system. In parallel the improvement is visible in the distance distributions for the 1-6 and 1-7 neighbors (see Figure 3.22, left side). It can be noted that the 1-7 B-B distribution is improved as well, even though the 1-7 B-B neighbors still interact with the CG nonbonded potential.

For syndiotactic chains the situation is slightly different. The slope of the internal distances for low n is not necessarily increasing with additional bonded interactions but can be also reduced. The reason for this is probably the fact that syndiotactic polystyrene prefers the all-trans conformation of the backbone and this is already provided by the 1-5 bonded interactions. Therefore, the addition of further bonded interactions is more of a

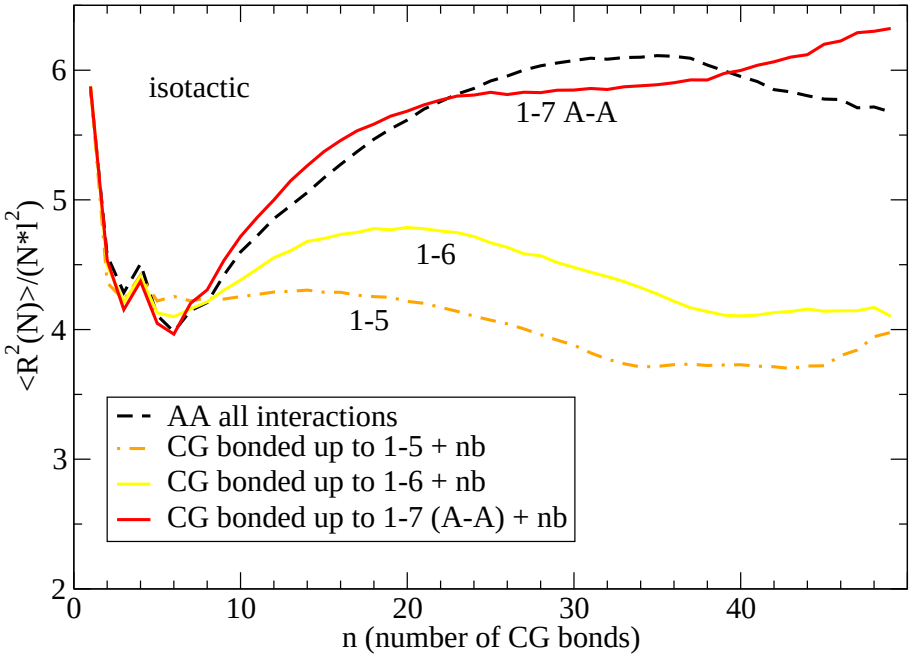

Figure 3.21: Internal distances in isolated atomistic (dashed) and CG (continuous and dashed-dotted) chains in vacuum. All nonbonded interactions are included in the sampling. The range of bonded interactions in CG chains is varied from 1-5 to 1-6 and to 1-7 A-A (for 1-7 B-B the nonbonded potential is used).

fine-tuning here and not a compensation of a lack of stiffness as in the case of isotactic polystyrene. Nevertheless, improving the agreement for 1-6 and 1-7 distributions can be used as an indicator for the quality of the model as well. This can be seen as a general criterion, because an agreement in the distributions between all pairs of neighbors, separated by up to *n* bonds, means an agreement of internal distances up to *n*, hence also an agreement in the slope of internal distances and finally an agreement in chain stiffness. The improvement of the distributions for syndiotactic chains due to the use of bonded 1-6 and 1-7 interactions can be seen in Figure 3.22 (left side).

Based on these considerations bonded interactions in the range up to 1-7 have been used in the final CG model for stereoregular chains. In the case of isotactic chains only 1-7 A-A bonded potentials are used, while the interaction between 1-7 B-B neighbors is modeled by the standard nonbonded interaction. This choice reproduces the chain stiffness very well. In the case of syndiotactic chains bonded potentials are used for 1-7 A-A and 1-7 B-B neighbors, since this reproduces the distributions up to the 1-7 distances very well.

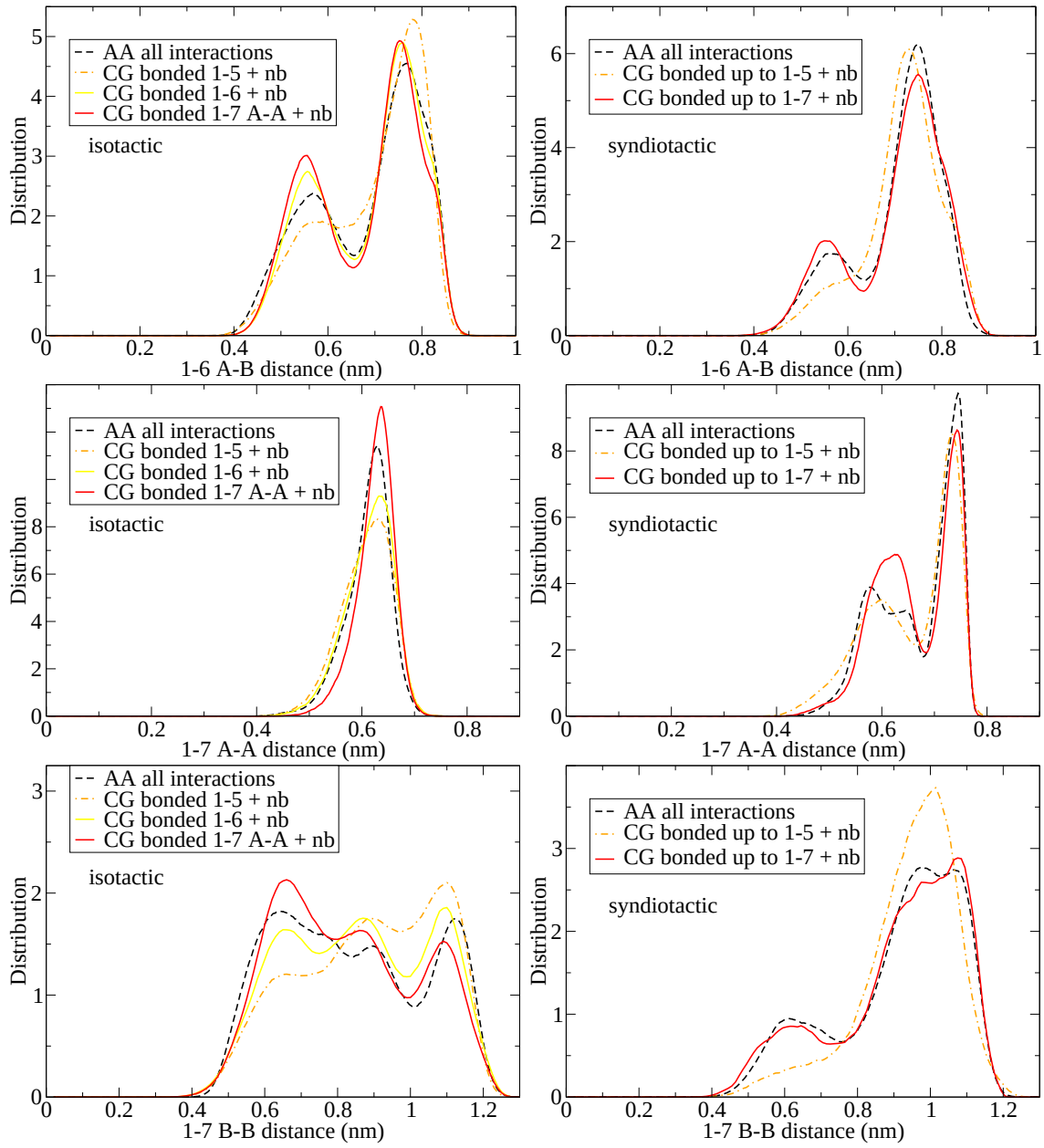

Figure 3.22: Distributions of A-B 1-6 distances (upper row), A-A 1-7 distances (middle) and B-B 1-7 distances (lower) in isotactic (left) and syndiotactic (right) chains: Comparison between atomistic chains including all nonbonded interactions (dashed) and CG chains with nonbonded interactions for 1-6 distances and above. The range of CG bonded potentials is varied from only 1-5 (dash-dotted) to 1-7 (continuous); in the isotactic case only bonded A-A 1-7 interactions are used, in the syndiotactic case also bonded B-B 1-7 interactions.

3.4.6 Combining different potentials: Atactic polystyrene

To simulate *atactic* chains, in which the two types of diads are randomly distributed, we have to check how the two sets of bonded potentials for purely iso- and syndiotactic chains can be combined to simulate chains that include meso diads and racemo diads. We therefore test, whether the local distributions for bonds, angles and dihedrals only depend on the type of diad that is involved in these sequences of two, three or four CG beads, or if the neighboring diads have a strong influence, too. To this end we sampled a chain consisting of a sequence of diads of alternating meso and racemo type. In this chain the phenyl rings are pointing pairwise to alternating sides. Each diad has two neighboring diads of the opposite type, which is the environment differing the most from the stereoregular chains. This tacticity is referred to as "block tacticity" in the following.

It turned out that the influence of neighboring diads on local distributions of CG bonded degrees of freedom is small. The comparison of these distributions is shown in Figure 3.23. Even though some deviations appear, they are much smaller than the differences between the two different diads and the type of diads can be clearly recognized by the distributions. Furthermore, if the CG model, whose potentials are developed based on stereoregular chains, is simulated with block tacticity, the CG distributions tend to deviate in the same direction as the distributions in AA chains with block tacticity.

Based on this test it is assumed in the following that bonded potentials can be used independently of the tacticity of the neighboring diads in the chain. This opens the way to describe atactic polystyrene with the CG model by using the CG potentials that have been developed from stereoregular (isotactic and syndiotactic) chains and combining them in atactic chains.

Bonded 1-5 interactions

Concerning the transfer of 1-5 potentials to the case of alternating diads in a chain we have to distinguish between A-A and B-B 1-5 interactions. For the case of the A-A 1-5 interaction we can still use the potentials which were used for stereoregular chains, since the two B beads between the connected A beads can just form a meso or racemo diad. For the B-B 1-5 interaction, however, two subsequent diads are involved, formed by the three B beads. Therefore we have three different types of B-B 1-5 potentials: Meso-meso, racemo-racemo and the symmetric cases of meso-racemo and racemo-meso. Meso-meso and racemo-racemo correspond to the cases of iso- and syndiotactic chains, as discussed above. The case of meso-racemo or racemo-meso has to be considered separately in the following.

In order to get the B-B 1-5 potential for a meso-racemo triad, we use the B-B 1-5 distribution of the atomistic single chain in vacuum with block tacticity. As discussed before, the bonded distributions up to 1-4 and A-A 1-5 depend mainly on their own tacticity but not on the environment. For this reason we developed the B-B 1-5 potential by using the corrected A-A 1-5 potentials from the iso- and syndiotactic chains to correct the B-B 1-5 potential. The Boltzmann-inverted B-B 1-5 distribution of the atomistic chain with block tacticity was corrected by the Boltzmann-inverted B-B 1-5 distribution of a CG chain,

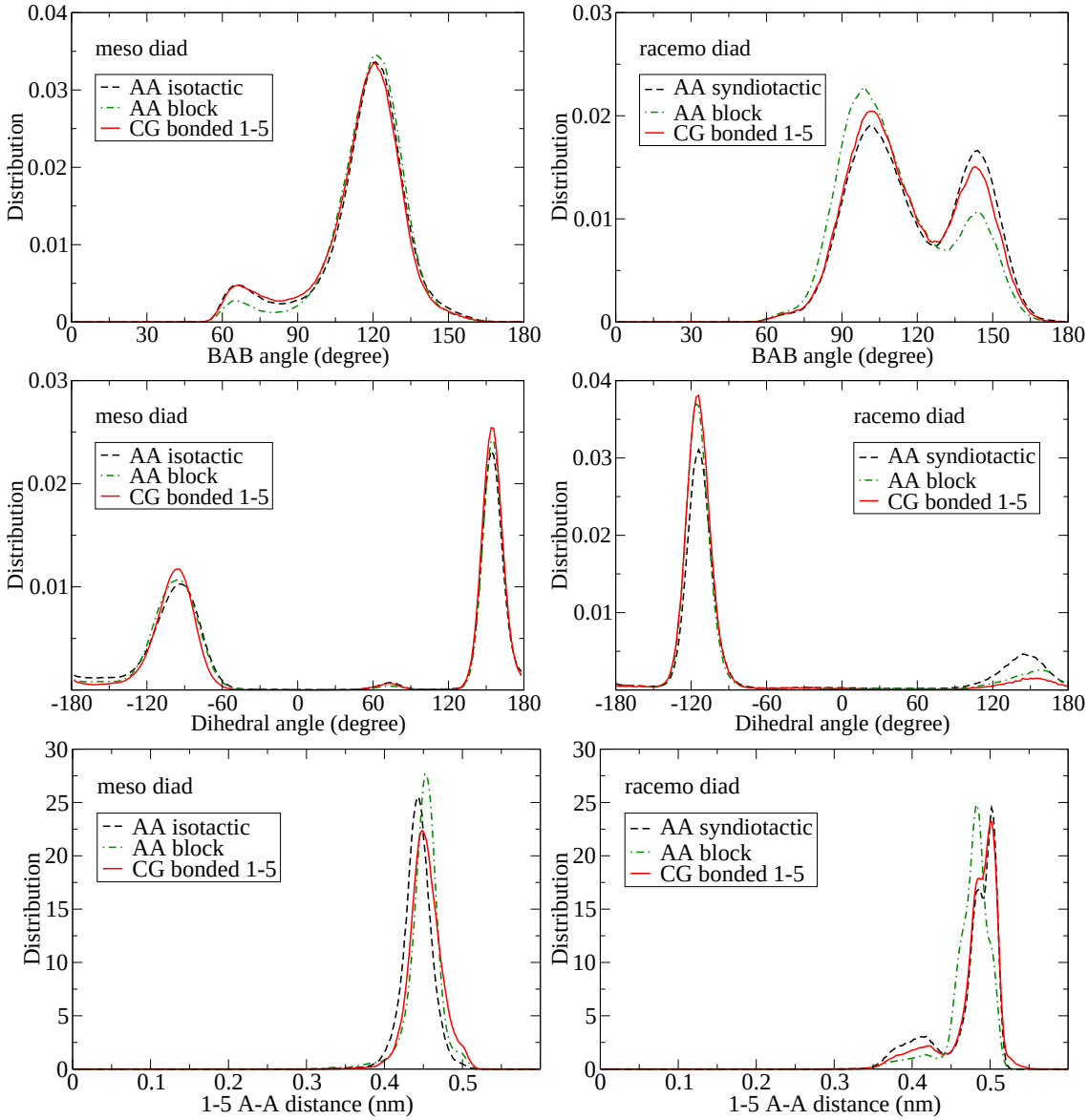

Figure 3.23: Distributions of BAB angles (top), ABAB dihedrals (middle) and A-A 1-5 distances (bottom) for meso (right) and racemo (left) diads: comparison between stereoregular all-atom single chains (dashed), all-atom chains with block tacticity (dash-dotted) and CG chains with block tacticity (continuous) with bonded interactions up to 1-5. It can be seen that the influence of neighboring diads (the difference between the two AA distributions for each degree of freedom) is negligible in comparison to the influence of the type of diad (the difference between left and right side in each row).

having only bonded potentials up to 1-4 and the two A-A 1-5 potentials. The distributions of B-B 1-5 distances with block tacticity are given in Figure 3.24.

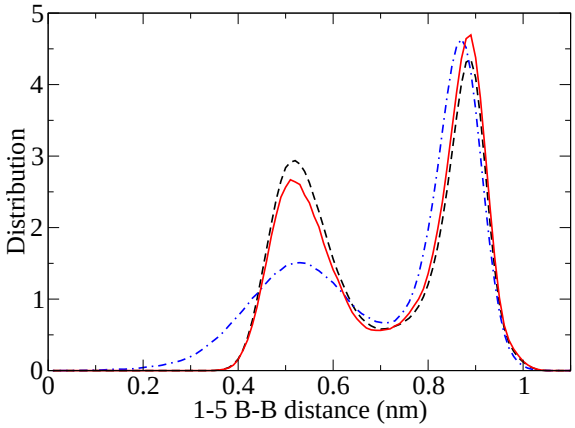

Figure 3.24: Distributions of B-B 1-5 distances in chains with block tacticity: The target distribution from an all-atom single chain (dashed), the correcting distribution from a CG chain with bonded interactions up to 1-4 and A-A 1-5 interactions from iso- and syndiotactic chains (dashed-dotted) and final CG distribution of a CG chain with the additional corrected 1-5 potential (continuous).

At this point we can simulate CG chains with block tacticity and compare their distributions to atomistic simulations. This comparison has already been shown in Figure 3.23 for BAB angles, dihedral angles and for A-A 1-5 distances. We see a good agreement between the CG and atomistic distributions. The CG distributions stay similar to the distributions in the stereoregular cases, on which they have been parameterized, but the deviations tend to the same directions as the distributions in atomistic block tacticity chains. This gives a hint that the careful treatment of local conformations and correlations in the development of the model has been successful and it confirms the assumption that it is possible to combine separately developed bonded potentials in the way described before.

The question of the maximum range for the bonded interactions also has to be answered for the block tacticity or, more general, for random atactic chains. In our final CG model we limit the range of bonded interactions in atactic chains to 1-5 neighbors (contrary to the stereoregular chains that have bonded interactions in a range up to 1-7 neighbors) and use the standard nonbonded interactions for 1-6 neighbors and beyond. This is reasonable, because the stiffness of the block chains (reflected by the internal distances) is already reproduced well with bonded 1-5 interactions. The other reason to not extend the range of bonded interactions is the rapidly increasing number of combinations of diads in atactic chains. 1-6 and 1-7 interactions include chain segments of two or three diads, where the diads appear in a random sequence, and therefore three or six different combinations of these interactions are possible. Bonded interactions would have to be developed for each combination and might be interdependent (as the 1-5 interactions in syndiotactic chains in section 3.4.4).

3.4.7 Correlations in coarse-grained chains

After finishing the development of bonded interaction potentials we have a look again at correlations between CG degrees of freedom, which we have investigated before for atomistic chains (in section 3.4.2). Now we can compare CG simulations and their correlations.

We simulated isolated, stereoregular chains of 25 monomers in vacuum with the all-atom model and the CG model (details can be found in the Appendix A.2.1). In these runs the nonbonded interactions were not excluded, as in the cases before, where the interaction range was varied. The CG runs also used all the bonded potentials up to 1-7, as presented before, and CG nonbonded interactions from 1-6 upwards, whose development will be presented in the following section. Even though the concept of not excluding any nonbonded interactions in a chain in vacuum does not result in chain dimensions comparable to chains in melts, the local conformations and correlations are not disturbed. This can be seen if the atomistic dihedral-dihedral plots in Figure 3.25 and 3.26 are compared to the ones in Figure 3.13 and 3.14. It is also a hint that the chain conformations are not changed strongly in melt simulations, because they are dominated by neighboring beads in a range up to 1-5.

The agreement between atomistic and CG chains is very good for both tacticities, especially for the combinations of two subsequent dihedral angles. In the isotactic case in Figure 3.25, for example, all dihedral-dihedral combinations sampled by the atomistic chain are reproduced by the CG chain, except for the region around $(160, 200)$ that deviates slightly. More important, however, the CG chain does *not* sample the region $(270, 90)$, indicating that the final CG model reproduces the local correlations between adjacent torsional degrees of freedom in polystyrene.

The syndiotactic case in Figure 3.26 shows that angle-dihedral combinations favor certain ranges in the atomistic chain of $(100, 250)$ and $(140, 150)$ that are less correlated in the CG chain, i.e. also the corresponding combinations of $(100, 150)$ and $(140, 250)$ appear. But also in this case the angle-dihedral combinations around $(90, 0)$ (and equally around $(90, 360)$, since the dihedral angle is periodic) are not sampled in CG and atomistic simulations. The correlations are pronounced for the syndiotactic dihedral-dihedral combinations, which are the more relevant ones for the overall chain structure. The comparison between AA and CG picture is not only confirming that local conformations and correlations are reproduced, but it also depicts a difference between the models concerning the dynamics of the two. In the AA picture it seems that combinations of $(120, 200)$ and $(200, 120)$ are only accessed via the neighboring combination $(225, 225)$ but not from $(120, 120)$. The latter combination is only reached, if one of the two dihedrals rotates by 360 degree (and the other by 80 degree). The CG model, in contrast, samples the same combinations but the direct transition from $(120, 200)$ or $(200, 120)$ to $(120, 120)$ is possible by rotating only one dihedral by 80 degree, without requiring the other move at all. This suggests that the CG model will show faster dynamics than the atomistic model due to lowered barriers in the energy landscape, which allow for shorter connecting paths between local minima.

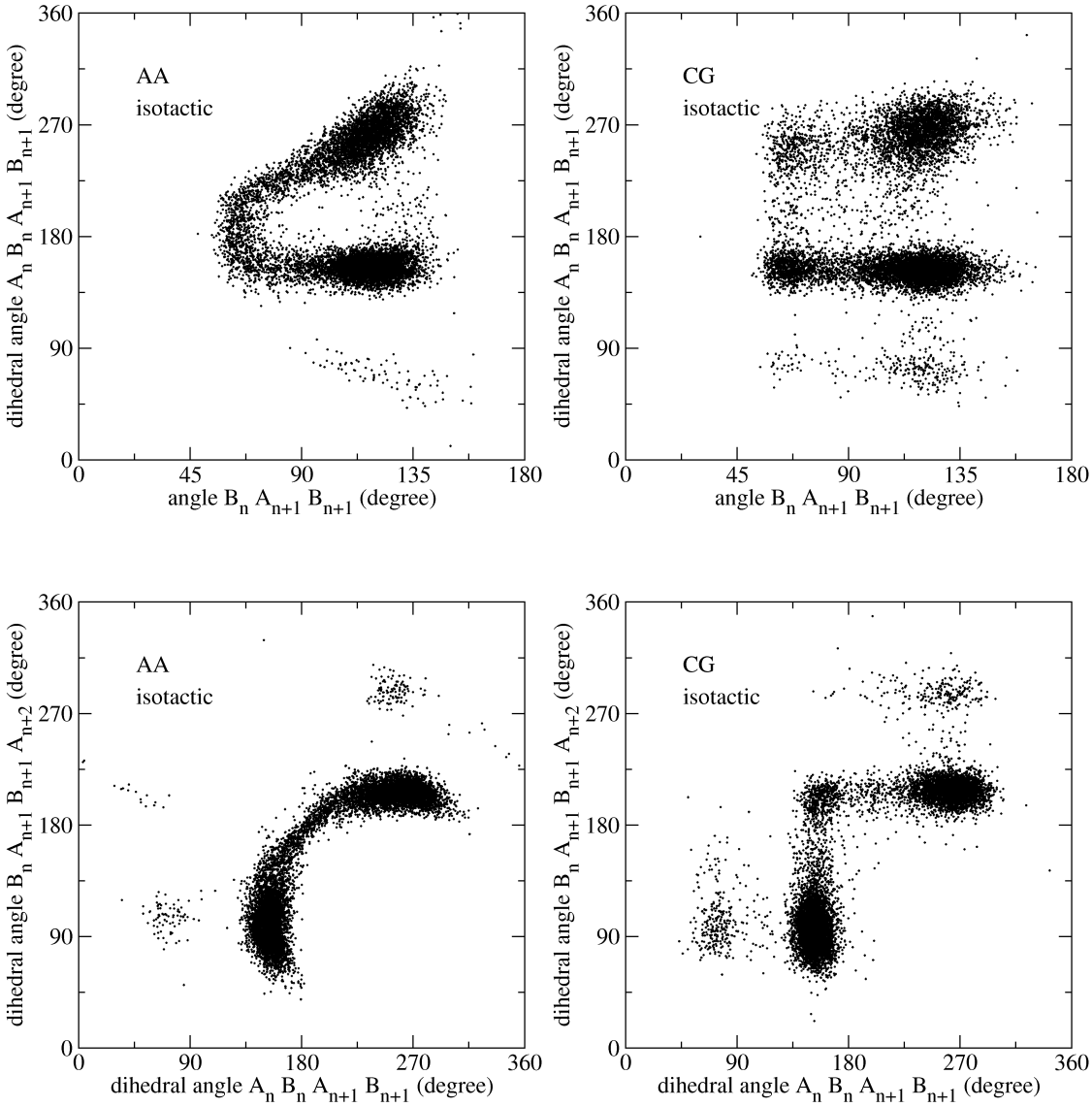

Figure 3.25: Combinations of CG angles and dihedrals (top) and of two subsequent CG dihedrals (bottom) in single isotactic chains: comparison between atomistic simulations with all interactions (left) and CG simulations with bonded potentials up to 1-7 A-A and non-bonded interactions (right). For better visibility the dihedral values in the range from -180 to 0 are shifted to the range from 180 to 360.

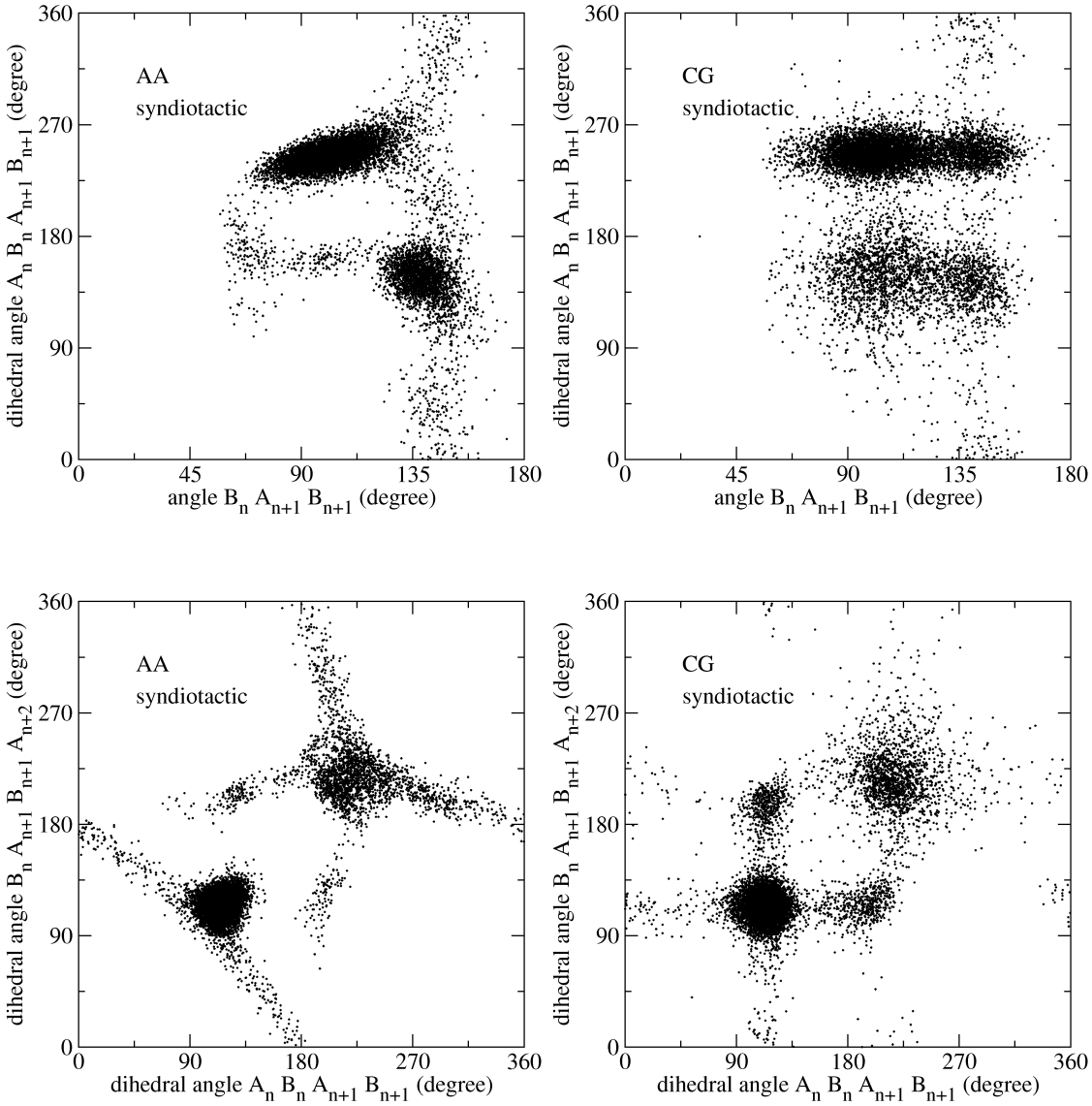

Figure 3.26: Combinations of CG angles and dihedrals (top) and of two subsequent CG dihedrals (bottom) in single syndiotactic chains: comparison between atomistic simulations with all interactions (left) and CG simulations with bonded potentials up to 1-7 and non-bonded interactions (right). For better visibility the dihedral values in the range from -180 to 0 are shifted to the range from 180 to 360.

3.5 Nonbonded interactions

One aim of the CG model presented in this work is its applicability in simulations under ambient pressure conditions. For this reason we develop nonbonded interactions including an attractive tail as opposed to the purely repulsive potentials that were used for a previous CG model of PS that used the same mapping scheme. [55] The approach we chose for the development is based on the sampling of pairs of short oligomers (compare section 2.1.3). It is different from most other structure-based CG methods, which use structures of equilibrated atomistic melts as target structures and fit the nonbonded potentials in order to reproduce these target structures.

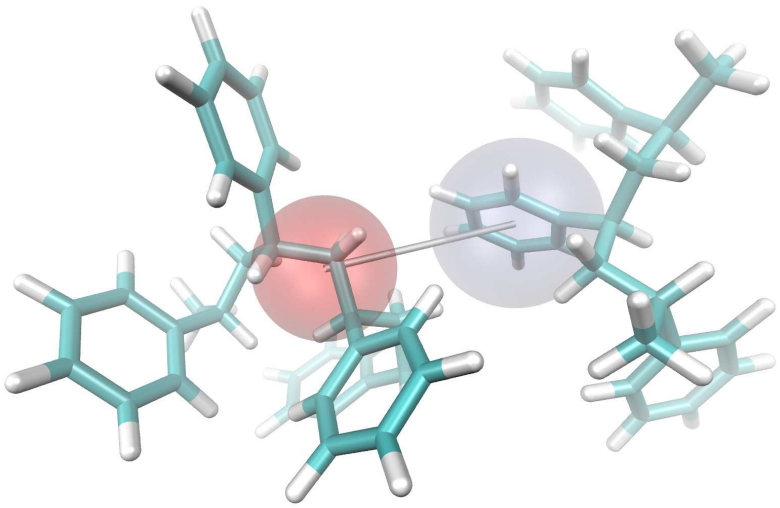

Figure 3.27: To develop nonbonded interaction potentials for the CG beads, pairs of oligomers are sampled in atomistic simulations with fixed distances between the two groups of atoms representing the CG beads of interest. In this picture the distance between an A bead (red) and a B bead (blue-gray) is fixed. Repeating these simulations at different distances and integrating the resulting constraint forces delivers a potential of mean force.

As in the case of the bonded potentials before we develop effective pair interactions between CG beads through a potential of mean force (PMF), which is the free energy along one degree of freedom. Unlike the PMF for the bonded potential, where a distribution for one degree of freedom is Boltzmann-inverted, the PMF for the nonbonded interaction is obtained from constraint dynamics runs with the all-atom model of two trimers (or fourmers) in vacuum, see Figure 3.27. In these runs the two groups of atoms, which represent the CG beads for which we calculate the PMF, are held at fixed distances r (not at fixed cartesian coordinates). The average constraint force f_c, required to satisfy the constraint, is the negative of the mean force. Repeating the constraint dynamics runs stepwise at different distances, allows integrating the constraint force to arrive at a PMF

(more accurately, it is the free energy difference between the integration limits):

$$V(r_2) - V(r_1) = \int_{r_1}^{r_2} \langle f_c \rangle_r dr \tag{3.2}$$

Using this method, two noninteracting masses experience an entropic force that pulls them apart, because larger volume elements in phase space are sampled at larger constraint lengths r. This entropic force is given by

$$-\frac{d}{dr}\left[-k_B T \log(4\pi r^2)\right] = \frac{2k_B T}{r} \tag{3.3}$$

where k_B is the Boltzmann constant and T the temperature. The PMF between the two beads is obtained by adding the entropic term to the constraint force and integrating backwards from infinity. In practice, simulations are limited to finite distances and the integration is performed backwards from the maximum distance r_m, adding an integration constant C. [78]

$$V_\mathrm{PMF}(r) = \int_{r_\mathrm{m}}^{r} \left[\langle f_c \rangle_s + \frac{2k_B T}{s}\right] ds + C \tag{3.4}$$

For two small molecules, where each molecule is represented by one single CG bead, this PMF would be already the effective interaction potential for the corresponding CG beads. We are using trimers or fourmers in the constraint dynamics runs, i.e. the molecules, whose conformations we are sampling, are larger than the groups of atoms, whose interactions we want to develop. The idea for this choice is the following: By using oligomers that represent several CG beads instead of small molecules that correspond to only one CG bead, we take into account the important effect that the CG beads are part of a chain and their relative orientations are strongly influenced by neighboring chain segments. This influence of the chain neighbors, which is a multibody effect, is incorporated in the development of the CG nonbonded interactions by sampling pairs of oligomers. In addition to the desired modification of the sampling of the two constrained groups of atoms, which represent the two CG beads for which the CG potential is developed, the PMF also includes contributions from interactions between all atoms in the two oligomers that enter into the constraint force. To get the effective interaction between two individual CG beads, this influence of the surroundings has to be taken out.

The PMF obtained by eq. 3.4 is denoted $V_\mathrm{PMF}^\mathrm{A\text{-}A}(r)$ (for the case we constrain the A-A distance). To obtain an effective A-A interaction potential $V_\mathrm{eff}^\mathrm{A\text{-}A}(r)$, we calculate a second PMF along the same coordinate r but exclude all direct A-A atomistic interactions[3] while maintaining all other interactions with and between neighboring parts of the oligomers. This PMF we denote $V_\mathrm{PMF}^\mathrm{excl,A\text{-}A}$. Then the effective, nonbonded bead-bead interaction potential is obtained from

$$V_\mathrm{eff}^\mathrm{A\text{-}A}(r) = V_\mathrm{PMF}^\mathrm{A\text{-}A}(r) - V_\mathrm{PMF}^\mathrm{excl,A\text{-}A}(r) \tag{3.5}$$

[3] Direct A-A interactions are all atomistic interactions between pairs of atoms, where one of the atoms is located in the central A group of oligomer 1 and the other in the central A group of oligomer 2.

The so-obtained potential $V_{\mathrm{eff}}^{\mathrm{A\text{-}A}}(r)$ may be viewed as the free energy of introducing intermolecular interactions between the two groups of atoms representing the A beads at distance r. Because bead A is part of an oligomer (trimer, fourmer), steric effects due to chain connectivity limit the set of relative orientations in which these beads can approach, which is realistically captured by V_{eff}. Although V_{eff} is a pair potential obtained from PMF calculations between PS fragments in vacuum, its use in simulations of the condensed melt state can be justified. Multibody contributions to the effective potential applicable in the melt are to a large extent similar to those present in vacuum and are determined by the relative orientations that chain segments can sample relative to each other.

The two beads, whose relative distance is fixed, are located in the middle of the oligomers. The size of the oligomers is chosen in such a way that these beads are located in a symmetrical configuration; A beads are located in fourmers and B beads in trimers, see Figure 3.28. In this work we used a maximum constraint distance r_{m} of 1.2 nm and performed constrained runs at distances r between 0.2 and 1.2 nm in steps of 0.02 nm. Details can be found in Appendix A.1.2.

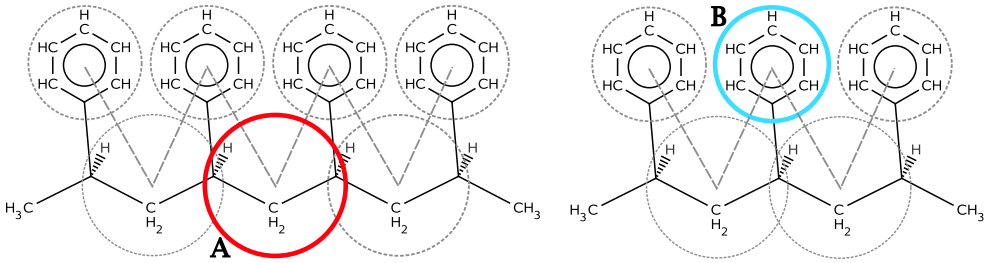

Figure 3.28: Molecules used in the sampling at constraint distances: fourmers (left) are used for A beads and trimers (right) are used for B beads, because they provide a symmetrical configuration for the respective beads. The distance constraint between two of these oligomers is applied between the centers of mass of the central groups of atoms (A-A, A-B or B-B).

Figure 3.29 shows the two potentials of mean force, $V_{\mathrm{PMF}}^{\mathrm{B\text{-}B}}$ and $V_{\mathrm{PMF}}^{\mathrm{excl,B\text{-}B}}$, and the resulting effective potential $V_{\mathrm{eff}}^{\mathrm{B\text{-}B}}$ for the interaction between two B beads (phenyl rings). As a technical note we point out that the PMFs with the exclusions of direct interactions, e.g. $V_{\mathrm{PMF}}^{\mathrm{excl,A\text{-}A}}(r)$, were obtained by using the simulation trajectories of the runs without these exclusions (used to determine e.g. $V_{\mathrm{PMF}}^{\mathrm{A\text{-}A}}$) and recalculating the forces for the given conformations but excluding the direct interactions between the two beads at fixed distances. Thus, strictly speaking, $V_{\mathrm{PMF}}^{\mathrm{excl,A\text{-}A}}$ is not a PMF since the sampling was not done with the Hamiltonian for which the forces were evaluated. However, in our tests the difference to a PMF with a repeated sampling was within the error bars for distances beyond the first minimum of the potential. The advantage of reusing the trajectory is a saving of half of the CPU time.

In principle the above procedure can be iterated to reproduce the all-atom A-A, A-B and B-B PMFs of trimers (or fourmers) in vacuum with the effective A-A, A-B and B-B potentials. Such an approach has been used before by McCoy and Curro [64] to derive united-atom models for small molecules and resembles the IBI approach (see sec-

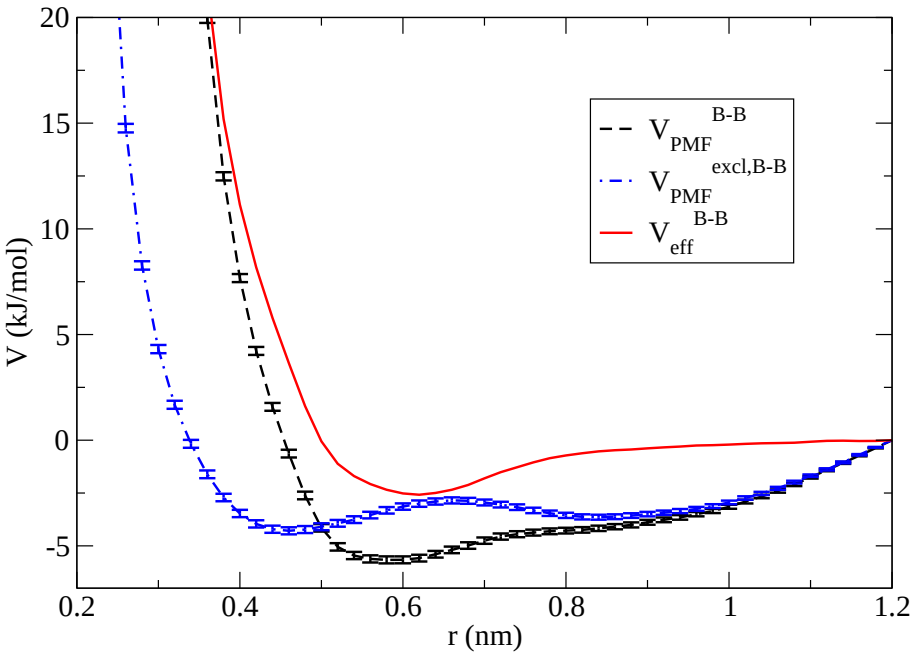

Figure 3.29: Coarse-grained B-B nonbonded interaction: The two potentials of mean force for runs with all interactions $V_{\mathrm{PMF}}^{\mathrm{B\text{-}B}}(r)$ (dashed) and for reruns with exclusions between all atoms of the central B beads $V_{\mathrm{PMF}}^{\mathrm{excl,B\text{-}B}}(r)$ (dashed-dotted) as well as the effective potential $V_{\mathrm{eff}}^{\mathrm{B\text{-}B}}(r)$, obtained by taking the difference (eq. 3.5) of the two potentials of mean force (continuous). The error estimates of the constraint forces that are integrated are obtained from block averaging. [79] ($k_{\mathrm{B}}T = 4.2\,\mathrm{kJ/mol}$ at 503 K)

tion 2.1.3), which is often used in the melt, in the sense that it employs iteratively refined CG potentials. A similar approach has been used to develop CG nonbonded interactions for polyethylene by Fukunaga et al. (see section 2.1.3). [65] A potential, obtained following their method, is shown in Figure 3.30 and compared to our effective potential from the sampling of two trimers and to a PMF between two benzene molecules. Their method uses a PMF between two isolated beads, which is a PMF between two benzene molecules in the case considered here (adding one hydrogen atom to the isolated B bead gives a benzene molecule). As expected, the benzene PMF coincides with our effective potential for longer distances (above 0.7 nm) and deviates for short distances, where the relative orientations of the two beads are influenced by the chain neighbors and different orientations are sampled. In order to take into account the constraints imposed by the chain neighbors, the method of Fukunaga et al. adds the Boltzmann-inverse of the radial distribution function (RDF) to the benzene-benzene PMF for short distances (shorter than the first peak in the RDF). This leads to a larger repulsive radius of their CG potential compared to the benzene-benzene PMF. Our effective potential deviates in the same direction and its repulsion radius is between the two.

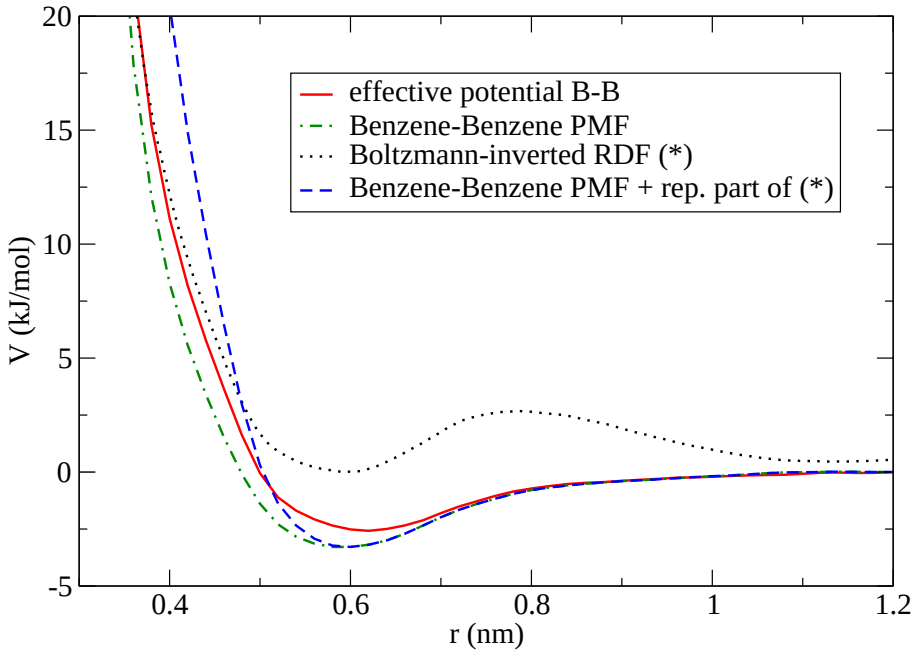

Figure 3.30: Coarse-grained B-B nonbonded interaction: The effective potential $V_{\text{eff}}^{\text{B-B}}(r)$ used in this work (continuous) is compared to a PMF between two benzene molecules (dashed-dotted) and to a potential developed with the method of Fukunaga et al. (dashed) that modifies the benzene PMF by adding the repulsive part of the Boltzmann-inverted radial distribution function (dotted).

We note that the effective potential may change, if instead of the distance between the exact mapping points, the distance between the centers of mass of the two beads (neglecting that the CH-groups are only weighted with half of their mass) is used as

distance coordinate. For our model this is of course only an issue if the center of mass of the A bead is used, calculated with the full masses of the two CH-groups instead of their half masses. Test calculations showed that this difference is indeed significant, leading to very different effective A-A and A-B nonbonded interaction potentials.

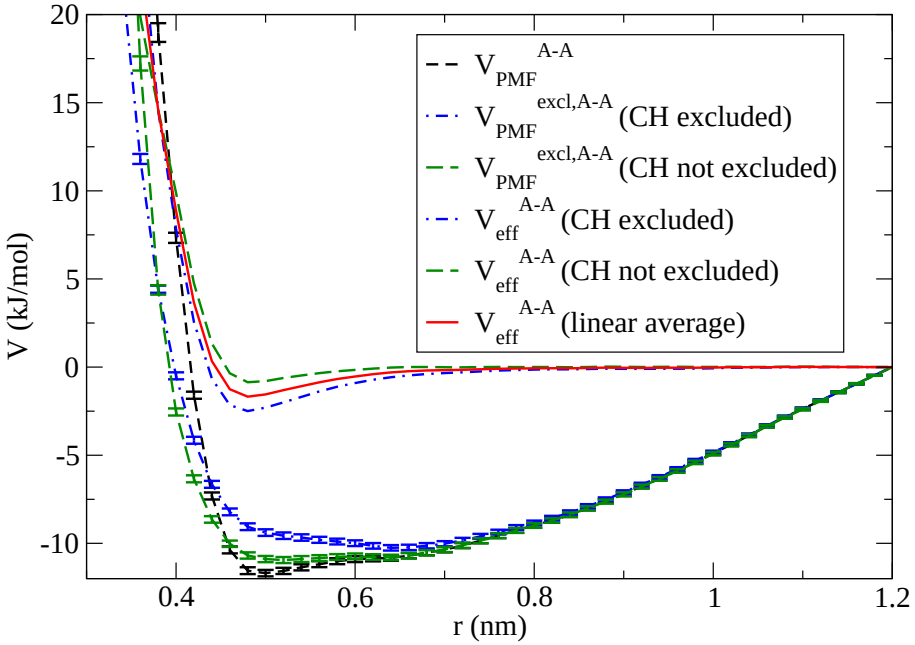

Figure 3.31: Coarse-grained A-A nonbonded interaction: The potentials of mean force for runs with all interactions (dashed) and for reruns with exclusions for the two cases of excluding all atoms in the A bead (dashed) or excluding only the CH_2-groups (dashed-dotted). The two resulting effective potentials are shown as well as their linear average, which is the A-A potential used in the final CG model.

Another important question is which all-atom interactions need to be excluded in the calculation of $V_{\mathrm{PMF}}^{\mathrm{excl,A\text{-}A}}$ and $V_{\mathrm{PMF}}^{\mathrm{excl,A\text{-}B}}$. Because each of the two CH-groups in a bead of type A is shared with another A bead, we have two choices (see mapping scheme in Figure 3.5). We can exclude the all-atom interactions involving only the CH_2 group, or exclude the all-atom interactions involving the CH_2 and the CH groups. If we consider the A-A CG interaction, the first choice leads to an effective potential in which the contributions of the CH groups are not accounted for, the second choice leads to an effective A-A potential in which the contributions of the CH groups are counted twice. We calculated the effective potentials with both choices for treating the CH groups and took their linear average as the effective potential in further simulations, see Figure 3.31. In our simulations of CG PS melts we get the best agreement with detailed atomistic structures of the melt (A-A, A-B and B-B radial distribution functions), if we take the linear average of the two effective potentials.

The potentials obtained by this method combine a short range repulsive and a longer ranged attractive part and are used for CG simulations of polystyrene melts, which are

presented in the next chapter 4. The B-B nonbonded potential was obtained from PMF calculations of two trimers in which the coordinate *r* was chosen between the central B beads. The A-A nonbonded potential was calculated from PMF calculations of two fourmers in which the coordinate *r* was chosen between the central A beads. To determine the A-A nonbonded interaction potential, trimers are too small and exhibit a non-symmetric environment around the central A bead (see Figure 3.28). The A-B nonbonded potential was obtained based on PMF calculations with a fourmer (A bead) and a trimer (B bead). In all calculations the stereoregular sequence was isotactic. The potentials were also calculated with syndiotactic sequences, which yielded nonbonded potentials that were identical within the error bars. In Figure 3.32 the effective potentials are plotted for the three interaction pairs A-A, A-B and B-B in isotactic oligomers. The short range repulsion for the B-B interaction is "softer" than for the A-A interaction, because the level of coarse-graining of the B bead (11 atoms) is larger than the one of the A bead (5 atoms).

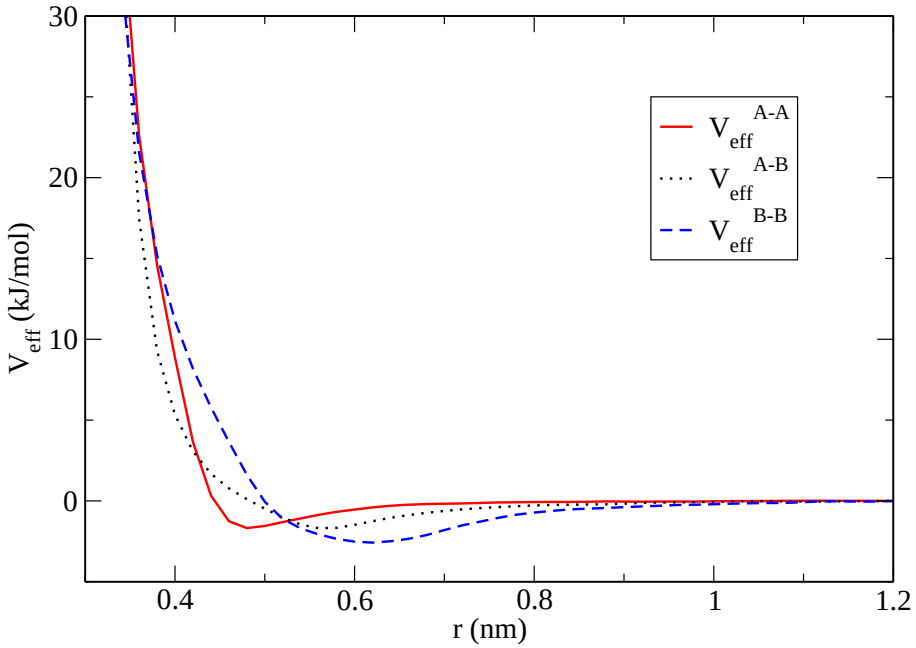

Figure 3.32: Comparison of the nonbonded potentials used in this work, $V_{\text{eff}}^{\text{A-A}}(r)$ (continuous), $V_{\text{eff}}^{\text{A-B}}(r)$ (dotted) and $V_{\text{eff}}^{\text{B-B}}(r)$ (dashed). ($k_{\text{B}}T = 4.2\,\text{kJ/mol}$ at $503\,\text{K}$)

4 Melt simulations

The previously developed CG model (chapter 3) is validated by simulating polymer melts and comparing them to atomistic melt simulations. [74] The CG model is parameterized only on *static* properties of atomistic chains, which can be compared directly. The dynamics of CG and AA simulations are different. Their relationship is investigated in the following chapter 5.

In this chapter static properties of CG and AA polymer melts are compared for melts of short chains, which are still feasible to be simulated at atomistic resolution. The first comparison is aimed at intrachain conformations. At the most local level these are the distributions for the CG degrees of freedom, at the level viewing the whole chain these are internal distances. The internal distances are also investigated for CG melts of long chains and compared to experimental data on chain dimensions. Besides the conformations of single chains the collective packing of chains in a melt is an important static property. It is typically expressed by pair- or radial distribution functions (RDF). Further assessment of the quality of the CG model can be obtained by checking densities or pressure in atomistic and CG systems. These points are discussed in the following.

Polymer melts of different tacticities of 10-mers (56 chains) have been simulated at ambient pressure (1 atm) and a temperature of 503 K, which is also the temperature at which the CG model was developed. The MD simulations were performed using an atomistic model (for details see Appendix A.1.3) and the CG model that was presented in the previous chapter (for details see Appendix A.2.2). The CG model for the atactic melt uses bonded interactions for 1-5 neighbors, the models for the stereoregular use bonded interactions in a range up to 1-7 neighbors (in isotactic chains up to 1-7 A-A; in syndiotactic chains up to 1-7 A-A and 1-7 B-B). In all CG systems nonbonded interactions are employed for neighbors in the range of 1-6 and beyond, as well as for interchain interactions.

4.1 Conformations in melts

4.1.1 Local distributions

Distributions of coarse-grained degrees of freedom in isolated atomistic chains have been used to develop the CG bonded potentials and have been shown to reproduce these distributions very well in CG simulations of isolated chains. If we check these distributions in melt simulations, we can distinguish two questions: Are the distributions in atomistic simulations different, if a chain is not surrounded by vacuum anymore, but by other chains?

And, secondly, in case there are changes, does the CG model display the same behavior in melt simulations?

The first question can be answered, if we compare the distributions in Figure 4.1 for melts and isolated chains (the distributions for isolated chains in vacuum are repeated here, they have been shown before in Figure 3.23). The distributions for angles, dihedrals and 1-5 A-A distances in the atomistic systems are hardly dependent on the surroundings, i.e. the distributions are almost the same in atomistic melts and in isolated chains (where they are furthermore independent from the types of neighboring diads).The 1-5 B-B distances in Figure 4.2 are the only cases, in which the distributions in atomistic melts deviate slightly from the distributions in isolated chains, but the deviations are still small compared to the differences between the different tacticities.

In CG melts the influence of the surroundings is small and the distributions in CG melts stay close to the distributions in single chains. Since this influence is also small in atomistic simulations and the CG model reproduces the distributions in isolated chains correctly, the agreement between CG and atomistic melts is very good. Slight deviations between the CG and atomistic distributions only appear for the degrees of freedom that connect B beads, i.e. for angles and 1-5 distances that act on three or five subsequent CG beads, where the end beads of these groups are B beads. In these cases the relative height of the peaks can deviate moderately, while their general shape is still obtained correctly, e.g. for the BAB angles (Figure 4.1, top) and for the 1-5 B-B distances that consist of two diads of the same type (Figure 4.2, top). A possible explanation why the B beads are slightly more influenced by surrounding chains in the melt, is the position of the B beads (representing the phenyl rings), which stick out from the chain to the side (even though they are not treated as side groups in the CG mapping), where they are more exposed to interchain influences of neighboring beads than the A beads, which are located closer to the backbone of the polymer.

The disturbing influence of the slight deviations, mentioned before, on overall chain dimensions is decreased further for two reasons. As discussed before, the 1-5 B-B distance connects two B beads, which are located in two neighboring diads. Therefore, three different combinations of diads can appear: two meso diads, two racemo diads and the combined case of one meso and one racemo diad. In an atactic melt, where diads are randomly distributed, half of all 1-5 B-B distances include one meso and one racemo diad, the other half contains two diads of the same type. The 1-5 B-B distance distribution for the most common, mixed case (see Figure 4.2, middle left, which contains also the distributions in isolated chains shown before in Figure 3.24) is exactly reproduced in CG simulations. The second reason is the very good reproduction of the dihedral distributions and the 1-5 A-A distances. These distributions govern the positions of the A beads, which are mapped onto the backbone of the polymer. The B beads can move more freely around the backbone and therefore, the slight deviations of their distributions hardly disturb the A beads that are mainly responsible for the dimensions of the polymer chain. The dihedral distributions offer an additional advantage that reduces the effect of even small deviations: Because the dihedrals along the chain have two possible orientations that are oriented against each other (see Appendix A.3.2) their deviations tend to cancel.

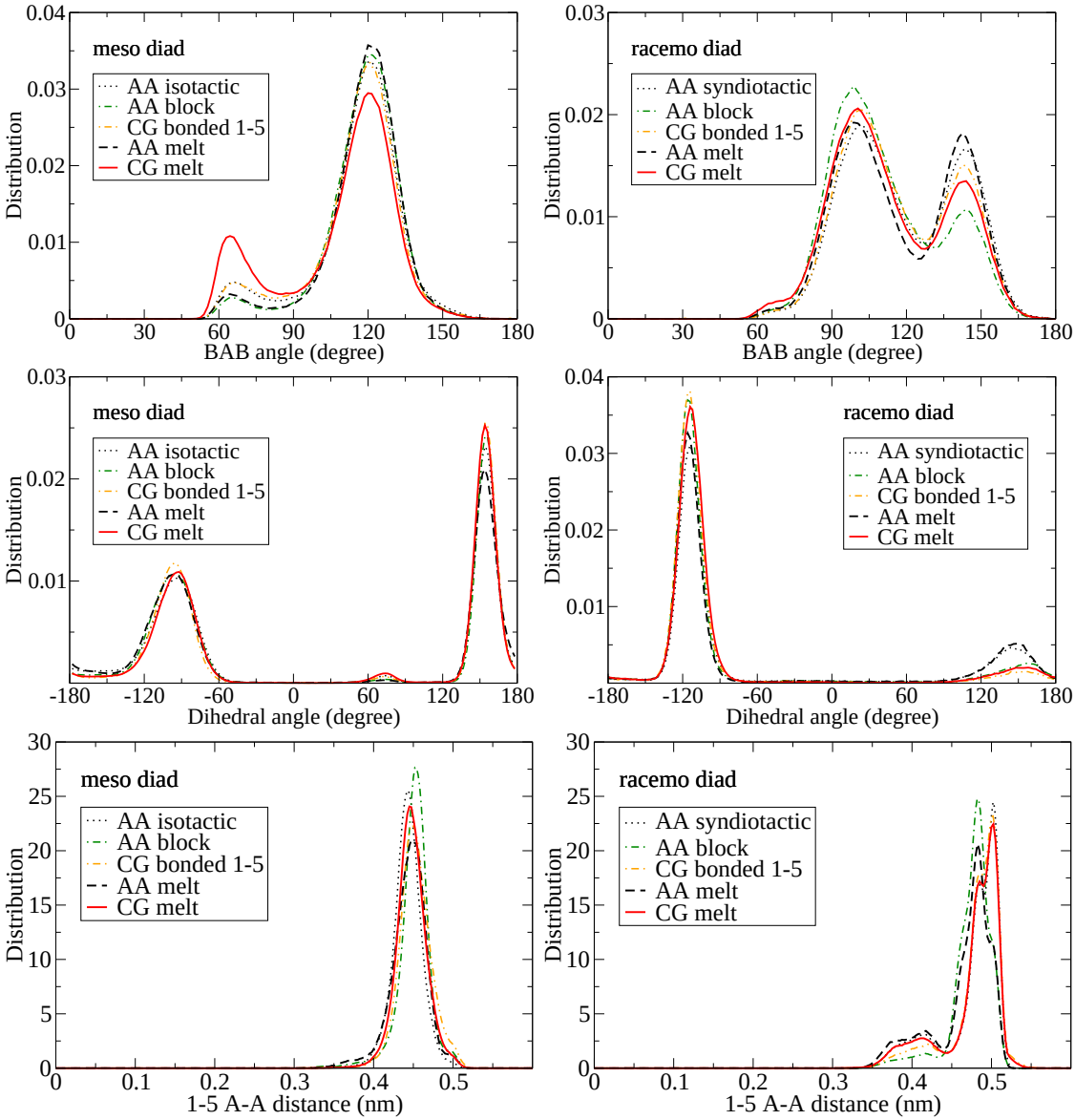

Figure 4.1: Distributions of BAB angles (top), ABAB dihedrals (middle) and A-A 1-5 distances (bottom) for meso (left) and racemo (right) diads: comparison between atactic melts of 10-mers in all-atom (dashed) and CG simulations (continuous), and corresponding distributions in isolated chains simulated in vacuum; these distributions are obtained by all-atom simulations of chains of stereoregular (dotted) or block (dashed-dotted) tacticity in vacuum or by CG simulations of stereoregular chains (dashed-double-dotted). A-B 1-2 bonds and ABA angles are not shown here, but their agreement is very good as well.

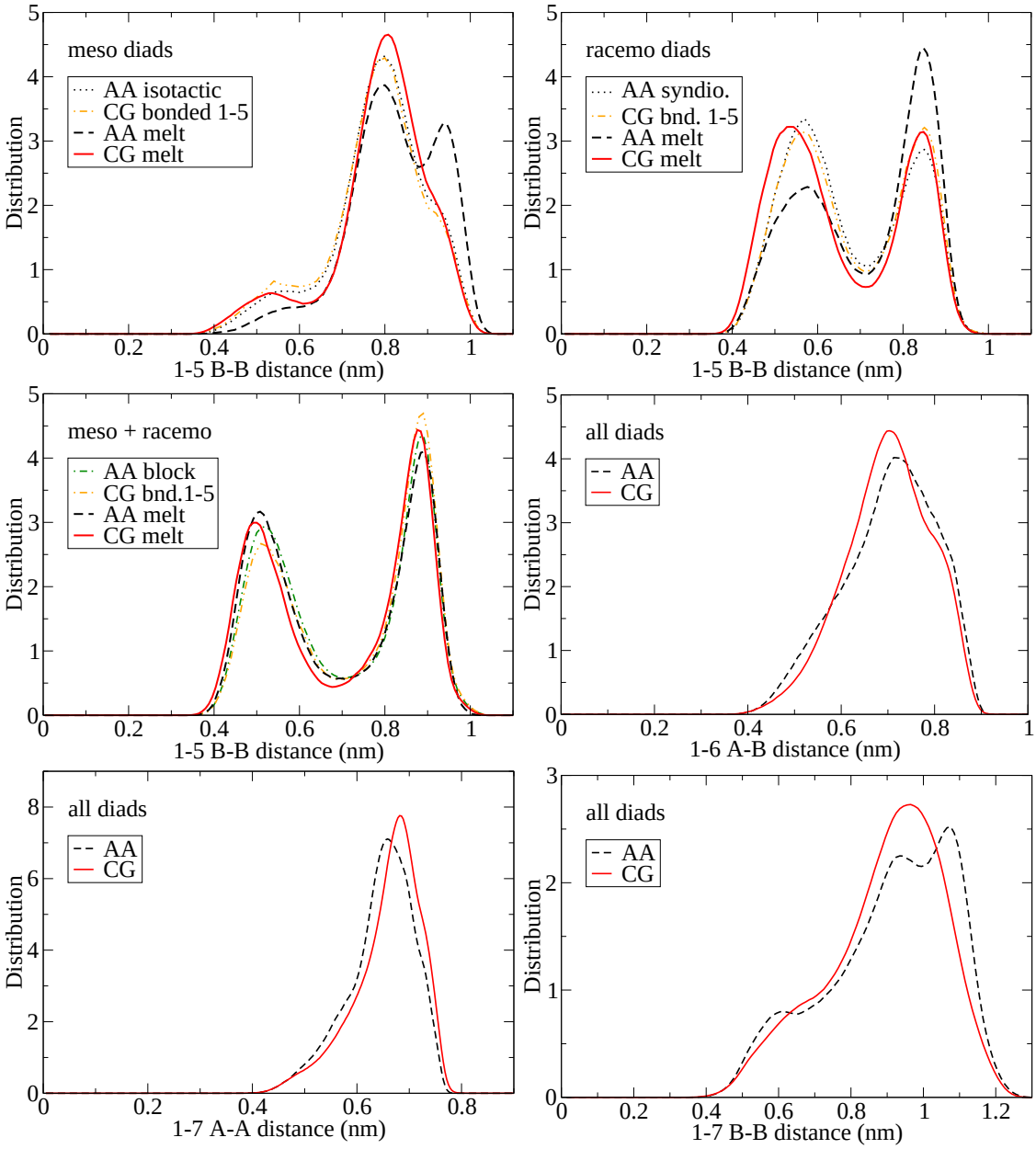

Figure 4.2: Distributions of B-B 1-5 distances (top panel and middle left; since two diads are involved in this pair, three different combinations can occur), A-B 1-6 distances (middle right), A-A 1-7 distances (bottom left; different combinations of diads are all included here) and B-B 1-7 distances (bottom right; also all combinations of diads): comparison between atactic all-atom melts of 10-mers (dashed) and atactic CG melt simulations (continuous) with bonded interactions up to 1-5.

The very good agreement between the distributions obtained from CG and atomistic melt simulations confirms that the development of CG potentials by sampling isolated chains in vacuum and the distinction between tacticities is a successful approach for the CG simulation of atactic and stereoregular melts. The correct reproduction of local distributions in the CG model leads to a consistency between the atomistic and the CG model for the overall chain dimensions and for the chain stiffness. These aspects are discussed in the following section.

4.1.2 Internal distances

To compare overall chain conformations in CG and atomistic melts we look at the internal distances within the chains. They are described by the characteristic ratio $C_n = \langle R^2(n)\rangle/(nl^2)$, where $\langle R^2(n)\rangle$ is the mean square distance between two repeat units, separated by n carbon-carbon bonds (two per monomer) of length l along the backbone. For CG systems we use the atomistic bond length $l = 0.153$ nm and have as well two CG bonds per repeat unit, therefore we can compare the internal distances for atomistic and CG systems directly and with experimental values for C_∞, which is the limit of the characteristic ratio for large n. For atomistic systems we apply the mapping scheme and evaluate the internal distances between the mapping points. By evaluating internal distances between CG beads (i.e. mapping points) instead of distances between whole monomers, we see more structure in the internal distances for small values of n, which reflect the local conformations for different tacticities. The internal distances for larger n, however, do not depend on the choice of evaluating them between CG beads or monomers.

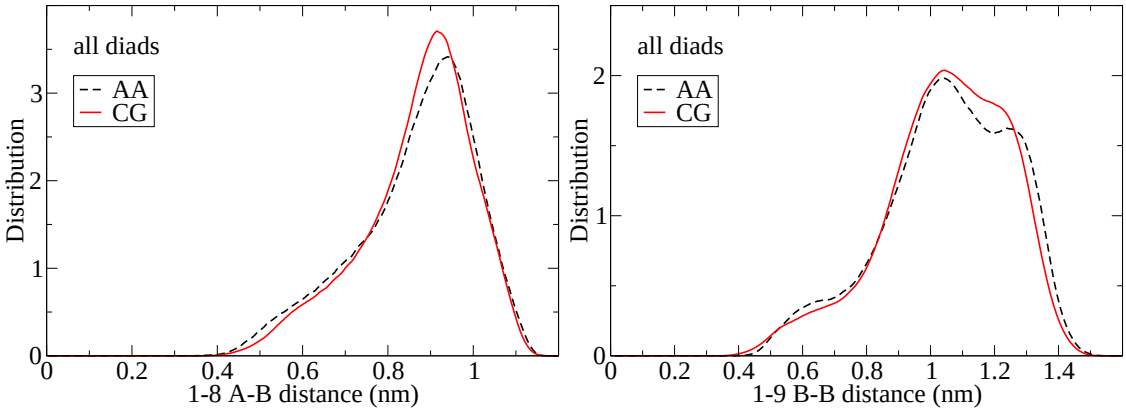

Figure 4.3: Distributions of A-B 1-8 distances (left) and B-B 1-9 distances (right; different combinations of diads are not distinguished): comparison between atactic all-atom melts of 10-mers (dashed) and CG melt simulations (continuous) with bonded interactions up to 1-5.

The internal distances are related to the distributions that were previously discussed. Contrary to the distributions, the internal distances give just an *average* value for pairs of beads separated by a certain nuber of bonds, but they allow a quick evaluation of these distances over the whole range of the polymer chain. If local distributions are reproduced

correctly in CG simulations, then the corresponding internal distance is reproduced correctly as well. Therefore, if the agreement in local distributions has been found to be good (as it is the case for the CG model presented here), then the internal distances provide sufficient information about chain conformations beyond the local range of a few neighboring beads. The agreement in the distributions between 1-6 and 1-9 is very good (see Figures 4.2 and 4.3). This is reflected in Figure 4.4 for the C_n in the corresponding range of n between 5 and 8, as well.

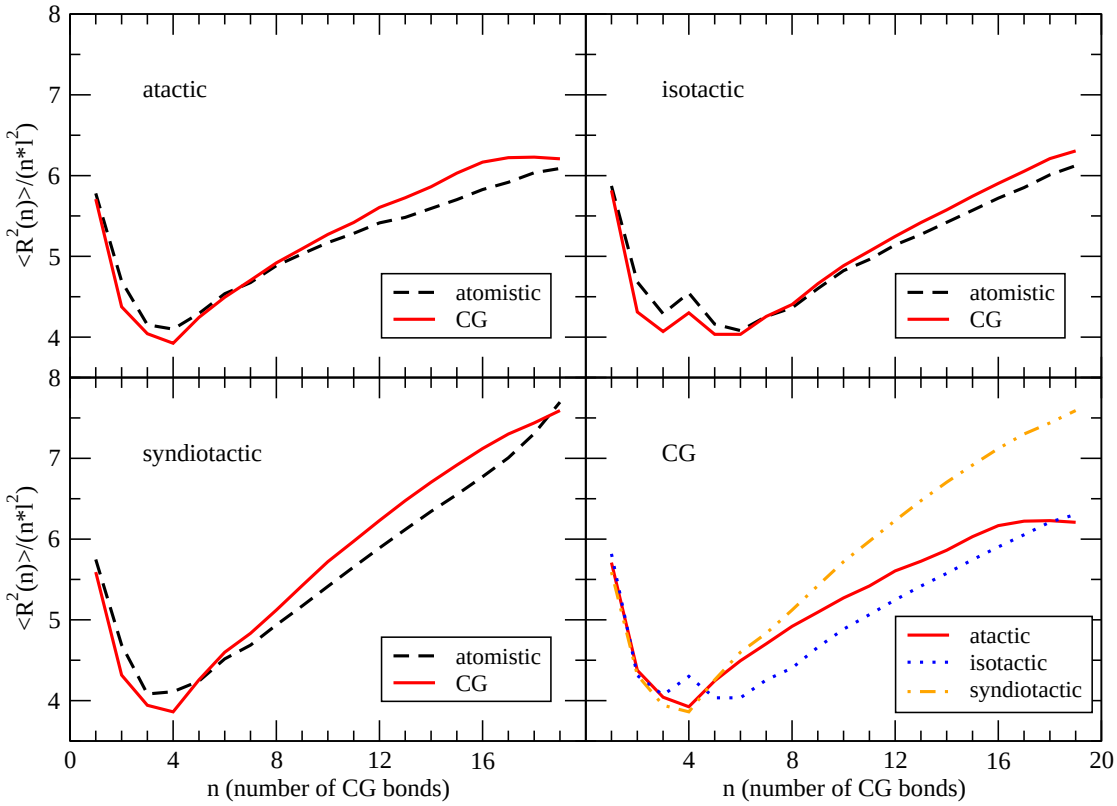

Figure 4.4: Simulations of 10-mer melts: Internal distances for atactic (top left), isotactic (top right) and syndiotactic (bottom left) PS melts comparing CG (continuous) and all-atom simulations (dashed) and comparison between the CG systems with different tacticities (bottom right). Plotted are the averages of the squared distances between beads, separated by n bonds, divided by the number of CG bonds and the squared bond length l^2. Since the number of CG bonds is equal to the number of carbon-carbon bonds in the backbone of the atomistic model, the CG distances are also normalized with the atomistic carbon-carbon bond length l of 0.153 nm and the CG and the atomistic model can be compared directly.

In Figure 4.4 the internal distances in atactic, iso- and syndiotactic melts of 10-mers are shown. Each melt consists of 56 chains with a length of 10 monomers simulated at 503 K.We see that the CG model reproduces the internal distances for the melts of different tacticities. The agreement already in the short internal distances indicates that the local conformations in the CG systems are correct. The increase of the distances along

the chain, especially the differences for different tacticities, suggests that the stiffness of the atactic, iso- and syndiotactic chains is modeled properly. This is important for melts of longer chains, where the characteristic ratio reaches a limit of C_∞, which can be compared to experimental results. This is done in the following.

Figure 4.5 shows internal distances of CG melts of chains of 192 monomers. The influence of the different tacticities can be seen clearly. The internal distances of these long chains agree well with the internal distances of the 10-mer melts presented above (which cover a range up to $n = 19$). They reach a plateau for about half the number of monomers in the chain already, i.e. if two CG bonds are separated by this number of bonds along the chain, the vectors indicating their direction are uncorrelated. If two bonds are connected by a smaller number of bonds along the chain, they are correlated. We can compare the plateau value of the internal distances with experimental results for the characteristic ratio C_∞. We get 7.8 for C_∞ of atactic PS, 8.9 for isotactic PS and 12.3 for syndiotactic PS. Experimental values are around 9.1 ± 0.4 for atactic PS [80], 9.3 for isotactic PS [81] and 14.4 ± 2.8 for syndiotactic PS. [82][1]

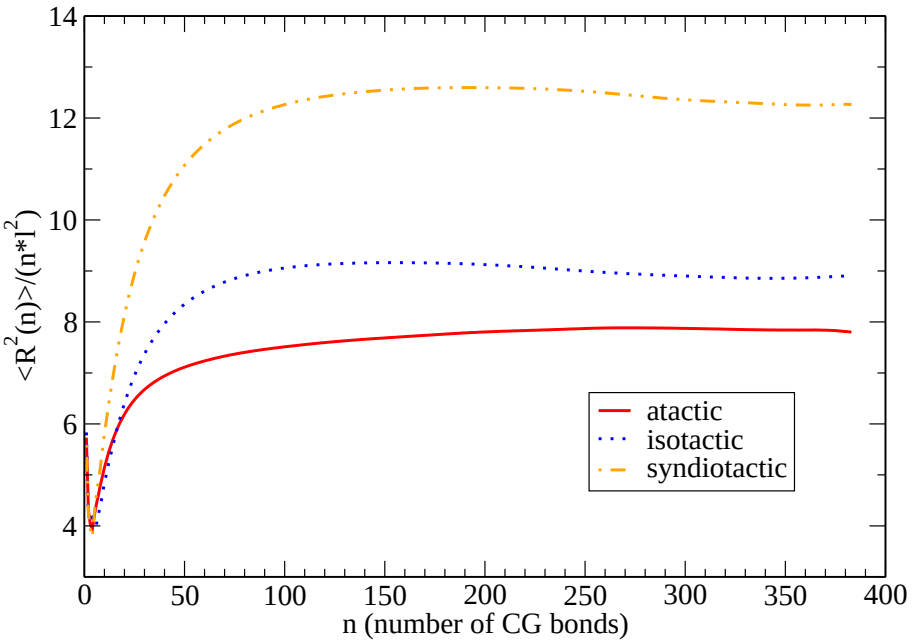

Figure 4.5: Internal distances for CG melts of chains of 192 monomers (20 kDa) with different tacticities: atactic (continuous), isotactic (dotted) and syndiotactic (dash-dotted).

The agreement for C_∞ between CG simulations and experimental values indicates two points: The atomistic model is capable to describe the stiffness of chains in melts correctly *and* the CG model reproduces the stiffness of the underlying atomistic model and

[1] Ref. 82 gives an experimental value of 10.6 for the C_∞ of syndiotactic PS. This value, however, is calculated with a monomer length l_m of 2.52 Å. Taking into account carbon-carbon bonds along the backbone (two per monomer) and their bond length l of 1.53 Å gives a value of 14.4 ± 2.8 for the C_∞. This way of defining C_∞ is used in this work as well as in ref. 83.

is efficient enough to simulate polymer systems, whose chain lengths are big enough to reach the plateau for the internal distances.

The simulated C_∞ for syndiotactic PS is higher than the value of 9 reported by Milano and Müller-Plathe in ref. 7. Their model is developed from stereoregular sequences in an atactic polymer, which might explain the difference in the syndiotactic case, whereas their atactic value of 8 is in agreement with our model. The relative differences between the characteristic ratios of the different tacticities agree also with the rotational isomeric state (RIS) model, which predicts values of 9 for atactic PS, 12 for isotactic PS and 18 for syndiotactic PS. [83] Even though our simulations, as well as experiments, show lower values for C_∞ than the RIS model for the stereoregular cases, we also observe that the atactic C_∞ is lower than the stereoregular cases and we find almost the same ratio between the C_∞ for isotactic and syndiotactic PS.

The previously discussed dimensions of chains in polymer melts can be finally compared to the dimensions of isolated chains in vacuum, especially to the case of isotactic chains. For these isolated chains the internal distances have been used as a criterion for the chain stiffness (see section 3.4.5), based on which the range of bonded interactions in the CG model has been chosen. As expected, the chains in the melt are more extended: in isotactic CG melts the characteristic ratio $C_{19} = 6.3$ (in both, the 10-mer and the 192-mer melt) is larger than in isolated chains with $C_{19} = 5.6$. The reason for this is that nonbonded interactions in vacuum lead to chain conformations, which are more coiled than in melts, where long-ranged nonbonded intrachain interactions are screened by the other chains.

4.2 Packing and density in melts

The local packing of the chains is examined by calculating radial distribution functions (RDF), which describe how the particle density varies as a function of the distance from one particular particle. In Figure 4.6 RDFs between A-A, A-B and B-B pairs for an atactic and an isotactic 10-mer melt at 503 K are shown. In these RDFs only intermolecular pairs of beads were included; pairs of beads in the same chain are left out, since the intrachain distributions are already reflected by the internal distances discussed before. We see a very good agreement between all-atomistic and CG RDFs for distances below 0.5 nm. For larger distances the agreement is still good with some deviations. The strongest deviation appears for the B-B RDF, where the position and height of the first peak and the following minimum differ from the atomistic RDF. The reason for this might be the representation of the atomistic phenyl group by a spherical CG bead. This has been also observed by Harmandaris et al. with their previous CG PS model. [55] The RDFs for isotactic and syndiotactic melts show a very good agreement as well. It can be noted that the CG simulations reproduce the small differences in the RDFs that atomistic simulations exhibit for different tacticities.

The density of the atomistic melt of atactic 10-mers (959 kg/m^{-3} at 503 K) is significantly above the reported experimental density of 895 kg/m^{-3} for short polystyrene chains ($M_w = 910$, $M_w/M_n = 1.16$). [84] There are two differences between the simulated sys-

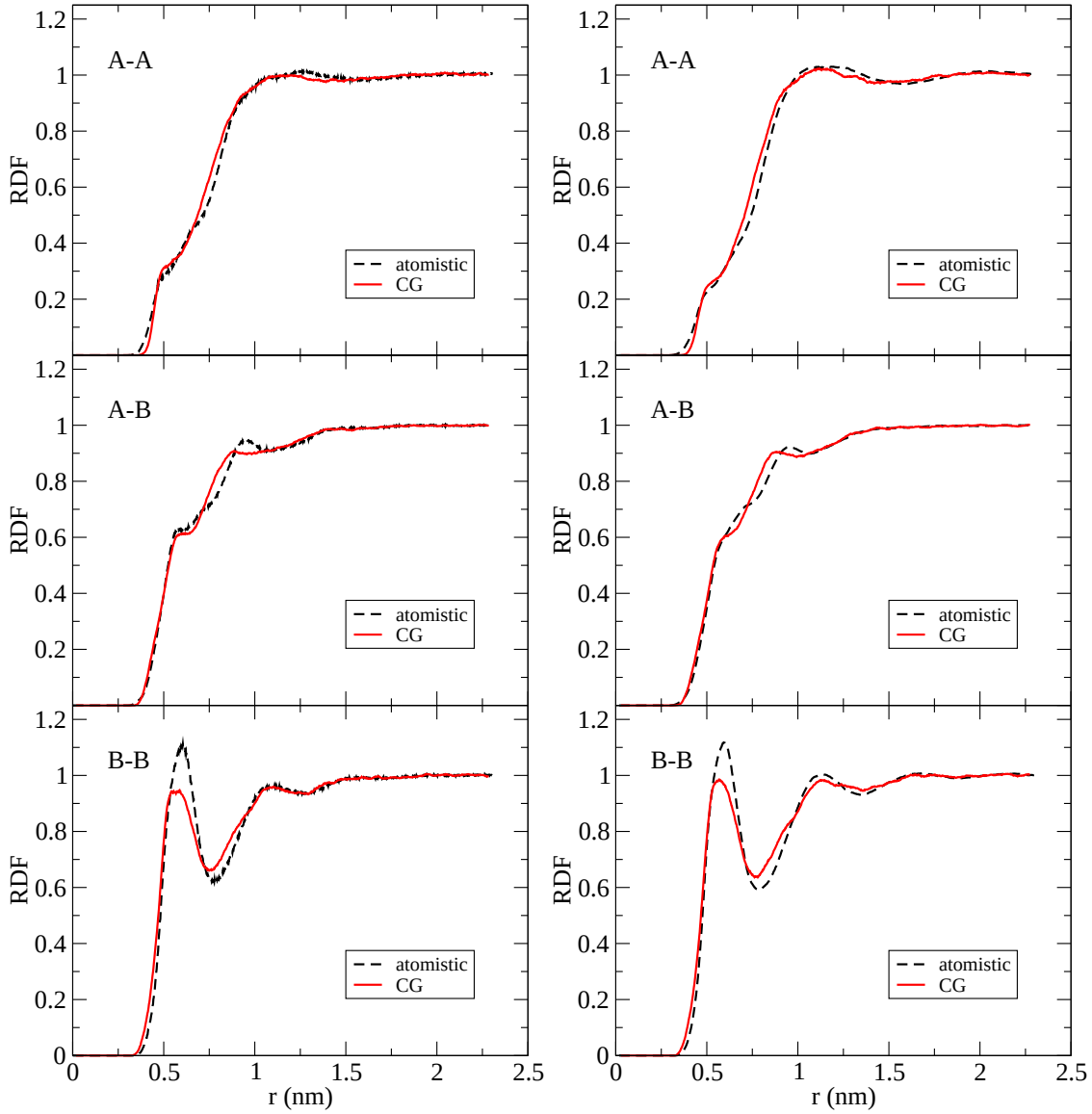

Figure 4.6: Radial distribution functions in atactic (left) and isotactic (right) melts in comparison between CG (continuous lines) and all-atom simulation (dashed lines).

tems and the experimental samples: The chain length of around 9 monomers in the experimental samples is slightly shorter than the chain lenth of 10 monomers that we simulate in the melt. Secondly, due to the M_w distribution a significant amount of shorter chains is included in the samples. These two factors lead to a lower density in experiments. Nevertheless, these effects may be not sufficient to explain the higher density predicted by the simulations. This is not a problem of the CG model, but an inaccuracy of the underlying atomistic force field. To be more close to experimental results one may have to adjust the density of the simulated systems. Especially the dynamics of atomistic systems react sensitive to density changes. [85] This will be also an issue lateron in this work for the study of additive diffusion in polymer melts (see section 5.3), where overestimated densities slow down diffusion processes significantly.

4.3 Temperature dependence and transferability

Coarse-grained models usually have state dependent potentials because left-out degrees of freedom are weighted differently at different temperatures. Following a strict procedure, all potentials have to be redeveloped at every temperature that is used in CG simulations. In practice it turned out that CG models can be used within a certain temperature range around the exact temperature, at which they have been developed, as long as they do not undergo a glass transition or another phase transition.

To test the temperature transferability of the CG model a series of runs over a range of temperatures from 403 K up to 523 K was performed. The potentials of the CG model were developed at 503 K and should therefore reproduce the distributions at this temperature in CG simulations at 503 K. All CG runs use these potentials, only the temperatures are varied by using a thermostat.

The densities predicted by the atomistic and CG model are shown in Figure 4.7. As discussed above, the densities predicted by both, the atomistic and the CG model, are higher than the experimental densities. [84] The thermal expansion of the simulated systems is similar to the experimental data, but seems to underestimate the expansion coefficient slightly. The CG model shows the same thermal expansion coefficient as the atomistic model, while the density is slightly overestimated compared to the prediction of the atomistic model. The agreement is strikingly good. A recent investigation by Qian and coworkers on the temperature transferability of another CG polystyrene model, developed based on the iterative Boltzmann inversion method, showed a similar good agreement between the thermal expansion coefficients of atomistic and coarse-grained melts. [9] There the authors show that with another location of the CG mapping point (on the methylene unit rather than on the bead center of mass) the temperature transferability is significantly worse. [86]

The thermal expansion of the CG system in comparison to the atomistic system is not the only criterion to judge the transferability of a CG model, but it gives a hint that the temperature dependence of the CG potentials must be quite weak. To confirm the temperature range of the CG model it was reparameterized at 423 K. If the potential has no temperature dependence, the distributions would be still temperature dependent. Con-

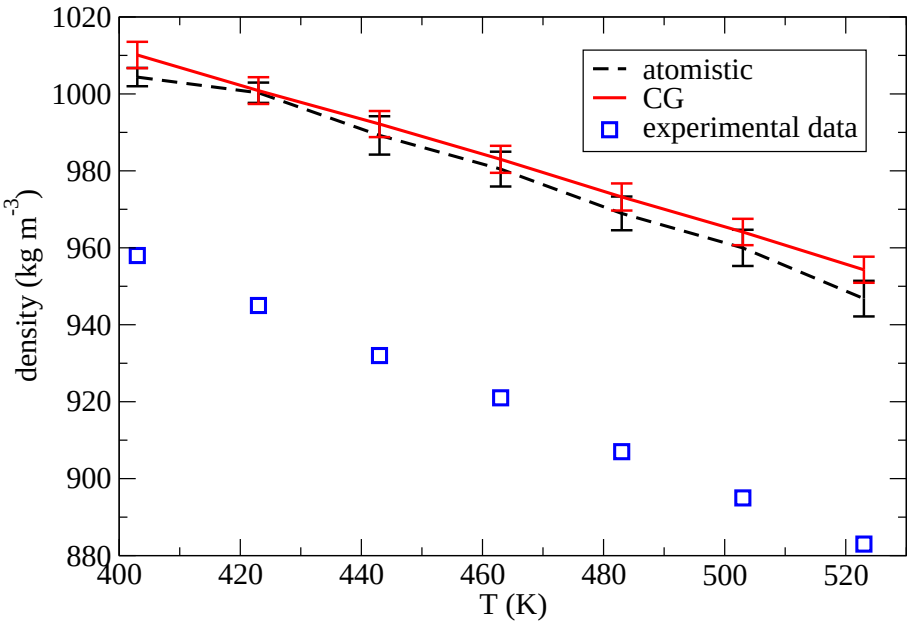

Figure 4.7: Densities of melts of 10-mers obtained from atomistic (dashed line) and CG simulations (continuous line) at constant pressure (1 atm) in a temperature range from 403 K to 523 K and experimental data (squares). [84]

sidering the case of an harmonic potential between two masses, the width of the bond length distribution would be more narrow for lower temperatures. The potential which is obtained by Boltzmann-inversion of the distribution, however, is the same for all temperatures due to the factor of $k_B T$ in equation 2.3. Therefore, to compare CG models at different temperatures, we have to compare the potentials directly, but not the distributions.

Some examples for the potentials at 423 and 503 K are shown in Figure 4.8. We see that the shape of the bonded potentials remains unchanged and that the barriers and potential differences between minima show slight deviations of around 1 kJ/mol ($k_B T = 3.5$ kJ/mol at 423 K). The errors in the distributions would be of the order of the actual deviations that we obtain between atomistic and CG simulations. The nonbonded potentials show even smaller deviations of 0.3 kJ/mol, which explains the good agreement of the thermal expansion behavior. The potentials not shown in Figure 4.8 for other degrees of freedom and for different types of diads do not have larger deviations. Based on these tests we used the CG model in the wide temperature range of 503 ± 100 K.

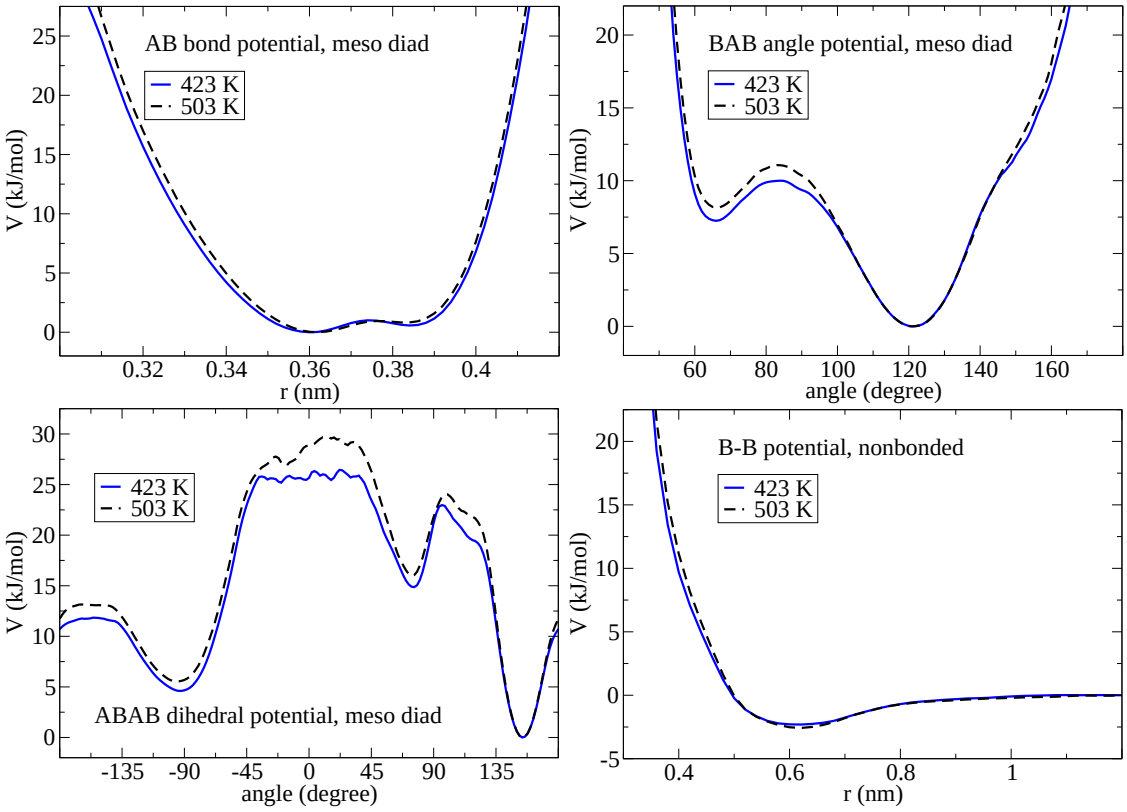

Figure 4.8: Comparison of potentials obtained at 503 K (dashed) and 423 K (continuous). Shown are the exemplary cases for CG bonds (top left), BAB angles (top right) and dihedrals (bottom left) in meso diads and the nonbonded B-B potential (bottom right).

5 Dynamics of multiscale polymer simulations

5.1 Time scales in atomistic and coarse-grained simulations

CG force fields are often developed to reproduce structures of the underlying detailed model. These static properties are typically chain conformations or packing of chains in melts, expressed by distributions for CG degrees of freedom or by radial distribution functions, respectively. Dynamical processes in CG systems are faster than corresponding processes in atomistic systems. The faster dynamics of CG systems can be discussed in terms of local friction coefficients. In the Rouse and in the reptation model, the local motion of monomers is governed by a scalar friction coefficient ζ. It is proportional to the melt viscosity, $\eta \propto \zeta$, and inversely proportional to the chains diffusion constant, $D \propto \zeta^{-1}$. The friction coefficient depends on the specific model that is used to simulate a polymer melt. Because the effective CG potentials are softer, the friction coefficient of the CG system, ζ^{CG}, is reduced compared to the friction coefficient of the atomistic system, ζ^{AA}. The atomistic friction coefficient is closer to the experimental situation and thus the dynamical predictions of the atomistic system are closer to experimental results. [87]

To obtain *quantitative* predictions of polymer dynamics from CG simulations, the time scale of the CG data has to be scaled in suitable way to fit atomistic simulation data or experimental results. This procedure has been discussed and used in the literature before. [44, 52, 54, 55, 66, 67, 85, 87, 88, 89, 90]

Following the above picture of friction coefficients, the time scaling factor $s = \frac{\zeta^{AA}}{\zeta^{CG}}$ provides the quantitative agreement between dynamics in atomistic and CG simulations. Calculating the mean square displacement from CG data, MSD(t_{CG}), and shifting it along the time axis, MSD(st_{CG}), results in an agreement with atomistic data, MSD(t_{AA}), for times longer than t_c (see below).

Analytical predictions how timescales in CG and atomistic systems are related are usually not available. The time scaling factor s is, in principle, dependent on the specific CG and atomistic model used, molecular weight, density, temperature and on other components in mixed systems.

A way to estimate the size of the time scaling factor s for a simple polymer system was proposed by Depa and Maranas. [89] They attribute the speed-up of CG systems not to the generally softer potentials between CG beads [91], but to a reduction of the nearest-neighbor attraction. They interpret the surroundings of nearest neighbors as a “cage”,

from which the CG atoms can escape easier, because their nonbonded potential is less attractive than the atomistic one in the range of the typical nearest-neighbor distance. They consider the transition of a particle from one local cage to another as an event, to which they apply an argument from the hyperdynamics method. [92, 93] The hyperdynamics method accelerates MD simulations to study transitions between minima of the potential energy surface $V(\mathbf{r}_n)$, which happen rarely and are difficult to study with pure MD simulations. The simulations are accelerated by modifying $V(\mathbf{r}_n)$ with a bias potential $\Delta V(\mathbf{r}_n)$, where $\mathbf{r}_n$ is the N-particle configuration. Provided that both potentials comply with certain requirements, the method gives a speed-up through a time-averaged "boost factor"

$$\frac{t_{\text{hyper}}}{t_{\text{MD}}} = \left\langle \exp\left(\frac{\Delta V(\mathbf{r}_n)}{k_B T}\right)\right\rangle_{\Delta t} \tag{5.1}$$

Adapting this method to the case of CG simulations, they interpret the difference between the atomistic and the CG potential (in the range of the first neighbor shell) as an ensemble-averaged bias potential per particle, $\langle \Delta V \rangle$,

$$\langle \Delta V \rangle = \int_0^\infty \langle N_{\text{CG}}(r)\rangle \, U_{\text{CG}}(r)\, dr - \int_0^\infty \langle N_{\text{AT}}(r)\rangle \, U_{\text{AT}}(r)\, dr \tag{5.2}$$

where the CG and atomistic potentials, U_{XX}, are weighted with the ensemble-averaged number density of neighbors for each bead, $\langle N_{\text{XX}}(r)\rangle$ (XX stands for CG or AT)

$$\langle N_{\text{XX}}(r)\rangle = \frac{\langle P_{\text{XX}}(r)\rangle}{n_{\text{XX}}} \tag{5.3}$$

n_{XX} is the number of particles and $\langle P_{\text{XX}}(r)\rangle$ is the averaged number density of intermolecular Lennard-Jones pairs. The speed-up of the CG system can be estimated using

$$s = \frac{t_{\text{CG}}}{t_{\text{AT}}} = \exp\left(\frac{\langle \Delta V \rangle}{k_B T}\right) \tag{5.4}$$

The predictions of the time scaling factor agree within 7% with simulation results for polyethylene. [89] The CG polyethylene system studied in their work offers certain advantages, which facilitate the application of this method. In the CG model, as well as in the atomistic model (united-atom), the polymer is modeled by only one type of bead or atom, i.e. on both simulation levels only one type of nonbonded interaction potential has to be considered. The application to systems with different atom and bead types, as the systems studied in this work, would be cumbersome. Furthermore, it is not investigated if the method can be used for polymers with extended side groups, as for polystyrene, where the packing becomes more complicated.

In the following, aspects of the behavior of the time scaling factor s are discussed for melts or liquids of short oligomers. For these short chains the dependence on molecular weight and tacticity is investigated, followed by a study of mixed systems, which contain two components of different molecular weight. For homopolymer melts it has been found

that the scaling factor reaches a constant value for high molecular weights. [85, 87, 90] For CG polystyrene this plateau value for s is reached approximately for the same molecular weight, at which the melt density becomes constant. [85, 87]

5.1.1 Time mapping by matching mean square displacements

The time mapping between time scales in atomistic and coarse-grained systems is expressed by the time scaling factor s. It is obtained by comparing corresponding dynamical quantities in atomistic and CG simulations. Various dynamical quantities can be used. In the systems studied in this work, two related quantities were chosen: diffusion coefficients as scalar dynamical quantities and mean square displacements (MSD) that span a certain range of time.

The self-diffusion coefficient D in a system of identical particles is calculated from the linear part of the mean square displacement of the center of mass, $\langle (R_{\mathrm{cm}}(t) - R_{\mathrm{cm}}(0))^2 \rangle$, as a function of time using the Einstein relation:

$$D = \lim_{t \to \infty} \frac{\left\langle (R_{\mathrm{cm}}(t) - R_{\mathrm{cm}}(0))^2 \right\rangle}{6t} \tag{5.5}$$

Time scaling factors based on diffusion coefficients compare only the asymptotic long time regime and require long atomistic trajectories that reach the diffusive regime. Using this quantity the CG time scale can also be mapped to experimental data.

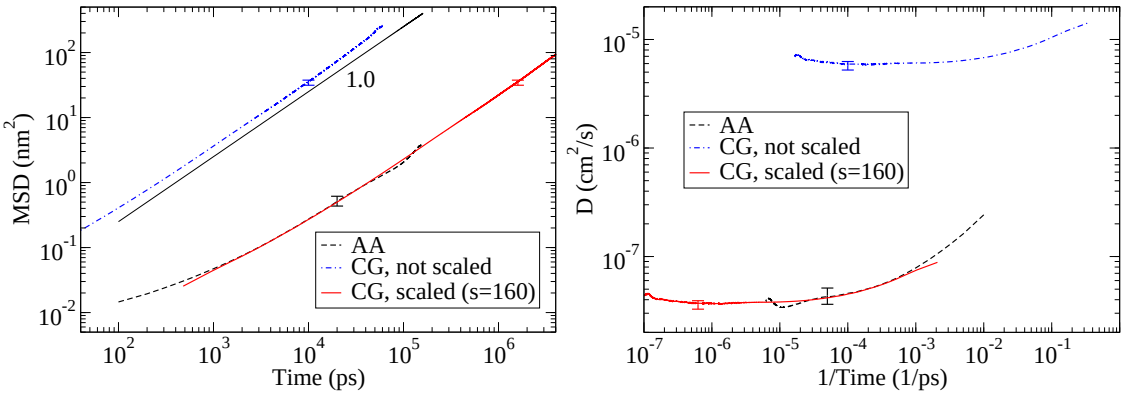

Figure 5.1: Mean square displacement (MSD) of the molecules center of mass in a melt of isotactic 10-mers in CG and AA simulations (left) and self-diffusion coefficient vs. inverse time (right). The unscaled CG data are taken directly from CG simulations, the scaled CG data are obtained by shifting the unscaled CG MSD along the time axis to match the MSD of the atomistic system. Typical error bars, obtained by block analysis over segments of the whole trajectory, are shown for each curve.

If data from atomistic MD runs are used, the time scaling factor s can be also obtained by matching the MSD of CG and AA simulations. This method was used in the following study and an example is shown in Figure 5.1, where the MSD from the CG run is shifted

by multiplying the time by a factor s of 160. The shifted MSD agrees with the atomistic MSD for long times, but also at times, where the diffusive regime is not yet reached completely. This can be seen more clearly in the right side of Figure 5.1, where the diffusion coefficient (obtained using eq. 5.5) is plotted vs. inverse time. For long times D approaches asymptotically to a constant value. The agreement between CG and atomistic D or MSD is reached for times t_c before the constant value for D is reached, in the example in Figure 5.1 for times around $t_c = 10^3$ ps. This provides a direct insight into the time- and length scales for which the particular CG model can be used.

5.1.2 Time mapping for oligomer systems

In this work the time scaling between CG and atomistic simulations was investigated for melts of low molecular weight. Systems up to 10-mers (represented by 20 CG beads) were simulated at a temperature of 503 K. For these small oligomers it is still feasible to reach the diffusive regime of the mean-square displacement in all-atom simulations and to obtain time scaling factors by directly comparing mean-square displacements of atomistic and CG simulations.

In a first series of simulations the influence of the tacticity on the time scaling factor was investigated. Systems of isotactic and syndiotactic polystyrene oligomers with varying molecular weight between 314 and 1044 g/mol (corresponding to a number of monomers N between 3 and 10) were studied. The systems were simulated at constant volume, using densities from atomistic constant pressure runs at ambient pressure. The densities range from 905 kg/m^3 for 3-mers to 959 kg/m^3 for 10-mers. Details about the simulations can be found in the Appendices A.1.4 and A.2.3. The time scaling factors s are determined by matching the MSD of atomistic and CG simulations.

Self-diffusion coefficients and scaling factors of iso- and syndiotactic oligomer systems are shown in Figure 5.2. The differences between iso- and syndiotactic systems are very small. Not only the differences between time scaling factors s of the two tacticities are within error bars, but also the differences between the self-diffusion coefficients. The time scaling factors, however, show a strong increase with increasing molecular weight. But in these systems not only the molecular weight is increasing, but also the density. To separate the influences of varying density and varying molecular weight, time scaling factors were investigated in a second series of runs, all performed at the same density. The density, which was chosen for these runs, was the density of the isotactic 10-mer system obtained by an atomistic NpT run at ambient pressure (955 kg/m^3). Since the differences between iso- and syndiotactic systems in their dynamics were very small (see Figure 5.2), the following studies were limited to one of the two tacticities, where the isotactic systems were chosen.

Self-diffusion coefficients and scaling factors of isotactic oligomer systems at constant density are shown in Figure 5.3. The increase in s with increasing molecular weight is still observed, but the slope is smaller compared to the previous Figure 5.2. As mentioned before, the systems with $N < 10$ are simulated at increased density (taken from the system with $N = 10$). Compressing the systems in such a way, slows down the diffusion processes

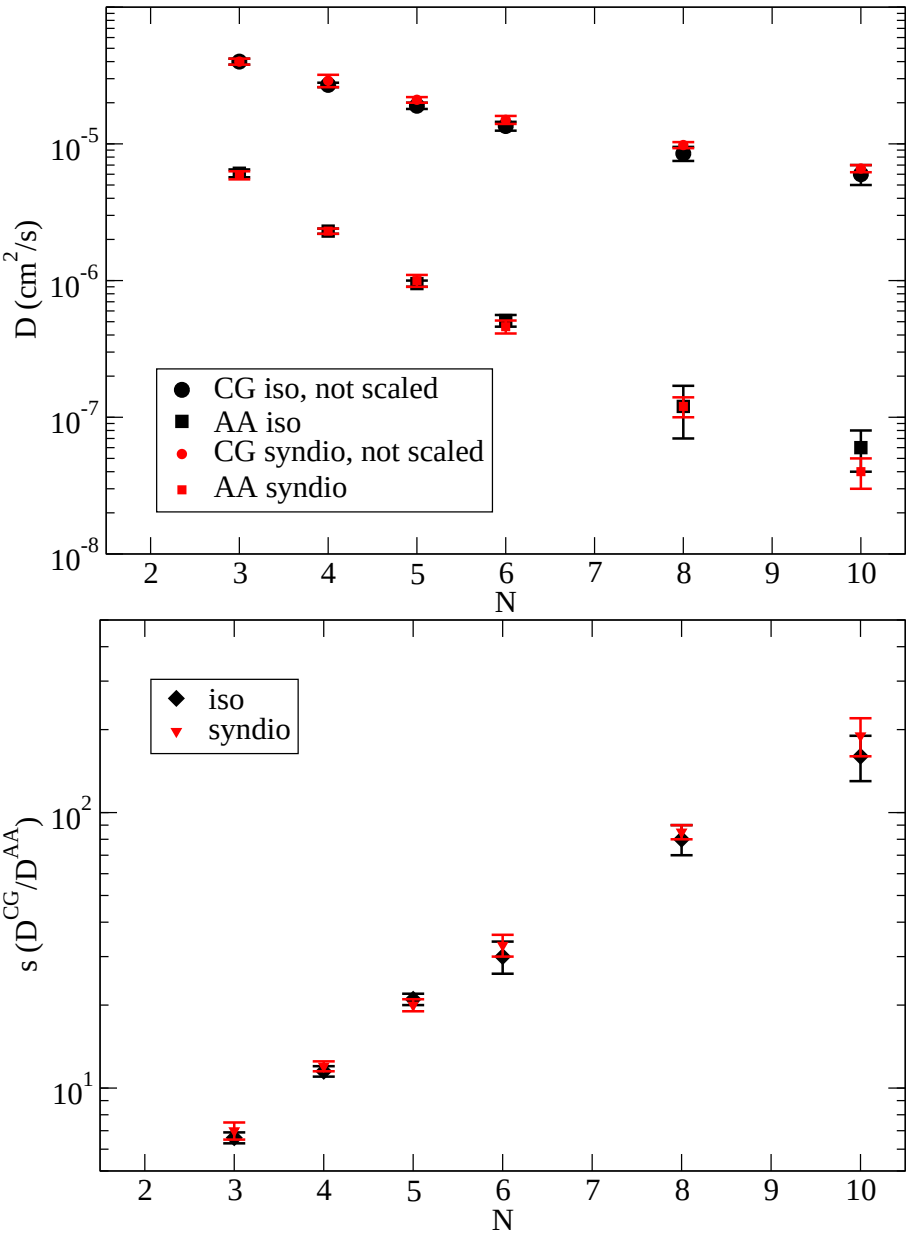

Figure 5.2: Self-diffusion coefficients (top) and time scaling factors (bottom) for oligomer melts of different molecular weight (number of monomers *N*) and different tacticity (isotactic and syndiotactic), obtained from all-atom (AA) and coarse-grained (CG) NVT simulations. The densities of the systems were obtained by atomistic NpT runs and are varying between 905 and 959 kg/m^3.

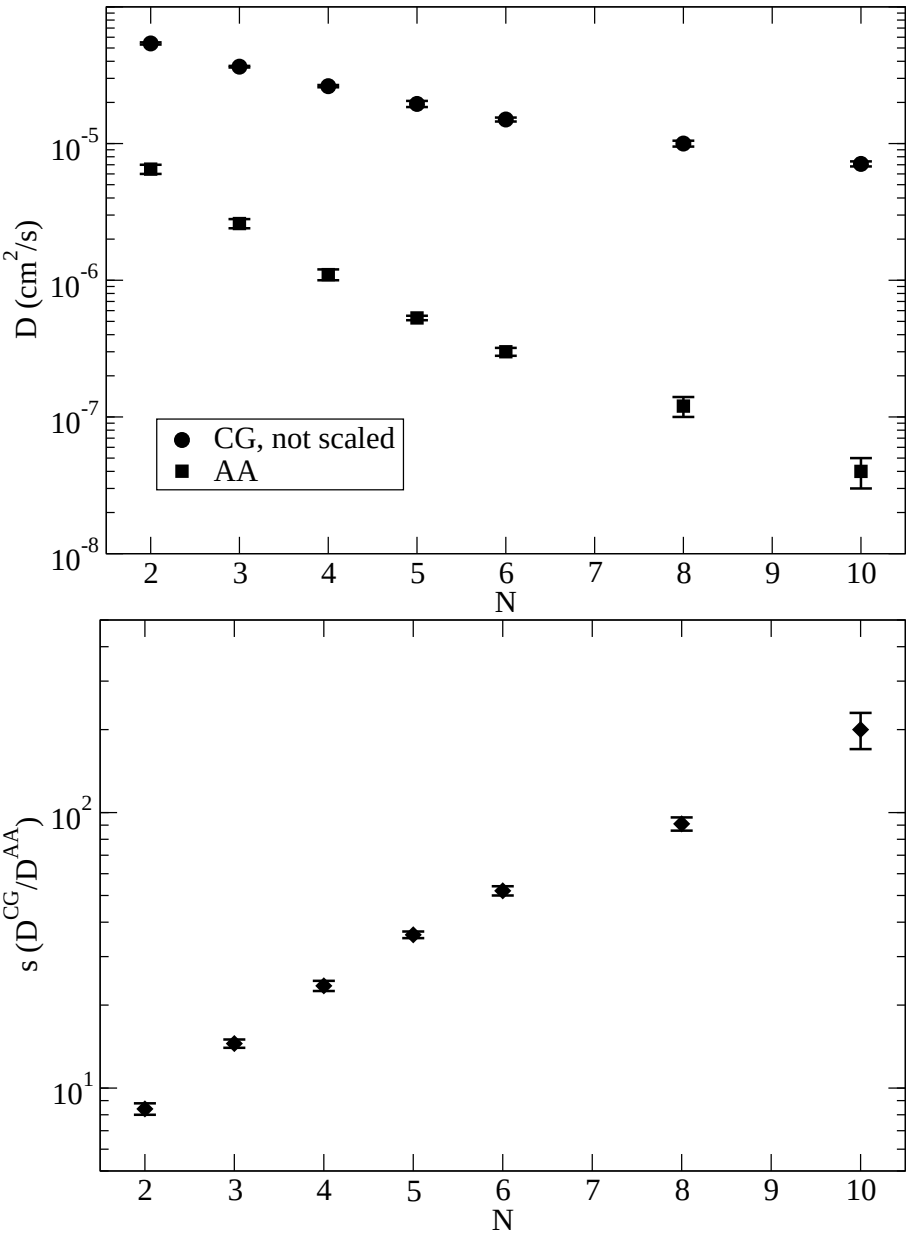

Figure 5.3: Self-diffusion coefficients (top) and time scaling factors (bottom) for isotactic oligomer melts of different molecular weight (number of monomers *N*), obtained from all-atom (AA) and coarse-grained (CG) NVT simulations. The densities of all systems were set to the density of the 10-mer system from an atomistic NpT run (955 kg/m^3).

in both, AA and CG simulations. But the smaller slope of s vs. N indicates that diffusion in the AA system is slowed down more than in the CG system, which can be also seen by directly comparing the self-diffusion coefficients in Figure 5.2 and 5.3.

The method to estimate the time scaling factor s for a melt of long polymer chains by performing the time mapping for a system of short chains, but at the higher density of the longer chains [85], cannot be applied for the very short oligomers studied here, i.e. the scaling factor for the 10-mer system is not the same as the scaling factor for the 2-mer system simulated at the higher density of the 10-mer system. The difference between the two systems is the strong influence of chain ends in the oligomer systems. Chain ends (the first and last few beads in a polymer chain) have a higher mobility than central beads, because they are only attached to neighboring monomers on one side, whereas beads in the middle of a polymer are attached to neighbors on both sides. Of course, the fraction of chain ends is increasing with decreasing the molecular weight of a polymeric system.

The CG force field in this work does not contain optimized potentials to treat chain end beads differently than central beads. The same nonbonded potentials are used for all monomers. Those potentials are developed for A and B beads separately, but the sampling of configurations is always done under the condition, that the beads are connected to two neighboring monomers on both sides, see section 3.5. To obtain special nonbonded potentials for chain ends, the sampled interacting beads should be connected to other monomers on only one side. This release of constraints would open additional possibilities how the two interacting beads can be oriented towards each other. These additional options would possibly result in a smaller beads size or in a stronger attraction, which would lead to an increased density of CG systems containing high amounts of chain ends. This consideration is consistent with the behavior of the density in CG NpT simulations[1] (without special end group potentials): While the density of 10-mer systems is in agreement with AA simulations, the density becomes more underestimated for shorter oligomers. For trimers the density predicted by the CG model is 12% below the density of the AA simulation. The opposite effect is observed for long chain melts, where the CG model predicts densities around 6% higher than the AA model.

[1] CG NpT simulations of oligomer systems were only performed during the setup of the CG systems. The CG oligomer systems that were used to study the time scaling were all simulated under NVT conditions at the same density as the corresponding atomistic systems.

5.1.3 Time mapping for mixtures of two components

Up to now the time scaling in one-component systems has been discussed. The time scaling in mixed systems has not been studied systematically before. The following direct comparison of scaling factors by simulating AA and CG systems is limited to mixtures of relatively short chains, in order to reach the diffusive regime of the MSD for the atomistic systems. Two series of mixtures are studied, which contain isotactic oligomers of two different molecular weights in varying weight fractions ($w_M = 0.25, 0.5, 0.75$ is the weight fraction of the smaller component):

- mixtures of 2-mers and 6-mers, with corresponding molar fractions $w_{mol} = 50$, 75, 90 of 2-mers
- mixtures of 3-mers and 10-mers, with corresponding molar fractions $w_{mol} = 53$, 77, 91 of 3-mers

All mixtures were simulated at the same density that was already used before for the one-component systems and that was obtained by an atomistic NpT run of the isotactic 10-mer system at ambient pressure. Details about the simulations can be found in the Appendices A.1.5 and A.2.4.

Diffusion coefficients of the two components and their time scaling factors s are shown in Figure 5.4 and 5.5. The mixed systems show the expected behavior for the diffusion coefficients: If the fraction of the smaller component is increased, the diffusion of both components becomes faster. This is observed in both, AA and CG systems. The scaling factors s for the two components, however, show an interesting behavior: They vary with the concentration of the two components and they are different for the two components by a factor, which is almost constant for the various molar fractions w_{mol}. Plotting $\log s$ vs. w_{mol} the dependence is almost linear for both components.

The difference in the scaling factors, both obtained from the same AA and CG simulation, gives a hint to possible problems, when different dynamical processes are involved in CG simulations. On the other hand, it has been shown before that the scaling factor s becomes independent of the molecular weight in CG melts of long polymer chains. Furthermore, it has been shown that in these systems a time mapping based on the mean-square displacement also describes other dynamical modes correctly, namely the mobility of polymer segments, expressed by the time dependent dynamic structure factor $S(q,t)$, which can be measured by neutron spin echo (NSE) spectroscopy. [94] Also orientational dynamical modes, as the end-to-end vector autocorrelation function, follow the same time mapping. [85, 87, 90]

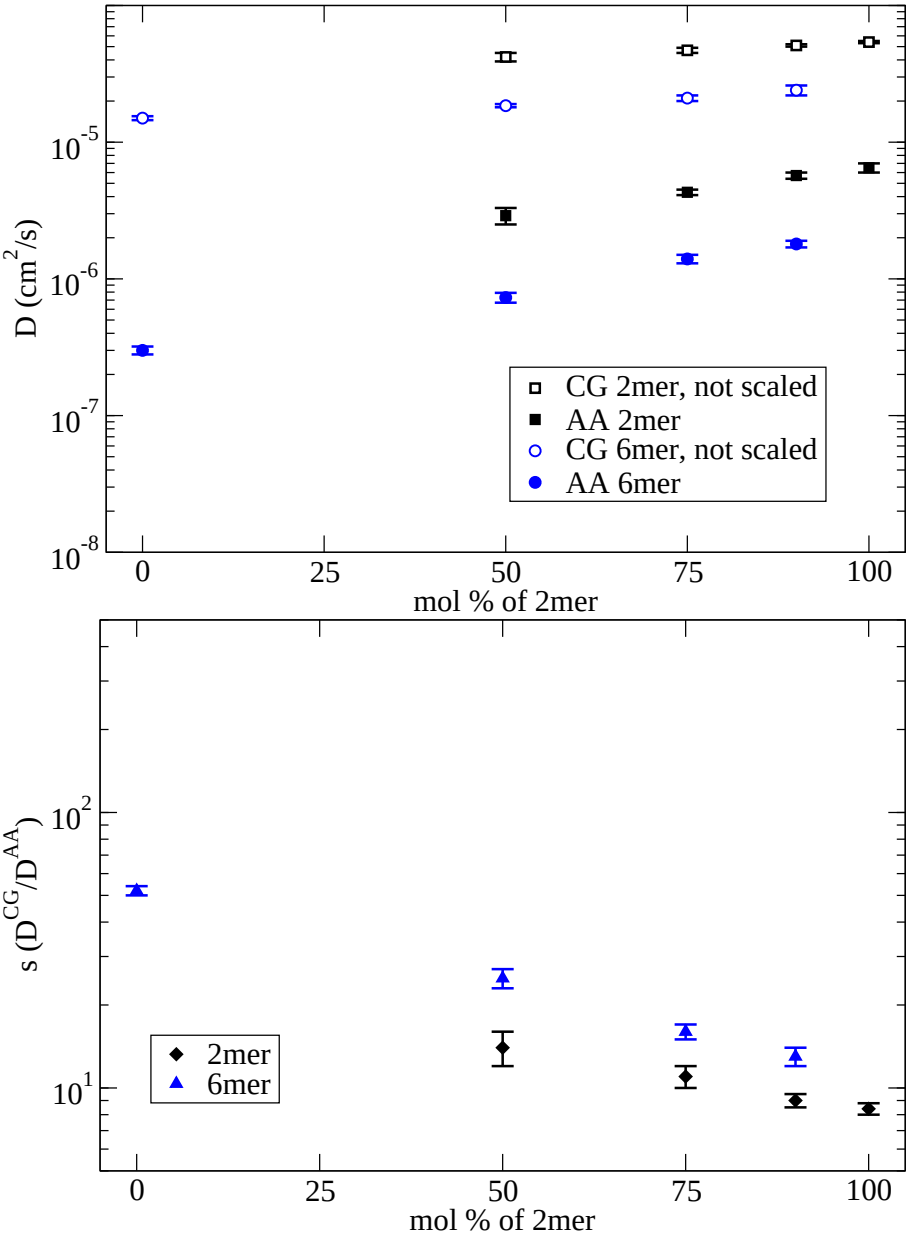

Figure 5.4: Diffusion coefficients for 2-mers and 6-mers in mixtures of those components with varying concentration (top) and time scaling factor for these systems (bottom). All simulations were performed at the same density of 955 kg/m^3.

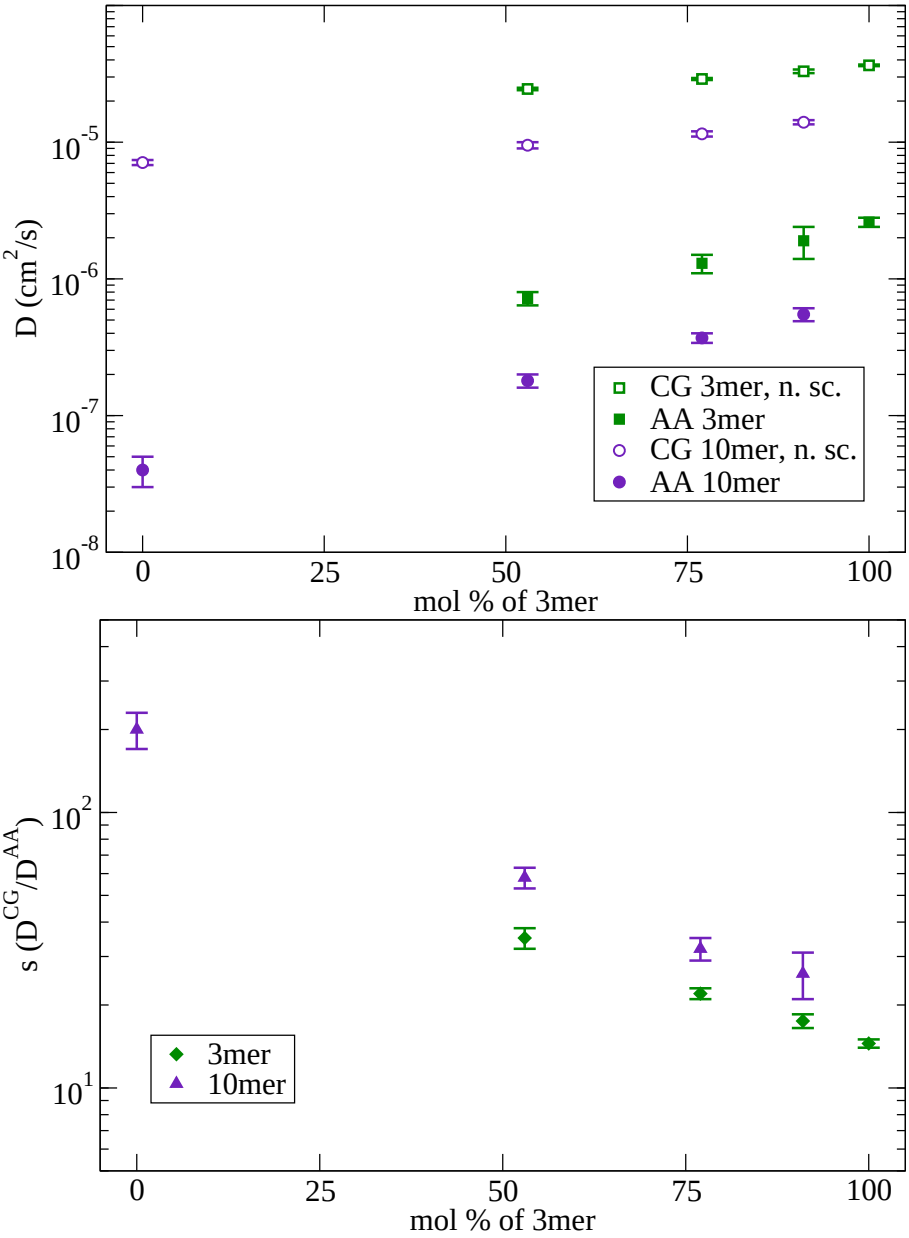

Figure 5.5: Diffusion coefficients for 3-mers and 10-mers in mixtures of those components with varying concentration (top) and time scaling factor for these systems (bottom). All simulations were performed at the same density of 955 kg/m^3.

5.1.4 Mean square displacements in pure and mixed systems

In the following the MSD, based on which the time scaling factors are determined, is studied in more detail for small molecules in very different surroundings: dimers diffusing in a pure dimer system are compared to ethylbenzene (one monomer) diffusing in a melt of long polymer chains (EB weight fraction $w_M = 0.1$). For the latter system, also the time mapping of the long chains can be determined and it will show a similar behavior as the previously presented mixtures of short oligomers.

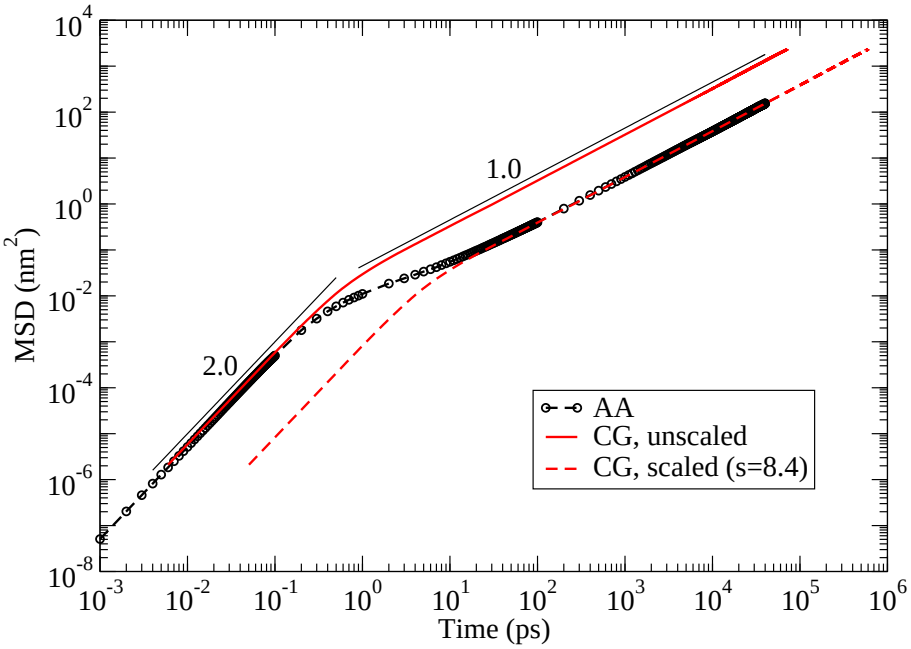

Figure 5.6: MSD of dimers (center of mass) in a pure dimer liquid, AA (circles) and CG. The CG MSD is shown with (dashed) and without (continuous) scaled times. The scaling factor $s = 8.4$ is obtained by matching the long-time, diffusive regime of atomistic and CG MSD. Drawn are also the slopes of 2 for the ballistic regime and of 1 for the diffusive regime.

In Figure 5.6 the MSD in dimer liquids is compared for AA and CG simulations. The MSD for shorter times has been obtained by shorter MD simulations with a more frequent output of the systems coordinates; the lowest value for the AA system shows the mean square displacement during one single integration time step of 1 fs.

For very short times below 0.1 ps the MSD increases with a slope of 2. This is the ballistic regime, in which the particles move freely and do not collide with their neighbors yet. Since the CG particles are also simulated with their real masses, AA and CG MSD are in perfect agreement. It is in the intermediate regime between 0.1 and 100 ps that the difference between atomistic and CG MSD evolves. In this intermediate regime the individual particles start to collide with each other and explore by that their interaction potential as well as the packing and the conformations of the surrounding molecules. Because the interaction potentials as well as the surrounding molecules are different, the

mobility of atomistic molecules is slowed down more than the mobility of CG molecules.

The AA MSD shows a clear subdiffusive regime (characterized by a slope < 1) before the diffusive regime (slope 1) is reached for times longer than 100 ps. This can be understood by the picture of molecules being trapped in a cage, which is formed by the neighboring molecules due to their attractive interaction. The time that is necessary to escape the cage is on average much longer than the time between two collisions, i.e. molecules wiggle around in the cage and collide frequently with their neighbors, before they eventually find a spot through which they escape from the cage. It is notable that the CG MSD does not exhibit any subdiffusive behavior but a smooth transition from the ballistic to the diffusive regime around a time of 1 ps. Due to the reduced number of "superatoms" (4 CG beads vs. 34 atoms per dimer) and their weaker attraction the picture of escaping a cage does not hold true here, because the "escape time" is comparable to the time between two collisions. The MSD of around 0.1 nm^2, where the diffusive regime in the CG system starts, corresponds to half of the bead size and is only slightly higher for the AA system.

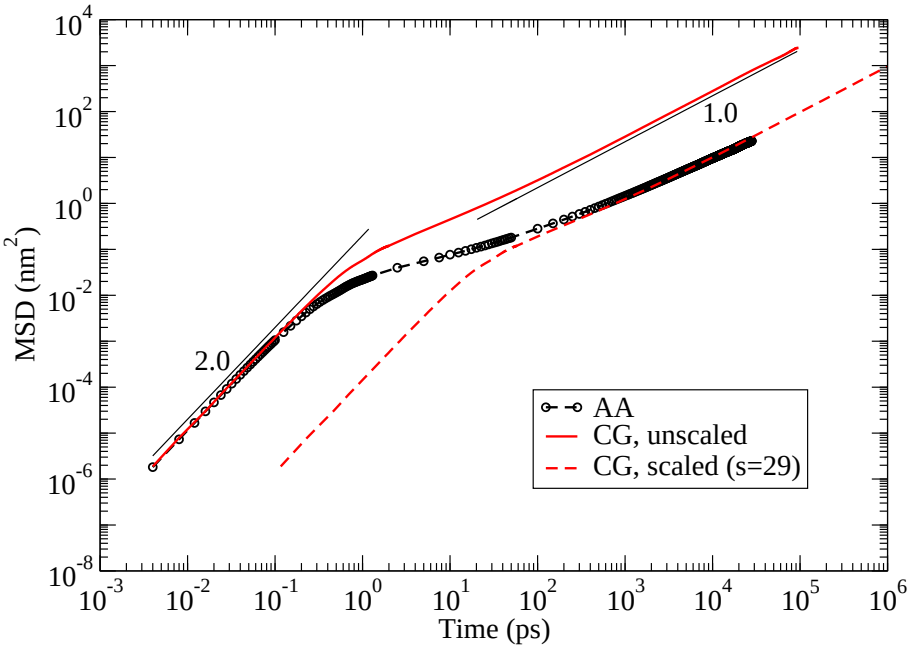

Figure 5.7: MSD of ethylbenzene (EB) in a matrix of long PS chains (96 monomers), AA (circles) and CG. The CG MSD is shown with (dashed) and without (continuous) scaled times. The scaling factor for EB is $s = 29$. Drawn are also the slopes of 2 for the ballistic regime and of 1 for the diffusive regime.

In comparison to the previous discussion of a liquid of short oligomers a different system is studied in Figure 5.7. It shows the MSD of ethylbenzene (EB) molecules in a matrix of long polystyrene (PS) chains (96 monomers). The weight fraction of EB is $w_M = 0.1$. EB is similar to the monomers of PS, the only difference are two extra hydrogen atoms in the AA representation. In the CG model it is represented by the same two beads as the monomers, which are part of a longer PS chain (see section 5.3).

As for the dimer system, in the short-time, ballistic regime the MSD of AA and CG molecules is in agreement, before a difference evolves in the intermediate regime between 0.1 and 1000 ps. In this intermediate regime also the CG system shows subdiffusive behavior, even though the EB molecule is smaller than the dimer, whose CG liquid did not show subdiffusive behavior. Another important difference to the dimer system is the length scale of the MSD of around 1 nm^2, on which the diffusive regime is reached. This MSD corresponds to more than the size of a CG bead (as opposed to half the bead size for the dimers liquid) and can have two explanations in the cage picture mentioned above: the size of the cage could be bigger due to the stiffness of the long polymer chains, which does not allow them to pack as closely as the smaller oligomers. In this case a cage or cavity could be even large enough to host more than one EB molecule. Another explanation is the mobility of the monomers in the long chains, which form the cage, which could lead to a motion of the whole cavity without releasing the EB molecule inside. The MSD of the beads in the polymer matrix can be found in Figure 5.8. It turns out that also the beads in the polymer matrix move around half of a CG bead size (the beads have a radius of around 0.4 nm) before the EB molecules reach the diffusive regime. In the CG simulation they move around 0.5 nm, whereas in the AA simulation they move around half of this distance. In both cases this is a significant displacement compared to the size of the EB molecule. This confirms that the dynamics of the long chain matrix is important for the diffusion of small penetrant molecules and the matrix cannot be seen *only* as a static arrangement of cavities, between which the small penetrant is hopping.

Looking at the time scaling factors of the mixed system of EB molecules in long PS chains, a similar situation as for the mixtures of short oligomers is observed. By mapping the MSD of EB from atomistic and CG simulations a time scaling factor $s = 29 \pm 6$ is obtained. This is higher than the scaling factor that would be obtained from an EB liquid at the same density (see Figure 5.3, which gives scaling factors for oligomer liquids at a density of 955 kg/m^3, whereas the the EB/PS mixture is simulated at constant pressure conditions, resulting in densities of 953 ± 2 kg/m^3 for the AA simulation and 946 ± 2 kg/m^3 for the CG simulation.). The time scaling factor for the matrix of the long PS chains is determind based on the MSD of individual beads and of the center of mass of the PS chains. It is clear that these two MSDs must have the same time scaling factor, because in the long-time limit the displacement of the whole chain becomes the same as the displacement of its constituent parts. They only differ on length scales, which are smaller than the chain dimension. Therefore, the time scaling factor for the motion of the polymer matrix can be determind by mapping these two MSDs simultaneously. They are shown in Figure 5.8.

A first observation is the perfect agreement in the ballistic regime (below 1 ps) of the MSD of the center of mass of the whole chain. The MSD of the individual beads, however, shows a small deviation in the ballistic regime. A possible reason for this small deviation might be found in the mapping of the CG model (see section 3.3), in which certain atoms in the backbone are involved in the definition of *two* CG mapping points. It has been shown that this can introduce a deviation between atomistic and CG simulation in the velocity distributions. [95]

The time scaling factor for the long polymer chains is $s = 300 \pm 50$; the scaling factor of the EB component, in comparison, is only $s = 29 \pm 6$. As in the case of the oligomer mixtures it is the smaller (and lighter) component, which has a lower s. The components of the small oligomer mixtures have a molecular weight ratio of around 3 (6-mers/2-mers and 10-mers/3-mers) and the time scaling factor for the heavier component is higher by a factor of roughly 1.5; the EB/PS system has a molecular weight ratio of 96 and the time scaling factor is higher by a factor of 10.

These similarities lead to the question, if the time scaling factor for the long polymer chains is independent from the concentration of added EB (at least in a range of low EB concentration before a dilute solution is formed), as it is independent of molecular weight for pure melts of long chains, or if it varies with the concentration, which is the case for the small oligomer mixtures (compare Figure 5.4 and 5.5).

The MSD for a pure melt of polystyrene chains (96 monomers, which is the same chain length as in the mixed EB/PS system) is shown in Figure 5.9. It delivers a time scaling factor $s = 700 \pm 200$, which is higher than the corresponding factor in the mixed system [2]. It is not surprising that the behavior of the time scaling factor s is qualitatively the same for mixtures of short oligomers and for a mixture of a small penetrant in a matrix of long chains, since both systems contain short molecules, for which the chain ends play an important role. Even though the chain end effect of the long polymer can probably be neglected, its time scaling depends on the concentration of EB, which contributes to the surroundings of the long chains.

[2] The comparison of the scaling factors has to take into account that the systems including the long polymer chains have been simulated at constant pressure. In the AA as well as in the CG simulation the reference pressure was set to ambient pressure. This choice leads to different densities of the four systems, which influence the values of the two time scaling factors. The densities for the atomistic systems are 953 kg/m^3 for the EB/PS system and 968 kg/m^3 for the pure PS system. The CG densities are 946 kg/m^3 and 1032 kg/m^3, respectively. Therefore, one has to check, if the scaling factors would be still different, when all systems would be simulated at the same density. Correcting the density of the CG systems, would increase the difference even further, because the system with the higher s has the higher density; decreasing this density, the diffusion coefficient D^{CG} of the system would be increased and by that also $s = D^{CG}/D^{AA}$. On the other hand, the density of the AA systems has the opposite influence and has to be checked carefully. To this end, simulation data of a second atomistic EB/PS system, simulated at a density of 924 kg/m^3, have been analyzed. Using the same CG system as before, a scaling factor of $s = 90 \pm 20$ is obtained. Extrapolating linearly from the two available densities to the density of the pure system a timescaling factor of around $s = 500$ is expected. This value reaches the error bar of the value for the pure system ($s = 700 \pm 200$), but taking into account that all influences of correcting the CG densities would increase the difference again, it is safe to state that the two time scaling factors are different and that the pure system has the higher one.

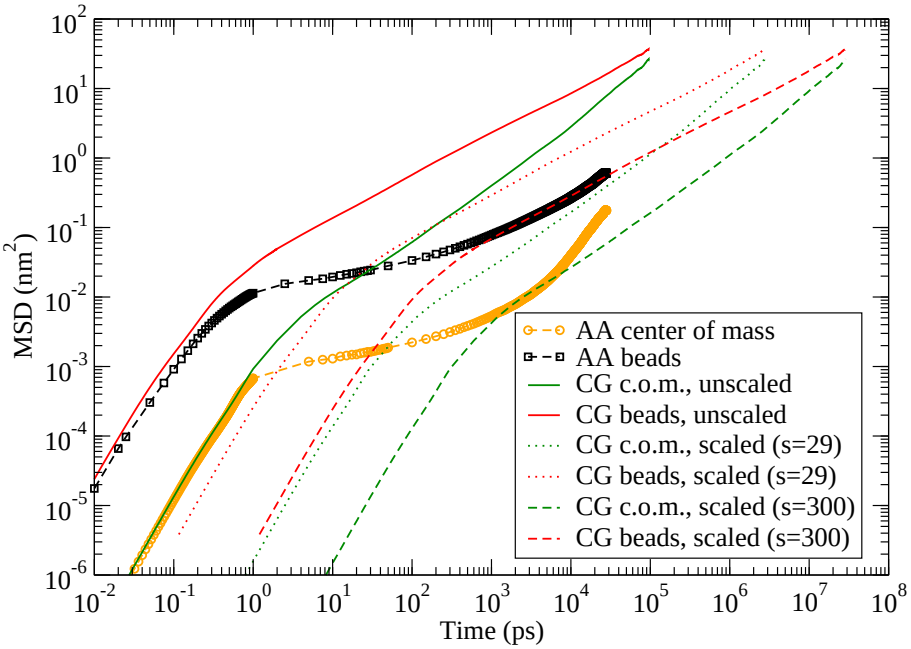

Figure 5.8: MSD of the matrix of long PS chains (96 monomers, 10 kDa) in a system mixed with EB for CG beads and the center of mass, AA and CG. (The MSD of the center of mass shows a long-time drift, which could be caused by a summation of small errors during the correction of motions of the center of mass of the whole system.)

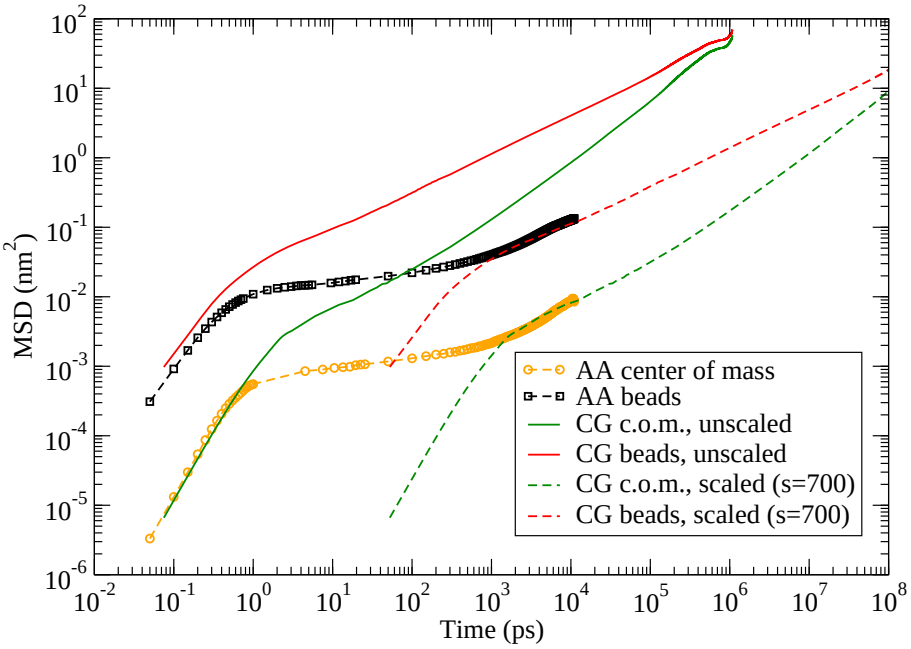

Figure 5.9: MSD of a melt of long PS chains (96 monomers, 10 kDa) for CG beads and the center of mass, AA and CG.

5.2 Dynamics of coarse-grained polystyrene melts

The CG model for polystyrene, which has been presented in this work, is very well suited to study polymer melts. It is efficient enough simulate systems of chains, which are long enough to form entanglements. These entanglements between polymer chains influence the dynamics, especially in longer time regimes, which are not accessible by atomistic simulations. In CG simulations, however, it is possible to observe these effects as well. On the basis of previous works done on the dynamics of polymer melts [38, 85, 87], at this point only a few aspects shall be presented, which demonstrate the applicability of the CG polystyrene model to study dynamics in polymer melts. The strength of the model is the consideration of all different tacticities of polystyrene. The influence of the tacticity on dynamical quantities of entangled systems has not been studied before and is possible to be studied with the presented CG model.

In Figure 5.10 the mean square displacement of the chain center of mass, $g_3(t)$, is presented for three polymer melts of different molecular weight (simulation details in Appendices A.2.2, A.2.5 and A.2.6). The systems show a subdiffusive behavior, related to the correlation hole effect, with a time dependence of $g_3 \propto t^{0.8}$ [10, 96, 85] in a short-time regime, which is shorter than the longest relaxation time. In the longer time regime the standard linear Fickian regime is observed. Another dynamical quantity is shown in Figure 5.11, where the mean square displacement of inner beads, $g_1(t)$, (the 30 most inner A beads of chains of 192 monomers) is presented for polymer melts of the same molecular weight (20000 g/mol, 20 kDa) but of different tacticity (simulation details in Appendix A.2.6).

In polymer melts the MSD of beads or chain segments, $g_1(t)$, is a property, whose behavior depends on how entangled the chains are. For unentangled systems the Rouse model [97] predicts a scaling as $t^{1/2}$ at short times and a scaling as t in the diffusive regime for longer times. In entangled systems the situation is more complicated. There, for times smaller than the disentanglement time, τ_d, the chains are confined to move in a tube, which is formed by the entanglements with other chains. This leads to a regime where $g_1(t)$ scales as $t^{1/4}$ as an combined effect of Rouse-like diffusion and the constraints of the tube. The motion of the chain along the contour of the tube is called reptation and the reptation theory explains four different regimes for $g_1(t)$ [97]:

$$g_1(t) \propto \begin{cases} t^{1/2}, & t \leq \tau_e \\ t^{1/4}, & \tau_e \leq t \leq \tau_R \\ t^{1/2}, & \tau_R \leq t \leq \tau_d \\ t, & \tau_d \leq t \end{cases} \tag{5.6}$$

τ_e is the entanglement time. This is the time at which the displacement of the segments reaches the tube diameter and the chain "realizes" that it is confined to a tube. In the long-time regime the chain has left its initial tube and a linear diffusive regime is reached.

The syndiotactic system shows a regime, where the slope is smaller than 0.5. This can be seen more clearly in Figure 5.12, where the MSD of the inner beads is normalized by $t^{1/2}$. This effect is a sign of entanglements and reptation behavior. It is less pronounced for

the other tacticities. In fact, the molecular weight of the chains (20000 g/mol) is similar to the entanglement molecular weight M_e (18100 g/mol for atactic PS [81]), for which the polymer chains only start to be entangled. In comparison to the inner beads, the outer beads at the chain ends do not reflect signs of entanglements, because they are not confined in a tube. This can be seen in Figure 5.13, which shows the MSD of the 5 outer A beads at each chain end normalized by $t^{1/2}$.

To explain the behavior of syndiotactic PS in this case, we remember the characteristic ratio C_∞, which has been presented before (see section 4.1.2). We found that the CG model reproduces the different characteristic ratios of 7.8 for atactic PS, 8.9 for isotactic PS and 12.3 for syndiotactic PS in good agreement with experimental results. The higher C_∞ of syndiotactic PS corresponds directly to a higher mean square end-to-end distance $\langle R^2 \rangle$, since $C_\infty \propto \langle R^2 \rangle$. The packing length describes the characteristic length scale, at which polymers start to interpenetrate, and is related to the mean square end-to-end distance, $p = (\rho_{\text{chain}} \langle R^2 \rangle)^{-1}$, where ρ_{chain} is the number density of chains. Finally, the packing length is related to the entanglement molecular weight, $M_e \propto p^3$. [81, 98, 99, 100] Following these relations, the M_e for syndiotactic PS is smaller than the one for atactic PS by a factor of around 4, due to the higher C_∞ of syndiotactic PS by a factor of 1.5. The molecular weight of the syndiotactic system studied here is around $4M_e$, whereas it is only around M_e for the isotactic and atactic system. Therefore, it is not surprising that the syndiotactic system shows stronger signs of entanglements. Future work can extend the scope of this study to polymer melts of higher molecular weight and study the influence of tacticity on entanglements in more detail.

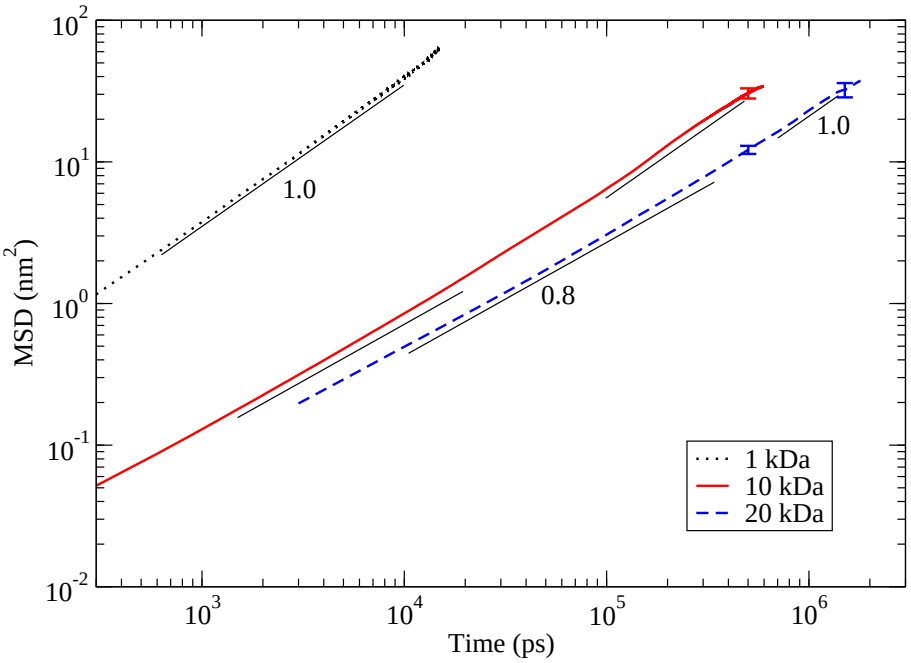

Figure 5.10: MSD $g_3(t)$ of the chain center-of-mass for atactic PS melts of different molecular weight. The time is taken directly from CG simulations and not scaled to fit atomistic time scales.

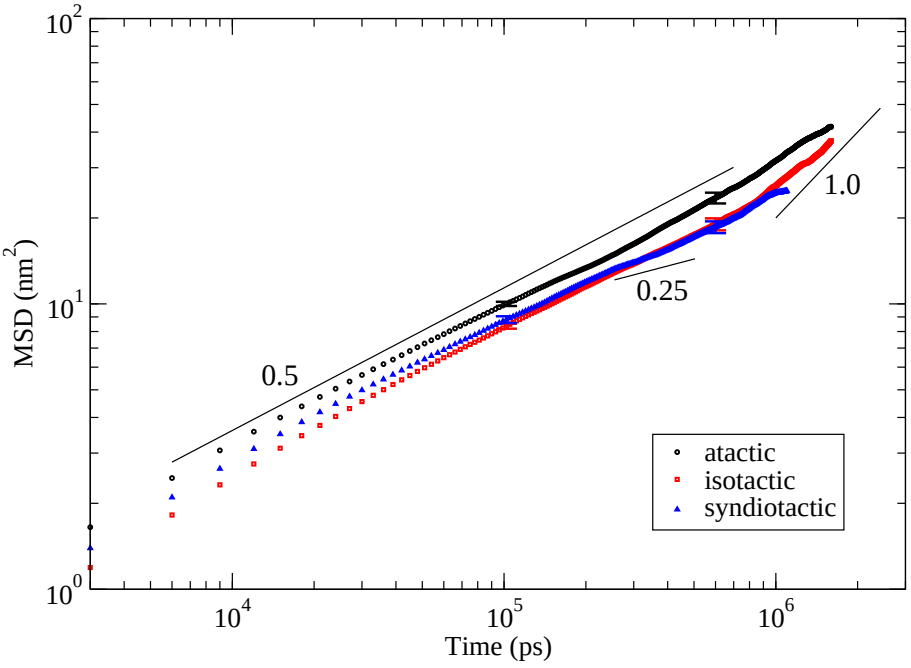

Figure 5.11: MSD $g_1(t)$ of inner A beads in PS melts (192 monomers, 20 kDa) of different tacticity. The time is taken directly from CG simulations and not scaled.

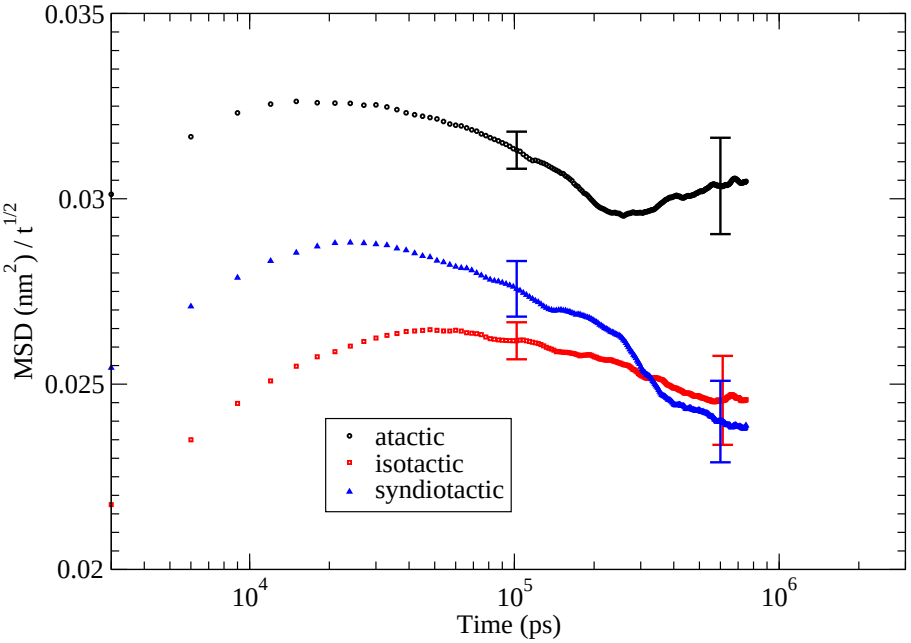

Figure 5.12: MSD $g_1(t)$ of inner A beads in PS melts (192 monomers, 20 kDa) of different tacticity, normalized by the Rouse slope of $t^{1/2}$. The drop of the syndiotactic MSD indicates a regime where $g_1(t)$ scales with a slope smaller than $t^{1/2}$.

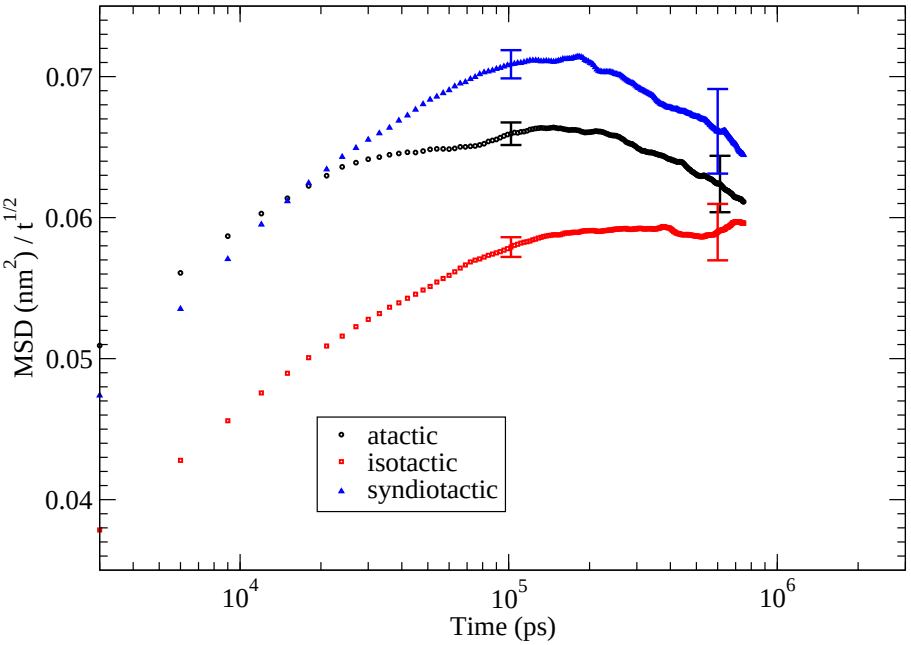

Figure 5.13: MSD $g_1(t)$ of outer A beads in PS melts (192 monomers, 20 kDa) of different tacticity, normalized by the Rouse slope of $t^{1/2}$.

5.3 Additive diffusion in polymer melts

In the following a study of the diffusion of ethylbenzene (EB) in a matrix of PS chains is presented. [101] This system has already been discussed in a previous section (5.1.4) under the aspect of time mapping in mixtures. There it became clear that for the motion of the small penetrant molecule, the motion of the polymer matrix cannot be neglected.

In this section the time scaling factor s is again of interest, in particular its dependence on temperature. The weight fraction of the additive is not varied, neither the molecular weight of any of the two components. The systems that are studied consist of 24 atactic PS chains with a length of 96 monomers (192 CG beads, molecular weight $M_W = 9984\,\mathrm{g/mol}$) and of 256 EB molecules, which corresponds to a weight fraction $w_{EB} = 0.1$. EB is similar to the monomers of PS, the only difference are two extra hydrogen atoms in the AA representation. In the CG model it is represented in the same way as the monomers in PS. All beads in the CG model interact with the same nonbonded potentials (see section 3.5). No special interactions were used for the beads at chain ends or in EB. All systems were simulated under NpT conditions, using a reference pressure of 1 atm (ambient pressure). Simulation details can be found in Appendices A.1.7 and A.2.7.

As discussed previously in section 5.1.1, the self-diffusion coefficient D_i of component i ($i = 1,2$) in the binary polymer/penetrant system is calculated from the linear part of the mean square displacement (MSD) of the center of mass of component i, $\langle (R^i_{\mathrm{cm}}(t) - R^i_{\mathrm{cm}}(0))^2 \rangle$, as a function of time using the Einstein relation:

$$D_i = \lim_{t\to\infty} \frac{\langle (R^i_{\mathrm{cm}}(t) - R^i_{\mathrm{cm}}(0))^2 \rangle}{6t} \tag{5.7}$$

To reach the linear part of the MSD long trajectories are needed. For all-atom systems these simulations are computationally very expensive at the temperatures (up to 473 K) at which experimental data are available. [88] The strategy in this study is to link diffusion coefficients from atomistic and CG simulations at higher temperatures (between 503 and 593 K) by determining time scaling factors. By extrapolating these time scaling factors to lower temperatures, the CG diffusion coefficients can be quantitatively compared to experimental data. The time scaling factor $s(T)$ is the ratio between the diffusion coefficients from CG and atomistic simulations (see above):

$$s(T) = D_{\mathrm{CG}}(T)/D_{\mathrm{AA}}(T) \tag{5.8}$$

In a first step the diffusion coefficients that are obtained from CG simulations in a temperature range between 398 and 593 K (The CG model was developed at 503 K) are analyzed. It is known that CG simulations for polymer dynamics can reproduce the characteristic Vogel-Fulcher behavior of diffusivity and bead friction exhibited by glass forming polymers. [66] A Vogel-Fulcher functional form, $D_{\mathrm{CG}}(T) = c\exp(-A/k(T - T_{\mathrm{VF}}))$, can be fitted to the CG data very well and delivers a $T_{\mathrm{VF}} = 185 \pm 30\,\mathrm{K}$ (see Figure 5.14). Even though the diffusion of additives and not the one of the long polymer chains is studied here, the observed Vogel-Fulcher behavior reflects that the mobility of additives is

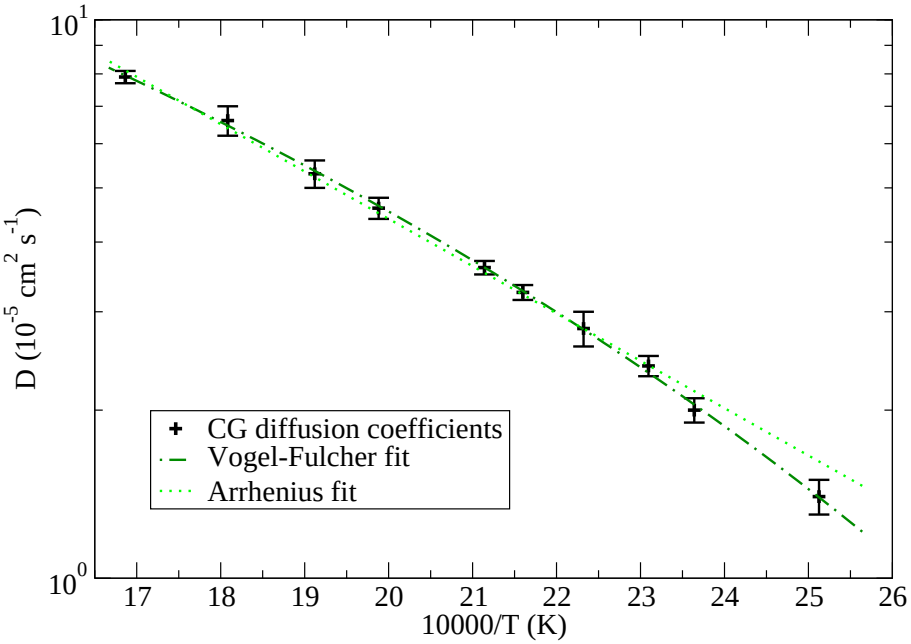

Figure 5.14: Fits of an Arrhenius and a Vogel-Fulcher form to the CG diffusion coefficients of 10% EB in PS. The diffusion coefficients for these CG systems are not scaled to match with diffusion coefficients of atomistic systems.

linked to the structural relaxation of the polymer melt, which includes the formation and destruction of larger cavities. This process happens on much larger time scales than the local spatial fluctuations of EB in these rather rugged cavities. [102]

If one assumes that in the atomistic simulations the connection between penetrant diffusivity and structural relaxations of the melt is the same as in the case of CG simulations (in section 5.1.4 it was shown that on the time scale, where the MSD of the EB molecules reaches a diffusive regime, the MSD of the PS beads exhibits a displacement of the order of at least half a bead size in both, AA and CG simulations, but the displacement for CG systems was higher by a factor of 2) and if one assumes the same Vogel-Fulcher temperature T_{VF} for the atomistic case, where the data are not sufficient to fit it directly, then the temperature dependence of the time scaling factor $s(T)$ also follows the Vogel-Fulcher equation:

$$s_{VF}(T) = c_{VF} \exp\left(\frac{A_{VF}}{k(T - T_{VF})}\right) \tag{5.9}$$

This assumption is compared with another empirical way to describe the temperature dependence of $s(T)$, which is the Arrhenius equation:

$$s_{Arrh}(T) = c_{Arrh} \exp\left(\frac{A_{Arrh}}{kT}\right) \tag{5.10}$$

These functional forms are used to fit s at high temperatures (above 500 K). In Figure 5.15 the fits for the Vogel-Fulcher form ($c_{VF} = 0.062 \pm 0.008$; $A_{VF}/k = 1952 \pm 50$ K; $T_{VF} =$

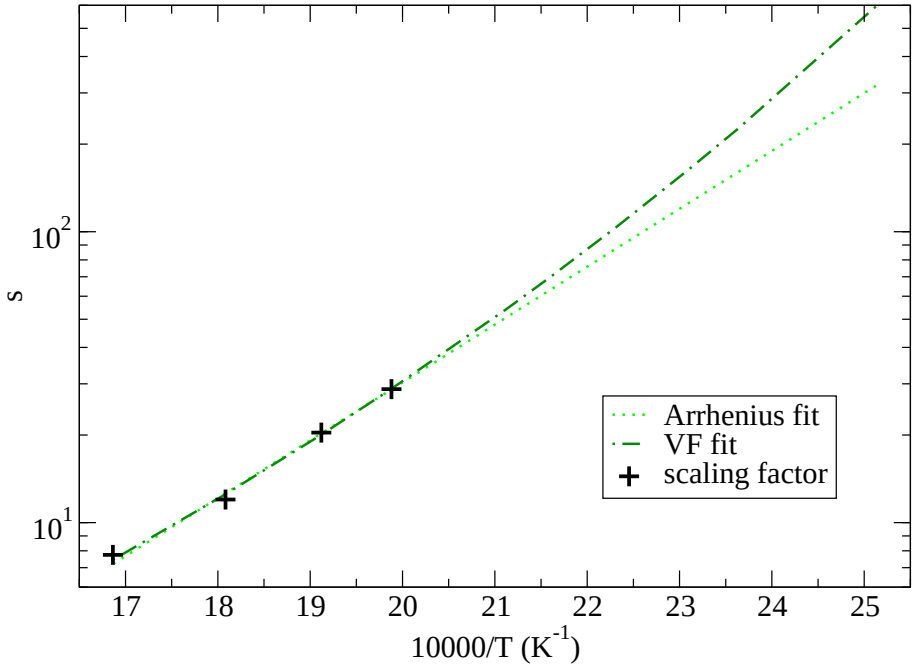

Figure 5.15: Fits of the time scaling factors $s = D_{CG}^{EB}/D_{AA}^{EB}$, obtained from the diffusion coefficients of EB.

185 K is set fixed) and for the Arrhenius form ($c_{Arrh} = 0.0032 \pm 0.001$; $A_{Arrh}/k = 4580 \pm 180$ K) are shown.

Applying the two relations for the time scaling factor from eq. 5.9 and 5.10 to the CG diffusion coefficients, they can be extrapolated to predict diffusion coefficients of the all-atom model D_{AA} in the range of experimental temperatures. These diffusion coefficients are shown in Figure 5.16. The scaled CG diffusion coefficients agree with the atomistic ones for the four temperatures above 503 K, to which the time scaling factor was fitted.

The comparison of the CG simulations to experimental diffusion coefficients [88] shows a clear vertical shift. The scaled diffusivities D_{CG} are too low by a factor of 7 (at all temperatures) for the Vogel-Fulcher scaling and by a factor between 7 (at high temperature) and 3 (at low temperature) for the Arrhenius scaling. It is remarkable that the Vogel-Fulcher scaling predicts a temperature dependence which is in perfect agreement with the experimental data, whereas the Arrhenius scaling predicts higher diffusivities for low temperatures. This is a clear indication that the CG model takes into account the structural aspects of the polymer matrix, which are responsible for the non-Arrhenius behavior of the dynamics, but the non-Arrhenius behavior also has to be taken into account for the time scaling factor $s(T)$.

To judge the quality of the simulation results, two characteristic differences to an experimental setup have to be considered, due to which simulated diffusion coefficients are expected to be lower compared to experimental ones. First, the experimental sample is polydisperse ($M_W/M_n = 1.07$). [88] The presence of shorter chains in the experimental system contributes to faster dynamics, the extent of which can be large but probably

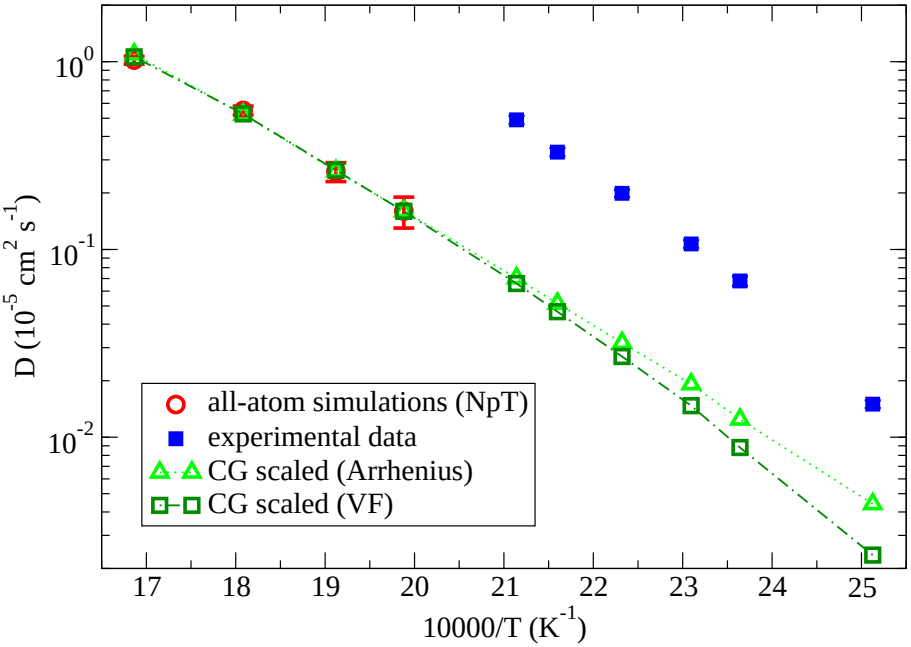

Figure 5.16: Diffusion coefficients from experiments, [88] all-atom simulations and CG simulations. CG data are scaled, using an Arrhenius and a Vogel-Fulcher (VF) form for the temperature dependence of the scaling factor.

not sufficient to explain the downward shift observed in Figure 5.16. The CG simulation with a polydisperse PS matrix requires a careful study of the time scaling behavior of these systems concerning the different time scaling factors for components with different molecular weight (as presented for two-component mixtures in sections 5.1.3 and 5.1.4). The second cause explaining the lower diffusion coefficients obtained from simulations is the density of the system, which is predicted 2-4% larger in comparison with experiment by the all-atom force field used in this work.[3] This is not only an effect of the all-atom force field but also a consequence of the presence of short chains in experimental samples. A slight overestimation of the density has a strong effect on the system dynamics and easily explains a factor of 7. We note that in a recent work based on the same all-atom model, all systems were simulated at constant volume corresponding to the experimental density. [85] There, a perfect agreement was obtained between the simulated and experimental polymer diffusion coefficients.

This strategy can also be applied in this case: In a first step, the temperature dependence of the diffusion coefficients, and by that also of the scaling factor $s(T)$, is simulated in NpT simulations, which describe the thermal expansion of the systems correctly. In a second step, the atomistic system at a single temperature is simulated in a constant volume simulation at a density corresponding to the experimental one. The difference of the

[3] Experimental density data for the EB/PS mixture are not available. But the density of the PS system without EB can be compared (at 503 K): The experimental density for PS (M_W = 9000 g/mol) is ρ_{exp} = 934 kg/m^3 [84], the density from atomistic NpT simulations is ρ_{AA} = 970 kg/m^3 for pure PS (M_W = 9984 g/mol) and $\rho_{\text{AA}}^{\text{EB/PS}}$ = 952 kg/m^3 for the EB/PS system.

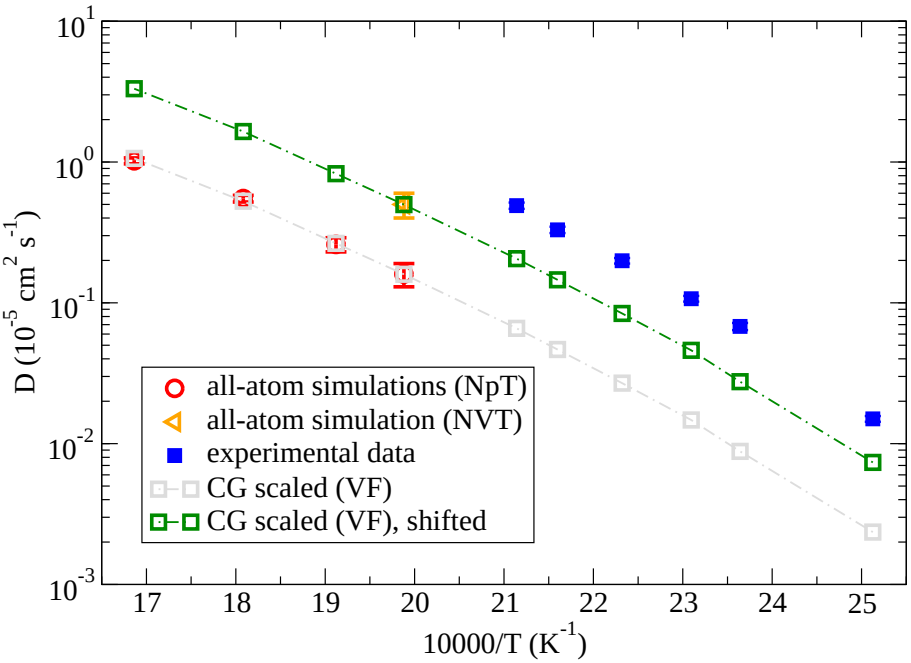

Figure 5.17: Diffusion coefficients from experiments, [88] NpT all-atom simulations and from CG simulations scaled with a Vogel-Fulcher (VF) form for the temperature dependence of the scaling factor. In addition, a diffusion coefficient from an NVT all-atom simulation at a density of 910 kg/m^3 (estimated density of the experimental sample) and 503 K is given, which defines a shift of the CG data.

atomistic diffusion coefficients between the NVT and the NpT simulation yields a factor, by which the extrapolated diffusion coefficients at *all* temperatures can be shifted. Following this method, the changes in density, and by that the whole temperature dependence of $D(T)$ and $s(T)$, are still obtained as predictions of the atomistic model, but the absolute value of $D(T)$ is "tuned" to fit closer to experimental conditions.

Simulating the PS/EB mixture under NVT conditions at a temperature of 503 K and a density of 910 kg/m^3, which is chosen based on the experimental density of the pure polymer (and taking into account a solvent swelling contribution obtained from the simulations) reduces the discrepancy between simulated and experimental diffusion data to a factor of 2, see Figure 5.17.

As mentioned above, using a polydisperse PS melt to host the EB molecules could be done in future work and would increase the simulated diffusion coefficients further. Moreover, this would extend the previously discussed aspects of time scaling in two-component mixtures (sections 5.1.3 and 5.1.4) to many-component systems.

Taking into account these two aspects of density and polydispersity the agreement between simulated and experimental diffusion coefficients is excellent. Hence, the hierarchical simulation approach outlined here to quantitatively obtaining penetrant diffusion data from CG simulations follows a sequence of well-defined procedures that may find potential future application in modeling diffusion in complex fluids.

Conclusion

A coarse-graining methodology for melts of linear polymer chains has been presented and applied to the case of polystyrene. Two new concepts were pursued in the CG model development, which turned out to improve the agreement of static properties of polymer melts with the underlying atomistic model. New components of the CG model are the introduction of longer-ranged intrachain potentials and the development of interchain potentials without atomistic melt systems as reference.

The longer-ranged intrachain potentials lead to a better control of the chain stiffness and to a description of local chain conformations in agreement with the detailed atomistic model. Local conformations depend strongly on the tacticity of the chain, i.e. on the stereochemical orientation of neighboring monomers, where side groups can be oriented randomly or in an ordered fashion. The correct description of local chain conformations allows the CG model to capture effects that are related to the local packing of chain segments. Due to the reproduction of the chain stiffness overall chain dimensions are described in agreement with the detailed atomistic model. Furthermore, they agree as well with experimental results for the characteristic ratio C_∞ for polystyrene of different tacticities.

The method to obtain longer-ranged intrachain potentials is especially useful for coarse-grained models, which use a mapping scheme that is close to the chemical structure (as in the presented case). In these systems the basic assumption of completely uncorrelated coarse-grained degrees of freedom is often not valid. However, the general method of structure-based coarse-graining can still be used, if the CG model is constructed in a way that takes into account these correlations and reproduces them also in the CG simulations.

The development of the CG interchain interaction potentials is based on the sampling of pairs of oligomers in vacuum. The presented method does not use atomistic melt structures as a reference system. Structure properties of melts are obtained as predictions of the CG model in contrast to other structure-based CG models, which are iteratively refined to reproduce the melt structure. Furthermore, the development of the CG potentials is computationally cheap, because no expensive atomistic melt simulations are needed. The presented CG model for polystyrene describes the melt packing and reproduces the density at ambient pressure between 400 K and 520 K in good agreement with the atomistic model.

The development of CG potentials from chain segments under vacuum conditions instead of melt conditions (which are, however, correctly reproduced) suggests a higher transferability of this CG method. Its application to further problems, such as two- or multi-component systems (blends, polymer/solvent mixtures) or polymer surfaces, appears promising.

The dynamics of CG systems have to be linked with the dynamics on the atomistic scale to obtain quantitative results. The connection of the CG and the atomistic time scale can be described by a time scaling factor, which depends on several specific system properties as molecular weight, density, temperature and other components in mixtures. The influence of selected aspects has been investigated in this thesis. In short oligomer melts the time scaling factor depends strongly on the molecular weight. In mixtures of two components the scaling factors can be different for each component, but it is still possible to obtain quantitative results: In mixtures of long polymer chains and small additive molecules the additive diffusion has been shown to obey a Vogel-Fulcher temperature dependency, which is also found experimentally, reflecting the importance of the motion of the chains for the motion of the additive.

CG simulations of polystyrene melts with different tacticities have been presented to demonstrate the applicability of the CG model to study dynamics in polymer melts. The influence of the tacticity on the dynamics of entangled systems has not been studied before. With the presented CG model it is possible to study this question and to gain more understanding how local, chemically specific conformations influence universal properties of polymer melts.

A Appendix

A.1 Simulation details of atomistic systems

For all atomistic simulations presented in this thesis an all-atom model has been used, which was adapted by Müller-Plathe to describe benzene-polystyrene systems. [3, 4] The model contains previously developed parameters [5, 6] and an adapted potential to describe torsional rotations properly. A description of the typical term of this force field has been given in section 1.2.1, the parameters of the force field are listed in the Appendix A.4.

Every PS monomer is described by 16 atoms. Atomistic bond lengths are constrained in all systems using the LINCS method (see section 1.3.2). Cutoff corrections were applied to energy and pressure using standard analytical expressions that assume a uniform density beyond the cutoff (see section 1.2.2), except for the simulations of isolated chains or pairs of oligomers in vacuum.

The tacticity of PS in the atomistic simulations depends on the initial configuration of the chains and does not change in the course of a simulation due to a high steric barrier. If a certain tacticity for a chain is needed, i.e. a defined sequence of meso and racemo diads, it can be imposed on the chain by applying improper dihedral potentials, which control the orientation of the phenyl rings. This is used for example during the backmapping procedure, where the atomistic chain, which is introduced in place of the CG chain, should have exactly the same tacticity.

All simulations reported in this thesis were performed using the molecular dynamics package GROMACS. [103]

A.1.1 Sampling of isolated chains

The sampling of atomistic chains in vacuum is done with atomistic PS chains of 25 monomers with different tacticities (isotactic, syndiotactic, block tacticity of alternating meso and racemo diads). The chain is simulated without periodic boundary conditions. For the sampling the stochastic dynamics (SD) method (see section 1.3.3) is used, which adds a friction and a noise term to the equations of motion. The reference temperature was set to 503 K and the inverse friction constant to $1/\xi_i = 0.1$ ps. For all nonbonded interactions a cutoff distance of 1 nm was used, without consideration of Coulombic interactions beyond the cutoff. At the cutoff charge groups were used to avoid artifacts caused by dipoles, which have one charge within the cutoff and the opposite charge outside. These dipoles were always considered to be in or out of the cutoff together. Since only one chain in vacuum was simulated, angular motion of the system was removed every few ps. The integration time step was 1 fs. The systems were simulated for 100 ns.

A.1.2 Sampling of isolated oligomer pairs

The sampling of atomistic pairs of oligomers in vacuum is done with atomistic PS chain segments of three or four monomers with isotactic tacticity. The systems are simulated without periodic boundary conditions. For the sampling the stochastic dynamics (SD) method (see section 1.3.3) is used, which adds a friction and a noise term to the equations of motion. The reference temperature was set to 503 K and the inverse friction constant to $1/\xi_i = 0.5$ ps. For all nonbonded interactions a cutoff distance of 1.8 nm was used, without consideration of Coulombic interactions beyond the cutoff. Since only one pair of oligomers in vacuum is simulated, angular motion of the system is removed every few ps. The distance between the centers of mass of the two groups of atoms, corresponding to the CG beads of interest, was constrained in a range of distances between 0.2 and 1.2 nm. Simulation runs were performed for all distances in steps of 0.02 nm. The integration time step was 1 fs. The systems were simulated for 12 ns at each distance.

A.1.3 10-mer melts

In the following paragraph technical details of the AA simulations presented in chapter 4 are given.

The simulated AA systems contain 56 chains of 10 monomers. Melts of atactic, isotactic and syndiotactic PS were simulated. For atactic systems five different random sequences of meso and racemo diads were used, the number of both types of diads is approximately the same. The initial configurations for the iso- and syndiotactic systems have been obtained by randomly placing 56 single chains in a box and slowly switching on the nonbonded interactions. For the atactic system an existing configuration, kindly provided by Milano and Müller-Plathe, was used. In principle, it is also possible to obtain atomistic configurations by backmapping CG configurations.

For nonbonded interactions a cutoff distance of 1 nm was used. Coulombic interactions beyond the cutoff were treated by reaction-field correction with a dielectric constant ϵ_{RF} of 2.5. The melts were simulated under isothermal-isobaric (NpT) conditions at various temperatures and 1 atm using the Berendsen thermostat (coupling time 0.2 ps) and barostat (coupling time 2.0 ps). The integration time step was 1 fs.

After the first equilibration of the systems production runs of 400 ns were performed for the systems at 503 K. To check the density dependence on temperature, shorter runs of 10 ns were performed. All systems are listed in table A.1.

tacticity	T (K)	C_N	ρ (kg m^{-3})
atactic	503	6.09	959
isotactic	503	6.12	956
syndiotactic	503	7.70	959
atactic	403		1004 ± 2
atactic	423		1000 ± 3
atactic	443		989 ± 5
atactic	463		980 ± 5
atactic	483		969 ± 5
atactic	503		960 ± 5
atactic	523		947 ± 5

Table A.1: Atomistic PS 10-mer systems: Shown are the tacticity of the chains, the temperature T as well as the resulting characteristic ratio between the two end beads of the chain C_N (where $N = 2N_{\text{Monomers}} - 1$, $N = 19$ in this case) and the density ρ.

A.1.4 Oligomer melts

In this paragraph technical details of the AA simulations presented in section 5.1.2 and 5.1.4 are given.

Each AA system contains the same number of 480 monomers (distributed onto $480/N$ oligomers of N monomers each), which was chosen as a common multiple of all N's studied. Therefore, at a given density each cubic simulation box has exactly the same volume. Initial coordinates for the atomistic systems were obtained by inverse mapping of atomistic details into equilibrated CG systems, which are described in section A.2.3.

In a first series of runs systems of isotactic and syndiotactic PS oligomers were simulated under NVT conditions at a temperature of 503 K and at a density, which was obtained by a NpT simulation for each system (Berendsen thermostat at 1 atm, coupling time 5 ps). The box sizes are between $L = 4.43$ and 4.52 nm. The velocity rescaling thermostat (coupling time 0.2 ps) was used. For nonbonded interactions a cutoff distance of 1 nm was used. Coulombic interactions beyond the cutoff were treated by the particle-mesh Ewald (PME) method with a direct-space cutoff of 1 nm and a grid spacing of 0.12 nm. The integration time step was 1 fs.

For the isotactic systems a second series of simulations was performed under the above described conditions, but the density of all systems was set to the same value of 955 kg/m^3 (the value of the isotactic 10-mer systems from the previous NpT simulation).

All atomistic (one component) oligomer systems are listed in table A.2.

N_{Monomers}	N_{chains}	tacticity	sim. time (ns)	D^{AA} ($10^{-5}\text{cm}^2\text{s}^{-1}$)	ρ (kg m^{-3})
3	160	isotactic	10	0.61 ± 0.04	906
4	120	isotactic	20	0.23 ± 0.01	925
5	96	isotactic	25	0.095 ± 0.005	935
6	80	isotactic	25	0.051 ± 0.005	943
8	60	isotactic	25	0.012 ± 0.005	954
10	48	isotactic	25	0.006 ± 0.002	955
3	160	syndiotactic	10	0.59 ± 0.04	905
4	120	syndiotactic	20	0.23 ± 0.01	925
5	96	syndiotactic	25	0.10 ± 0.01	936
6	80	syndiotactic	25	0.046 ± 0.005	943
8	60	syndiotactic	25	0.012 ± 0.002	952
10	48	syndiotactic	25	0.004 ± 0.001	959
2	240	isotactic	40	0.65 ± 0.05	955
3	160	isotactic	60	0.26 ± 0.02	955
4	120	isotactic	60	0.11 ± 0.01	955
5	96	isotactic	80	0.053 ± 0.002	955
6	80	isotactic	100	0.030 ± 0.002	955
8	60	isotactic	110	0.012 ± 0.002	955
10	48	isotactic	200	0.004 ± 0.001	955

Table A.2: Simulated atomistic one-component oligomer systems: Shown are the number of repeat units per chain N_{Monomers}, the number of chains in the simulation box N_{chains}, the tacticity of the chains, the simulation time, the diffusion coefficients D^{AA} and the density ρ.

A.1.5 Oligomer mixtures

In this paragraph technical details of the AA simulations of systems of two oligomer components, presented in section 5.1.3, are given.

As for the one-component oligomer systems each AA system contains the same number of 480 monomers, distributed onto isotactic oligomers of two different molecular weights (Dimer and 6-mer mixtures or Trimer and 10-mer mixtures).

Initial coordinates for the atomistic systems were obtained by inverse mapping of atomistic details into equilibrated CG systems, which are described in section A.2.4.

All systems of isotactic PS oligomer mixtures were simulated under NVT conditions at a temperature of 503 K and at the fixed density of 955 kg/m^3, which was used before for one-component oligomers. The velocity rescaling thermostat (coupling time 0.2 ps) was used. For nonbonded interactions a cutoff distance of 1 nm was used. Coulombic interactions beyond the cutoff were treated by the particle-mesh Ewald (PME) method with a direct-space cutoff of 1 nm and a grid spacing of 0.12 nm. The integration time step was 1 fs. The production runs were performed for 75 ns for the 2-mer/6-mer systems and between 170 and 200 ns for the 3-mer/10-mer systems.

The two-component oligomer systems are listed in table A.3 and A.4.

$N_{2\text{-mer}}$	$N_{6\text{-mer}}$	$w_{\text{M, 2-mer}}$	$w_{\text{mol, 2-mer}}$	$D^{\text{AA}}_{2\text{-mer}}$ ($10^{-5}\text{cm}^2\text{s}^{-1}$)	$D^{\text{AA}}_{6\text{-mer}}$ ($10^{-5}\text{cm}^2\text{s}^{-1}$)
60	60	0.25	0.5	0.29 ± 0.04	0.073 ± 0.006
120	40	0.50	0.75	0.43 ± 0.02	0.14 ± 0.01
180	20	0.75	0.9	0.57 ± 0.03	0.18 ± 0.01

Table A.3: Simulated atomistic two-component oligomer mixtures of Dimers and 6-mers: Shown are the numbers of oligomers of the two components $N_{2\text{-mer}}$ and $N_{6\text{-mer}}$, the fraction of the smaller component expressed by the weight fraction $w_{\text{M, 2-mer}}$ and the molar fraction $w_{\text{mol, 2-mer}}$, and the diffusion coefficients of both components $D^{\text{AA}}_{2\text{-mer}}$ and $D^{\text{AA}}_{6\text{-mer}}$.

$N_{3\text{-mer}}$	$N_{10\text{-mer}}$	$w_{\text{M, 3-mer}}$	$w_{\text{mol, 3-mer}}$	$D^{\text{AA}}_{3\text{-mer}}$ ($10^{-5}\text{cm}^2\text{s}^{-1}$)	$D^{\text{AA}}_{10\text{-mer}}$ ($10^{-5}\text{cm}^2\text{s}^{-1}$)
40	36	0.25	0.53	0.072 ± 0.008	0.018 ± 0.002
80	24	0.50	0.77	0.13 ± 0.02	0.037 ± 0.003
120	12	0.75	0.91	0.19 ± 0.05	0.055 ± 0.006

Table A.4: Simulated atomistic two-component oligomer mixtures of Trimers and 10-mers: Shown are the numbers of oligomers of the two components $N_{3\text{-mer}}$ and $N_{10\text{-mer}}$, the fraction of the smaller component expressed by the weight fraction $w_{\text{M, 3-mer}}$ and the molar fraction $w_{\text{mol, 3-mer}}$, and the diffusion coefficients of both components $D^{\text{AA}}_{3\text{-mer}}$ and $D^{\text{AA}}_{10\text{-mer}}$.

A.1.6 PS melt, 10kDa

In this paragraph technical details of the AA simulation of a PS melt with molecular weight M_W =9984 g/mol (96 monomers) presented in section 5.1.4 are given.

The PS melt consists of 24 atactic PS chains with a length of 96 repeat units. Initial coordinates for the atomistic systems were obtained by inverse mapping of atomistic details into an equilibrated CG system, which is described in section A.2.5.

The system was simulated under NpT conditions at a temperature of 503 K and a pressure of 1 atm using the Berendsen thermostat (coupling time 1.0 ps) and barostat (coupling time 5.0 ps), resulting in an average density of $\rho = 968 \pm 3\,\text{kg/m}^3$ and a cubic boxsize L^3 with $L = 7.43\,\text{nm}$. For nonbonded interactions a cutoff distance of 1 nm was used. Coulombic interactions beyond the cutoff were treated by the particle-mesh Ewald (PME) method with a direct-space cutoff of 1 nm and a grid spacing of 0.12 nm. The integration time step was 1 fs. The production run was performed for 16 ns.

A.1.7 EB/PS systems

In the following paragraph technical details of the AA simulations presented in section 5.1.4 and 5.3 are given.

The mixed systems of ethylbenzene (EB) and polystyrene (PS) consist of 24 atactic PS chains with a length of 96 repeat units ($M_W = 9984\,\text{g/mol}$) and of 256 EB molecules ($M_W = 106\,\text{g/mol}$). This corresponds to an EB weight fraction w_{EB} of 10%.

Initial coordinates for the atomistic systems were obtained by inverse mapping of atomistic details into equilibrated CG systems, which are described in section A.2.7.

The mixed EB/PS systems were simulated under isothermal-isobaric (NpT) conditions at temperatures between 503 K and 593 K. The velocity rescaling thermostat (coupling time 0.2 ps) was used independently for PS and EB. The Berendsen barostat (coupling time 5.0 ps) was used, resulting in cubic boxsizes L^3 with $L = 7.75$ nm up to $L = 7.91$ for the different temperatures. For nonbonded interactions a cutoff distance of 1 nm was used. Coulombic interactions beyond the cutoff were treated by the particle-mesh Ewald (PME) method with a direct-space cutoff of 1 nm and a grid spacing of 0.12 nm. The integration time step was 1 fs.

One additional simulation was performed at constant volume (NVT) with a density of 910 kg/m^3. The simulated systems are listed in table A.5.

T (K)	simulation time (ns)	$D_{\mathrm{EB}}^{\mathrm{AA}}$ (10^{-5}cm^{2}s^{-1})	ρ (kg m^{-3})
503	28	0.16 ± 0.03	953 ± 2
523	10	0.26 ± 0.03	942 ± 3
553	10	0.55 ± 0.03	922 ± 3
593	8	1.02 ± 0.05	897 ± 4
503	4	0.6 ± 0.1	910 (NVT)

Table A.5: Simulated atomistic systems of PS/EB: For different temperatures the simulation times, the EB diffusion coefficients $D_{\mathrm{EB}}^{\mathrm{AA}}$ and the densities ρ are given.

A.2 Simulation details of coarse-grained systems

The coarse-grained MD simulations in this work are performed with the CG model that has been presented in this thesis. For the CG simulations the MD package GROMACS has been used. [103] All interaction potentials were used in a tabulated form.

All times and dynamical properties, e.g. mean square displacements or diffusion coefficients, are given in real CG times, i.e. they have to be scaled in order to be compared directly to atomistic times or dynamical quantities.

The tacticity of the CG chains is implemented in the topology of the CG chains. For details see section A.3.

A.2.1 Sampling of isolated chains

The sampling of CG chains in vacuum is done with PS chains of 25 monomers with different tacticities (isotactic, syndiotactic, block tacticity of alternating meso and racemo diads). The chain is simulated without periodic boundary conditions. For the sampling the stochastic dynamics (SD) method (see section 1.3.3) is used, which adds a friction and a noise term to the equations of motion. The reference temperature was set to 503 K and the inverse friction constant to $1/\xi_i = 0.1$ ps. For nonbonded interactions a cutoff distance of 1 nm was used. Since only one chain in vacuum is simulated, angular motion of the

system is removed every few ps. The integration time step was 2 fs. The systems were simulated for 200 ns.

A.2.2 10-mer melts

In the following paragraph technical details of the CG simulations presented in chapter 4 and section 5.2 are given.

The simulated CG systems contain 56 chains of 10 monomers. Melts of atactic, isotactic and syndiotactic PS were simulated. For atactic systems the same five different random sequences of meso and racemo diads as for the AA systems were used. The setup of the starting configurations for the CG melts of these relatively short chains is not critical, because the chains move their own size during a first equilibration run of a few ns.

CG melts were simulated under isothermal-isobaric (NpT) conditions at 503 K and 1 atm using the Berendsen thermostat (coupling time 0.4 ps) and barostat (coupling time 4.0 ps). A second series of runs was performed at varying temperatures between 403 and 523 K. For nonbonded interactions a cutoff distance of 1 nm was used. The integration time step was 3 fs.

CG melts at 503 K with isotactic, syndiotactic and atactic tacticity were simulated for 15 ns. The CG 10-mer systems are presented in table A.6.

tacticity	T (K)	C_N	ρ (kg m^{-3})
atactic	503	6.21	964 ± 3
isotactic	503	6.30	968 ± 4
syndiotactic	503	7.59	962 ± 3
atactic	403	6.97	1010 ± 3
atactic	423	6.73	1001 ± 3
atactic	443	6.55	992 ± 3
atactic	463	6.48	983 ± 4
atactic	483	6.25	973 ± 4
atactic	503	6.23	964 ± 3
atactic	523	6.06	954 ± 3

Table A.6: Coarse grained PS 10-mer systems: Shown are the tacticity of the chains, the temperature T as well as the resulting characteristic ratio between the two end beads of the chain C_N (where $N = 2N_{Monomers} - 1$, $N = 19$ in this case) and the density ρ.

A.2.3 Oligomer melts

In this paragraph technical details of the CG simulations presented in section 5.1.2 and 5.1.4 are given.

Each CG system contains the same number of 480 monomers (distributed onto $480/N$ oligomers of N monomers each), which was chosen as a common multiple of all N's studied. Initial coordinates were obtained by randomly placing the oligomers in the simulation

box. During an initial equilibration run the molecules already move distances comparable to their own size.

In a first series of runs systems of isotactic and syndiotactic PS oligomers were simulated under NVT conditions at a temperature of 503 K and at the densities of the corresponding AA systems. The velocity rescaling thermostat (coupling time 0.2 ps) was used. For nonbonded interactions a cutoff distance of 1 nm was used. The integration time step was 3 fs.

For the isotactic systems a second series of simulations was performed under the above described conditions, but the density of all systems was set to the same value of 955 kg/m^3 (the value of the isotactic AA 10-mer systems from the previous NpT simulation). Furthermore, the system size was increased by replicating the system twice in each direction, thereby increasing the number of molecules by a factor of 8. The simulation box then has sides of $L = 8.87$ nm.

All (one component) oligomer systems are listed in table A.7.

N_{Monomers}	N_{chains}	tacticity	sim. time (ns)	D^{CG} (10^{-5}cm^{2}s^{-1})	ρ (kg m^{-3})
3	160	isotactic	60	4.0 ± 0.2	906
4	120	isotactic	60	2.7 ± 0.1	925
5	96	isotactic	60	1.9 ± 0.1	935
6	80	isotactic	60	1.35 ± 0.1	943
8	60	isotactic	60	0.85 ± 0.1	954
10	48	isotactic	60	0.6 ± 0.1	955
3	160	syndiotactic	60	4.0 ± 0.2	905
4	120	syndiotactic	60	2.9 ± 0.3	925
5	96	syndiotactic	60	2.1 ± 0.1	936
6	80	syndiotactic	60	1.5 ± 0.1	943
8	60	syndiotactic	60	0.98 ± 0.05	952
10	48	syndiotactic	60	0.66 ± 0.04	959
2	1920	isotactic	72	5.4 ± 0.1	955
3	1280	isotactic	72	3.65 ± 0.05	955
4	960	isotactic	72	2.63 ± 0.05	955
5	768	isotactic	72	1.95 ± 0.1	955
6	640	isotactic	72	1.5 ± 0.05	955
8	480	isotactic	72	1.0 ± 0.05	955
10	384	isotactic	72	0.71 ± 0.03	955

Table A.7: Simulated CG one-component oligomer systems: Shown are the number of repeat units per chain N_{Monomers}, the number of chains in the simulation box N_{chains}, the tacticity of the chains, the simulation time, the diffusion coefficients D^{CG} and the density ρ.

A.2.4 Oligomer mixtures

In this paragraph technical details of the CG simulations of systems of two oligomer components presented in section 5.1.3 are given.

To obtain configurations for the inverse mapping, each CG system was set up with the same number of 480 monomers, distributed onto isotactic oligomers of two different molecular weights (Dimer and 6-mer mixtures or Trimer and 10-mer mixtures). Initial coordinates were obtained by randomly placing the oligomers in the cubic simulation box of volume L^3 with $L = 4.43\,\text{nm}$. During an initial equilibration run the molecules already move distances comparable to their own size. For the CG production runs the system sizes was increased by replicating the system twice in each direction, thereby increasing the number of molecules by a factor of 8 and the boxsize to $L = 8.87\,\text{nm}$.

All CG systems of isotactic PS oligomer mixtures were simulated under NVT conditions at a temperature of 503 K and at the fixed density of $955\,\text{kg/m}^3$, which was used before for one-component oligomers. The velocity rescaling thermostat (coupling time 0.2 ps) was used for each of the two components independently. For nonbonded interactions a cutoff distance of 1 nm was used. The integration time step was 3 fs. The production runs were performed for 72 ns for all mixed systems.

The CG two-component oligomer systems are listed in table A.8 and A.9.

$N_{\text{2-mer}}$	$N_{\text{6-mer}}$	$w_{\text{M, 2-mer}}$	$w_{\text{mol, 2-mer}}$	$D^{\text{CG}}_{\text{2-mer}}$ ($10^{-5}\text{cm}^2\text{s}^{-1}$)	$D^{\text{CG}}_{\text{6-mer}}$ ($10^{-5}\text{cm}^2\text{s}^{-1}$)
480	480	0.25	0.5	4.2 ± 0.3	1.85 ± 0.05
960	320	0.50	0.75	4.7 ± 0.2	2.1 ± 0.1
1440	160	0.75	0.9	5.1 ± 0.1	2.4 ± 0.2

Table A.8: Simulated CG two-component oligomer mixtures of Dimers and 6-mers: Shown are the numbers of oligomers of the two components $N_{\text{2-mer}}$ and $N_{\text{6-mer}}$, the fraction of the smaller component expressed by the weight fraction $w_{\text{M, 2-mer}}$ and the molar fraction $w_{\text{mol, 2-mer}}$, and the diffusion coefficients of both components $D^{\text{CG}}_{\text{2-mer}}$ and $D^{\text{CG}}_{\text{6-mer}}$. The diffusion coefficients D^{CG} for these CG systems are not scaled.

$N_{\text{3-mer}}$	$N_{\text{10-mer}}$	$w_{\text{M, 3-mer}}$	$w_{\text{mol, 3-mer}}$	$D^{\text{CG}}_{\text{3-mer}}$ ($10^{-5}\text{cm}^2\text{s}^{-1}$)	$D^{\text{CG}}_{\text{10-mer}}$ ($10^{-5}\text{cm}^2\text{s}^{-1}$)
320	288	0.25	0.53	2.45 ± 0.05	0.95 ± 0.05
640	192	0.50	0.77	2.9 ± 0.05	1.15 ± 0.05
960	96	0.75	0.91	3.3 ± 0.1	1.4 ± 0.05

Table A.9: Simulated CG two-component oligomer mixtures of Trimers and 10-mers: Shown are the numbers of oligomers of the two components $N_{\text{3-mer}}$ and $N_{\text{10-mer}}$, the fraction of the smaller component expressed by the weight fraction $w_{\text{M, 3-mer}}$ and the molar fraction $w_{\text{mol, 3-mer}}$, and the diffusion coefficients of both components $D^{\text{CG}}_{\text{3-mer}}$ and $D^{\text{CG}}_{\text{10-mer}}$. The diffusion coefficients D^{CG} for these CG systems are not scaled.

A.2.5 PS melt, 10kDa

In this paragraph technical details of the CG simulation of a PS melt with molecular weight $M_W = 10$ kDa presented in section 5.1.4 and 5.2 are given.

The PS melt consists of 24 atactic PS chains with a length of 96 repeat units (192 CG beads, 96 monomers, M_W =9984 g/mol = 10 kDa). Four different random sequences of meso and racemo diads were used, the number of both types of diads is approximately the same. The initial configuration was obtained by randomly placing 24 chains with independent conformations in a simulation box at a density, which was about 20% below the final density. After a short steepest descent run, which removes strong overlaps between the molecules, the system reaches the final density in a NpT run of 2.5 ns. Afterwards the system is simulated for around 100 ns. During this simulation the internal distances are monitored and are found to agree with the previously simulated value of C_∞, indicating that the chain conformations are equilibrated. This procedure has been repeated at temperatures of 423, 463 and 503 K.

The CG system was simulated under NpT conditions at 503 K and 1 atm using the Berendsen thermostat (coupling time 0.5 ps) and barostat (coupling time 5.0 ps), resulting in a density of 1032 ± 2 kg/m^3 and a cubic boxsize L^3 with $L = 7.28$ nm. For nonbonded interactions a cutoff distance of 1 nm was used. The integration time step was 3 fs. The simulation time of the production run was 1080 ns.

A.2.6 PS melt, 20kDa

In the following paragraph technical details of the CG simulations presented in chapter 4 and section 5.2 are given.

The systems consist of 50 chains of polystyrene (384 CG beads, 192 monomers, M_W = 20000 g/mol = 20 kDa) with three different tacticities (atactic, isotactic and syndiotactic). As an initial configuration for the melts of long chains an atactic system was used, which was equilibrated with a previous CG model for PS, using the setup as described there. [55, 104]

The three systems were simulated under NpT conditions at 503 K and 1 atm using the Berendsen thermostat (coupling time 0.4 ps) and barostat (coupling time 4.0 ps) for 300 ns and then simulated under NVT conditions at the average density of these first 300 ns. The size of the cubic simulation box L^3 was $L = 11.71$ nm. For nonbonded interactions a cutoff distance of 1 nm was used. The integration time step was 3 fs. The simulation times of the production runs were between 1500 and 2000 ns. The simulated systems are listed in table A.10.

N_{Monomers}	N_{chains}	tacticity	T (K)	C_{N}	ρ (kg m^{-3})
192	50	atactic	503	7.80 ± 0.38	1035
192	50	isotactic	503	8.91 ± 0.30	1040
192	50	syndiotactic	503	12.27 ± 0.30	1031

Table A.10: Coarse grained PS systems (20kDa) studied in this work: Reported are the number of repeat units per chain N_{Monomers}, the number of chains in the simulation box N_{chains}, the tacticity of the chains, the temperature T as well as the resulting characteristic ratio between the two end beads of the chain C_{N} (where $N = 2N_{\text{Monomers}} - 1$) and the density ρ.

A.2.7 EB/PS systems

In the following paragraph technical details of the CG simulations presented in section 5.1.4 and 5.3 are given.

The mixed systems of ethylbenzene (EB) and polystyrene (PS) consist of 24 atactic PS chains with a length of 96 repeat units (192 CG beads, M_W = 9984 g/mol) and of 256 EB molecules (2 CG beads, M_W=106 g/mol). This corresponds to an EB weight fraction w_{EB} of 10%. Initial coordinates for the CG system were obtained by randomly placing the EB molecules in the equilibrated PS matrices (described in section A.2.5), followed by a short steepest descend run. This procedure has been repeated at temperatures of 423, 463 and 503 K. Afterwards the systems at all temperatures between 398 and 593 K were simulated in NpT runs of 32 ns, where the starting configuration at each temperature was taken from the nearest temperature, for which the system setup had been done before (423, 463 and 503 K).

Production runs of 96 ns were performed under isothermal-isobaric (NpT) conditions at 1 atm and at various temperatures between 398 and 593 K using the velocity rescaling thermostat (coupling time 0.5 ps) and the Berendsen barostat (coupling time 5.0 ps), resulting in cubic boxsizes L^3 with L = 7.62 nm up to L = 7.92 for the different temperatures. For nonbonded interactions a cutoff distance of 1 nm was used. The integration time step was 4 fs. For the bonded and nonbonded interactions of EB the same potentials were used as for PS. The simulated systems are listed in table A.11.

T (K)	D_{EB}^{CG} (10^{-5}cm^{2}s^{-1})	ρ (kg m^{-3})
398	1.4 ± 0.1	999 ± 2
423	2.0 ± 0.1	987 ± 2
433	2.4 ± 0.1	981 ± 2
448	2.8 ± 0.2	974 ± 2
463	3.3 ± 0.1	967 ± 2
473	3.6 ± 0.1	961 ± 2
503	4.6 ± 0.2	946 ± 2
523	5.3 ± 0.3	935 ± 3
553	6.6 ± 0.4	917 ± 3
593	7.9 ± 0.2	892 ± 3

Table A.11: Simulated CG systems of PS/EB: For different temperatures the EB diffusion coefficients D_{EB}^{CG} and the densities ρ are given. The diffusion coefficients D_{EB}^{CG} for these CG systems are not scaled.

A.3 Implementation of the coarse-grained topology

A.3.1 Chain direction

The torsions in the CG model can have two different orientations. The dihedral potentials describing these torsions exist in two versions, which are mirrored in their orientation around 0 degree (they range from -180 to 180 degree). To use correct orientations for the torsions, the beads in the CG model are not only distinguished by A and B beads. They also have to contain also information about their orientation (B beads) and the type of diad they are involved in (A beads). To this end, first a direction is assigned to the chains by numbering the beads with the following scheme: A_1, B_1, A_2, B_2, A_1, B_1, A_2, B_2, ... This direction is only used to define the orientation of the phenyl groups, but does not have a physical meaning.

The orientation of the phenyl rings is defined in the following way, see also Figure A.1: One imagines an atomistic chain with the backbone extended along a straight line (all-trans orientation of the backbone), the phenyl rings pointing upwards and the chain direction oriented from left to right. Looking from the top at this chain, the phenyl rings point upwards or downwards, see Figure A.1 (middle). This orientation of the phenyl rings (which are the B beads in the CG resolution) is used in the CG model to define tacticity. The B beads can have two types: B^{up} or B^{down}.

Two subsequent B beads define a diad. If both B beads are of the same type (B^{up}-B^{up} or B^{down}-B^{down}) it is a meso diad, if they are of different types (B^{up}-B^{down} or B^{down}-B^{up}) it is a racemo diad. The type of the A beads is already determined by the types of the two neighboring B beads.

For the nonbonded interactions only A and B beads are distinguished. Their specific type, which describes their orientation and the tacticity, does not influence the nonbonded interactions.

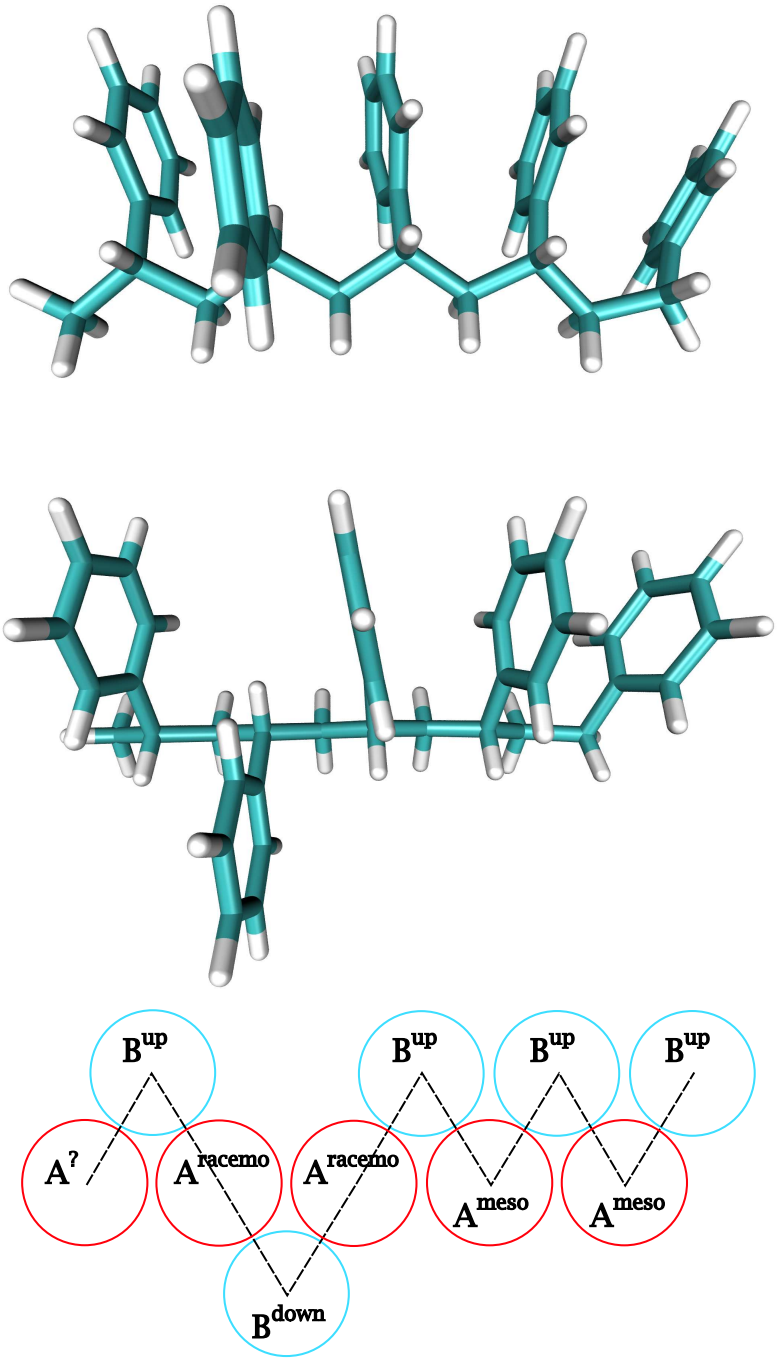

Figure A.1: Definition of different bead types to describe the tacticity in the CG model: The atomistic chain in all-trans conformation is viewed from the top (middle), with the phenyl rings pointing upwards, see also side view (upper picture). The two types of B beads are B^{up} or B^{down}, corresponding to the phenyl rings pointing up or down in the top view (bottom).

A.3.2 Dihedral orientation

With the previously defined chain direction and the orientations of the B beads, which keep the information about the chain tacticity, it is possible to distinguish two orientations of dihedral potentials. As before, isotactic and syndiotactic chains are treated separately, i.e. the final CG model has four different dihedral potentials.

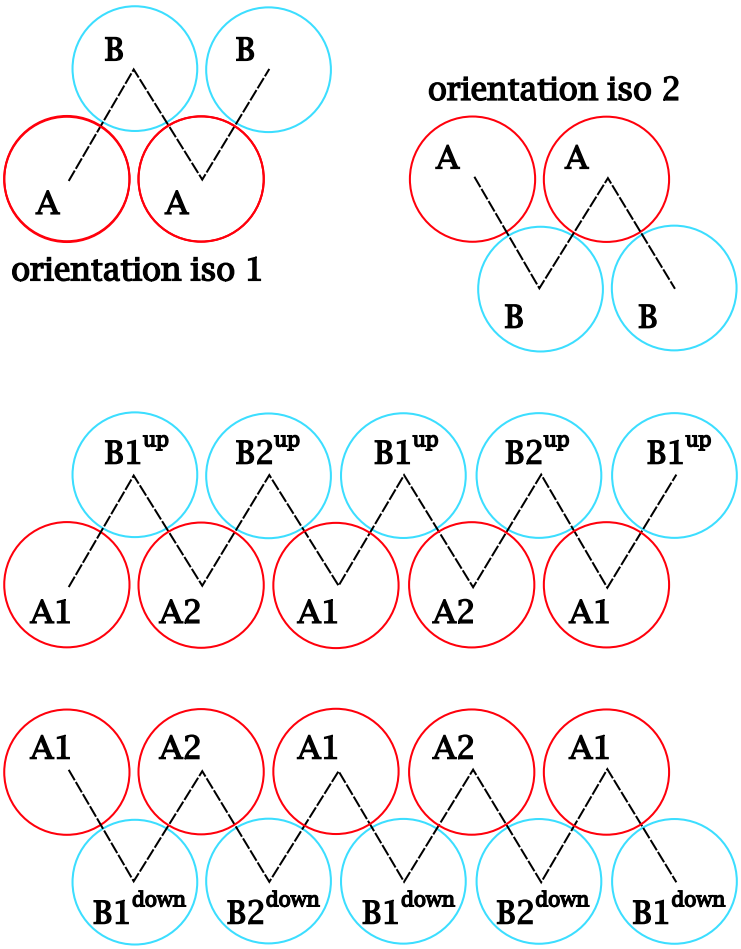

Figure A.2: Orientations of dihedral potentials in isotactic chains: The two orientations of meso diads (top) are identified with all congruent combinations of four subsequent beads in isotactic chains (middle and bottom).

The orientations for meso diads are shown in Figure A.2: in the upper row, the two orientations are shown, in the middle and below the two possible types of isotactic chains are given. Every sequence of four subsequent beads in the chain is congruent with either of the two orientations. Orientation “iso 1” applies to the following meso diads:

- A_1 - B_1^{up} - A_2 - B_2^{up}
- A_2 - B_2^{up} - A_1 - B_1^{up}

- A_1 - B_2^{down} - A_2 - B_1^{down}
- A_2 - B_1^{down} - A_1 - B_2^{down}

The mirrored orientation “iso 2” is used for the other combinations:

- A_1 - B_2^{up} - A_2 - B_1^{up}
- A_2 - B_1^{up} - A_1 - B_2^{up}
- A_1 - B_1^{down} - A_2 - B_2^{down}
- A_2 - B_2^{down} - A_1 - B_1^{down}

An analogous scheme is used for orientations of racemo diads, presented in Figure A.3. Orientation “syndio 1” applies to:

- A_1 - B_1^{up} - A_2 - B_2^{down}
- A_2 - B_2^{up} - A_1 - B_1^{down}
- A_1 - B_2^{down} - A_2 - B_1^{up}
- A_2 - B_1^{down} - A_1 - B_2^{up}

And finally the mirrored orientation “syndio 2” is congruent with:

- A_1 - B_2^{up} - A_2 - B_1^{down}
- A_2 - B_1^{up} - A_1 - B_2^{down}
- A_1 - B_1^{down} - A_2 - B_2^{up}
- A_2 - B_2^{down} - A_1 - B_1^{up}

These four orientations cover all possible combinations of bead types and allow the description of all tacticities: In isotactic chains only the potentials for meso diads with the orientations “iso 1” and “iso 2” are used, in syndiotactic chains only the potentials for racemo diads with the orientations “syndio 1” and “syndio 2” are used. In atactic chains, both types of diads appear in random sequences and all four orientations of the dihedral potentials are employed.

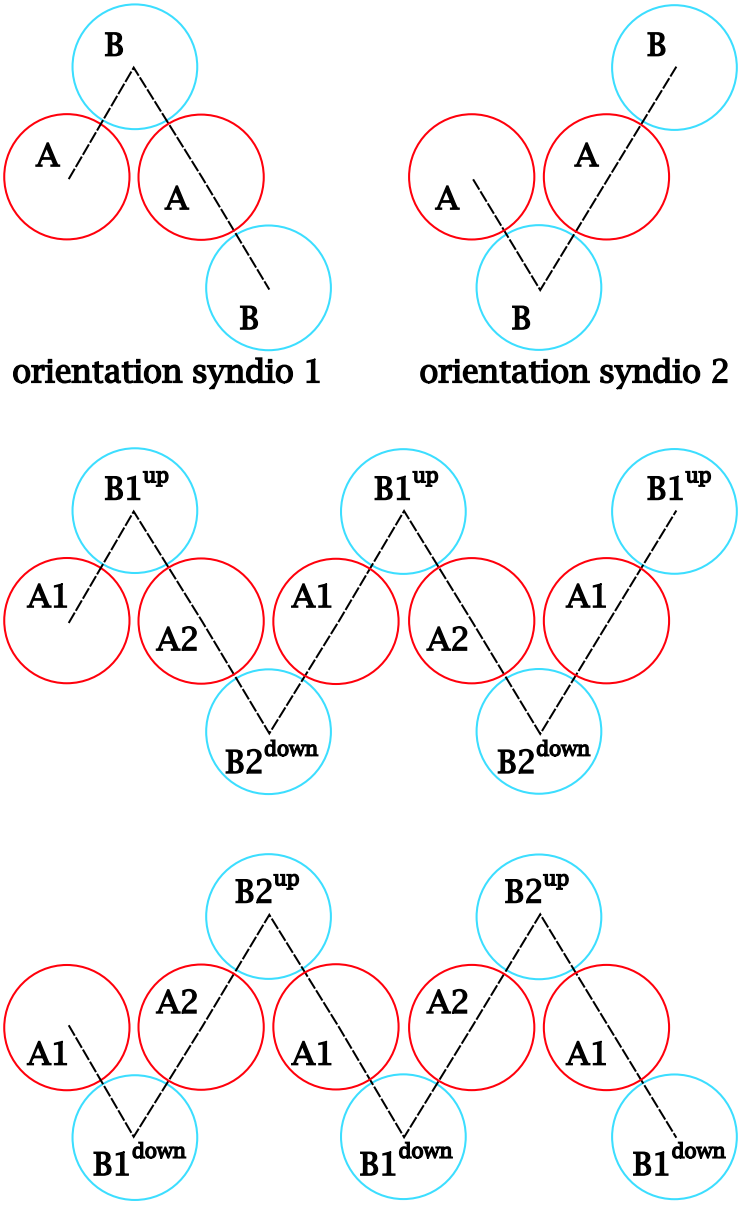

Figure A.3: Orientations of dihedral potentials in syndiotactic chains: The two orientations of racemo diads (top) are identified with all congruent combinations of four subsequent beads in syndiotactic chains (middle and bottom).

A.3.3 Bonded 1-5 interactions

An example for the different types of bonded 1-5 interactions is given in Figure A.4. There are two types of A-A 1-5 interactions, which depend on the type of diad (meso or racemo) formed by the two intermediate B beads. For the B-B 1-5 interactions three different types of interactions exist, since the three involved B beads form two subsequent diads. The three combinations are: iso (meso-meso), syndio (racemo-racemo) and block (meso-racemo or racemo-meso).

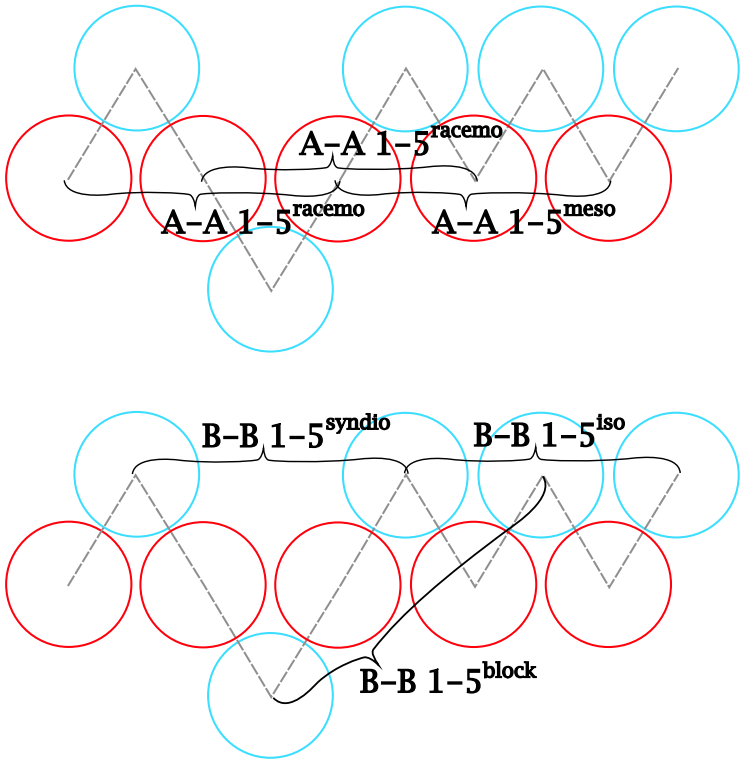

Figure A.4: Types of 1-5 intrachain potentials in the CG model: Depending on the bead types and the diads they form, two different potentials are used for A-A 1-5 interactions (top) and three different potentials for B-B 1-5 interactions (bottom). The bead types in the chain segment presented here are the ones from the example in Figure A.1.

A.4 Parameters of the atomistic force field

The components of the atomistic force field are described in section 1.2.1. The parameters for the nonbonded interactions are given in table A.12, the parameters for the bonded interactions in table A.13.

nonbonded interactions[a]	ϵ (kJ mol^{-1})	σ (nm)	q (e)
C_{ali}	0.3519	0.3207	0
H_{ali}	0.318	0.2318	0
C_{aro}	0.294	0.355	-0.115[b]
H_{aro}	0.126	0.242	+0.115

Table A.12: Potential energy function parameters of the all-atom force field for nonbonded potentials. [3] The subscripts ali and aro denote aliphatic and aromatic atoms, respectively. [a]Nonbonded interactions are excluded between first and second neighbors and, in addition, between all atoms of a given phenyl group. [b]The charge on the aromatic carbon of the phenyl group, which is connected to the aliphatic carbon of the backbone is 0.

bond	distance (nm)
C_{ali}-C_{ali}	0.153
C_{ali}-H_{ali}	0.110
C_{aro}-C_{aro}	0.139
C_{aro}-H_{aro}	0.108
C_{ali}-C_{aro}	0.151

bond angles	θ_0 (deg)	k_θ (kJ mol^{-1} rad^{-2})
H-C_{ali}-H	109.45	306.4
C_{ali}-C_{ali}-H	109.45	366.9
C_{ali}-C_{ali}-C_{ali}	109.45	482.3
C_{aro}-C_{ali}-H	109.45	366.9
C_{ali}-C_{ali}-C_{aro}	109.45	482.3
C_{ali}-C_{aro}-C_{aro}	120.00	376.6
C_{aro}-C_{aro}-C_{aro}	120.00	376.6
C_{aro}-C_{aro}-H	120.00	418.8

proper dihedral angles	ϕ_s (deg)	k_ϕ (kJ mol^{-1})	n
C_{ali}-C_{ali}-C_{ali}-C_{ali}	0	6.0	3
C_{ali}-C_{ali}-C_{ali}-H (terminal methyl)	0	6.0	3

improper dihedral angles	ξ_0 (deg)	k_ξ (kJ mol^{-1} rad^{-2})
C_{aro}-C_{aro}-C_{aro}-C_{aro}	0	176.4
$C2_{aro}$-$C3_{aro}$-$C1_{aro}$-H[on C2]	0	176.4
$C2_{aro}$-$C3_{aro}$-$C1_{aro}$-C_{ali}[on C2]	0	176.4

Table A.13: Potential energy function parameters of the all-atom force field for bondod potentials. [3] The subscripts ali and aro denote aliphatic and aromatic atoms, respectively.

Acknowledgments

Acknowledgments are not available in the electronic version.

Bibliography

[1] Berendsen, H. J. C. *Simulating the Physical World*. Cambridge University Press, New York, 1st edition, 2007.

[2] Wick, C. D.; Martin, M. G.; Siepmann, J. I. *J. Phys. Chem. B*, **2000**, *104*, 8008–8016.

[3] Müller-Plathe, F. *Macromolecules*, **1996**, *29*, 4782–4791.

[4] Milano, G.; Guerra, G.; Müller-Plathe, F. *Chem. Mater.*, **2002**, *14*, 2977–2982.

[5] Jorgensen, W. L.; Severance, D. L. *J. Am. Chem. Soc.*, **1990**, *112*(12), 4768–4774.

[6] Müller-Plathe, F.; Rogers, S. C.; van Gunsteren, W. F. *J. Chem. Phys.*, **1993**, *98*(12), 9895–9904.

[7] Milano, G.; Müller-Plathe, F. *J. Phys. Chem. B*, **2005**, *109*, 18609–18619.

[8] Sun, Q.; Faller, R. *Comput. Chem. Eng.*, **2005**, *29*, 2380–2385.

[9] Qian, H.; Carbone, P.; Chen, X.; Varzaneh, H. A. K.; Liew, C. C.; Müller-Plathe, F. *Macromolecules*, **2008**, *41*, 9919–9929.

[10] Binder, K., Ed. *Monte Carlo and Molecular Dynamics Simulations in Polymer Science*. Oxford University Press, New York, 1st edition, 1995.

[11] Allen, M. P.; Tildesley, D. J. *Computer Simulations of Liquids*. Oxford Science Publications, Oxford, 1987.

[12] Berendsen, H. J. C.; van Gunsteren, W. F. (Dordrecht [usw.]: Reidel, The Netherlands). chapter Molecular dynamics simulations: Techniques and approaches, pp 475–500. NATO ASI series, Ser. C, 135, 1984.

[13] Barker, J. A.; Watts, R. O. *Mol. Phys.*, **1973**, *26*(3), 789–792.

[14] Ewald, P. P. *Ann. d. Phys.*, **1921**, *369*(3), 253–287.

[15] Darden, T.; York, D.; Pedersen, L. *J. Chem. Phys.*, **1993**, *98*(12), 10089–10092.

[16] Deserno, M. *Counterion condensation for rigid linear polyelectrolytes*. PhD thesis, Universität Mainz, 2000.

[17] Goldstein, H.; Poole, C.; Safko, J. *Classical Mechanics*. Addison Wesley, San Francisco, 3rd edition, 2002.

[18] Frenkel, D.; Smit, B. *Understanding Molecular Simulation*. Academic Press, San Diego, 2nd edition, 2002.

[19] Verlet, L. *Phys. Rev.*, **1967**, *159*(1), 98–103.

[20] Hockney, R. W.; Eastwood, J. W. *Computer Simulation using Particles*. Taylor & Francis Group, New York, 1988.

[21] van Gunsteren, W. F.; Berendsen, H. J. C. *Mol. Sim.*, **1988**, *1*(3), 173–185.

[22] Swope, W. C.; Andersen, H. C.; Berens, P. H.; Wilson, K. R. *J. Chem. Phys.*, **1982**, *76*(1), 637–649.

[23] Tuckerman, M.; Berne, B. J.; Martyna, G. J. *J. Chem. Phys.*, **1992**, *97*(3), 1990–2001.

[24] Martyna, G. J.; Tuckerman, M. E.; Tobias, D. J.; Klein, M. L. *Mol. Phys.*, **1996**, *87*, 1117–1157.

[25] Ryckaert, J.-P.; Ciccotti, G.; Berendsen, H. J. C. *J. Comput. Phys.*, **1977**, *23*(3), 327–341.

[26] de Leeuw, S. W.; Perram, J. W.; Petersen, H. G. *J. Stat. Phys.*, **1990**, *61*(5), 1203–1222.

[27] Hess, B.; Bekker, H.; Berendsen, H. J. C.; Fraaije, J. G. E. M. *J. Comput. Chem.*, **1997**, *18*, 1463–1472.

[28] Schneider, T.; Stoll, E. *Phys. Rev. B*, **1978**, *17*(3), 1302–1322.

[29] Hoogerbrugge, P. J.; Koelman, J. M. V. A. *Europhys. Lett.*, **1992**, *19*, 155–160.

[30] Soddemann, T.; Dünweg, B.; Kremer, K. *Phys. Rev. E*, **2003**, *68*(4), 046702.

[31] Español, P. *Phys. Rev. E*, **1995**, *52*(2), 1734–1742.

[32] Berendsen, H. J. C.; Postma, J. P. M.; van Gunsteren, W. F.; DiNola, A.; Haak, J. R. *J. Chem. Phys.*, **1984**, *81*, 3684–3690.

[33] Hoover, W. G.; Ladd, A. J. C.; Moran, B. *Phys. Rev. Lett.*, **1982**, *48*(26), 1818–1820.

[34] Evans, D. J. *J. Chem. Phys.*, **1983**, *78*(6), 3297–3302.

[35] Nosé, S. *Mol. Phys.*, **1984**, *52*, 255–268.

[36] Hoover, W. G. *Phys. Rev. A*, **1985**, *31*(3), 1695–1697.

[37] Bussi, G.; Donadio, D.; Parrinello, M. *J. Chem. Phys.*, **2007**, *126*(1), 014101.

[38] Kremer, K.; Grest, G. S. *J. Chem. Phys.*, **1990**, *92*(8), 5057–5086.

[39] Malevanets, A.; Kapral, R. *J. Chem. Phys.*, **2000**, *112*(16), 7260–7269.

[40] Abrams, C. F.; Delle Site, L.; Kremer, K. *Phys. Rev. E*, **2003**, *67*(2), 021807.

[41] Villa, E.; Balaeff, A.; Mahadevan, L.; Schulten, K. *Multiscale Model. Simul.*, **2004**, *2*(4), 527–553.

[42] Praprotnik, M.; Delle Site, L.; Kremer, K. *J. Chem. Phys.*, **2005**, *123*(22), 224106.

[43] Praprotnik, M.; Delle Site, L.; Kremer, K. *J. Chem. Phys.*, **2007**, *126*(13), 134902.

[44] Marrink, S. J.; de Vries, A. H.; Mark, A. E. *J. Phys. Chem. B*, **2004**, *108*(2), 750–760.

[45] Marrink, S. J.; Risselada, H. J.; Yefimov, S.; Tieleman, D. P.; de Vries, A. H. *J. Phys. Chem. B*, **2007**, *111*(27), 7812–7824.

[46] Müller-Plathe, F. *ChemPhysChem*, **2002**, *3*(9), 754–769.

[47] Reith, D.; Pütz, M.; Müller-Plathe, F. *J. Comput. Chem.*, **2003**, *24*, 1624–1636.

[48] Lyubartsev, A. P.; Laaksonen, A. *Phys. Rev. E*, **1995**, *52*(4), 3730–3737.

[49] Izvekov, S.; Voth, G. A. *J. Phys. Chem. B*, **2005**, *109*(7), 2469–2473.

[50] Noid, W. G.; Chu, J.-W.; Ayton, G. S.; Voth, G. A. *J. Phys. Chem. B*, **2007**, *111*(16), 4116–4127.

[51] Ayton, G. S.; Noid, W. G.; Voth, G. A. *Curr. Opin. Struct. Biol.*, **2007**, *17*(2), 192 – 198.

[52] Tschoep, W.; Kremer, K.; Batoulis, J.; Bürger, T.; Hahn, O. *Acta Polym.*, **1998**, *49*, 61–74.

[53] Abrams, C. F.; Kremer, K. *Macromolecules*, **2003**, *36*(1), 260–267.

[54] Harmandaris, V. A.; Adhikari, N. P.; van der Vegt, N. F. A.; Kremer, K. *Macromolecules*, **2006**, *39*, 6708–6719.

[55] Harmandaris, V. A.; Reith, D.; van der Vegt, N. F. A.; Kremer, K. *Macromol. Chem. Phys.*, **2007**, *208*, 2109–2120.

[56] Poma, A. B.; Delle Site, L. *Phys. Rev. E*, **2008**, *78*(5), 056703.

[57] Villa, A.; Peter, C.; van der Vegt, N. F. A. *Phys. Chem. Chem. Phys.*, **2009**, *11*, 2077–2086.

[58] Villa, A.; van der Vegt, N. F. A.; Peter, C. *Phys. Chem. Chem. Phys.*, **2009**, *11*, 2068–2076.

[59] Henderson, R. L. *Phys. Lett. A*, **1974**, *49*(3), 197–198.

[60] Rühle, V.; Junghans, C.; Lukyanov, A.; Kremer, K.; Andrienko, D. *J. Chem. Theory Comput.*, **2009**, *5*(12), 3211–3223.

[61] Soper, A. K. *Chem. Phys.*, **2000**, *258*, 121–137.

[62] Wang, H.; Junghans, C.; Kremer, K. *Eur. Phys. J. E*, **2009**, *28*(2), 221–229.

[63] Johnson, M. E.; Head-Gordon, T.; Louis, A. A. *J. Chem. Phys.*, **2007**, *126*(14), 144509.

[64] McCoy, J. D.; Curro, J. C. *Macromolecules*, **1998**, *31*, 9362–9368.

[65] Fukunaga, H.; Takimoto, J.; Doi, M. *J. Chem. Phys.*, **2002**, *116*, 8183–8190.

[66] Tschoep, W.; Kremer, K.; Hahn, O.; Batoulis, J.; Bürger, T. *Acta Polym.*, **1998**, *49*, 75–79.

[67] Hess, B.; Leon, S.; van der Vegt, N. F. A.; Kremer, K. *Soft Matter*, **2006**, *2*, 409–414.

[68] Santangelo, G.; Di Matteo, A.; Müller-Plathe, F.; Milano, G. *J. Phys. Chem. B*, **2007**, *111*(11), 2765–2773.

[69] Peter, C.; Delle Site, L.; Kremer, K. *Soft Matter*, **2008**, *4*, 859–869.

[70] Chen, X.; Carbone, P.; Santangelo, G.; Di Matteo, A.; Milano, G.; Müller-Plathe, F. *Phys. Chem. Chem. Phys.*, **2009**, *11*, 1977–1988.

[71] Hess, B.; Peter, C.; Ozal, T.; van der Vegt, N. F. A. *Macromolecules*, **2008**, *41*(6), 2283–2289.

[72] Ozal, T. A.; Peter, C.; Hess, B.; van der Vegt, N. F. A. *Macromolecules*, **2008**, *41*(13), 5055–5061.

[73] Hess, B.; van der Vegt, N. F. A. *Macromolecules*, **2008**, *41*(20), 7281–7283.

[74] Fritz, D.; Harmandaris, V. A.; Kremer, K.; van der Vegt, N. F. A. *Macromolecules*, **2009**, *42*(19), 7579–7588.

[75] Humphrey, W.; Dalke, A.; Schulten, K. *Journal of Molecular Graphics*, **1996**, *14*, 33–38.

[76] Spyriouni, T.; Tzoumanekas, C.; Theodorou, D. N.; Müller-Plathe, F.; Milano, G. *Macromolecules*, **2007**, *40*, 3876–3885.

[77] Sun, Q.; Faller, R. *Macromolecules*, **2006**, *39*, 812–820.

[78] Hess, B.; Holm, C.; van der Vegt, N. *J. Chem. Phys.*, **2006**, *124*(16), 164509.

[79] Hess, B. *J. Chem. Phys.*, **2002**, *116*(1), 209–217.

[80] Boothroyd, A. T.; Rennie, A. R.; Wignall, G. D. *J. Chem. Phys.*, **1993**, *99*, 9135–9144.

[81] Fetters, L. J.; Lohse, D. J.; Graessley, W. W. *J Polym Sci Part B: Polym Phys*, **1999**, *37*, 1023–1033.

[82] Stölken, S.; Ewen, B.; Kobayashi, M.; Nakaoki, T. *J Polym Sci Part B: Polym Phys*, **1994**, *32*(5), 881–885.

[83] Yoon, D. Y.; Flory, P. J. *Macromolecules*, **1976**, *9*(2), 294–299.

[84] Zoller, P.; Walsh, D. J. *Standard Pressure-Volume-Temperature Data for Polymers*. Technomic, Lancaster, 1995.

[85] Harmandaris, V. A.; Kremer, K. *Macromolecules*, **2009**, *42*, 791–802.

[86] Carbone, P.; Varzaneh, H. A. K.; Chen, X.; Müller-Plathe, F. *J. Chem. Phys.*, **2008**, *128*, 064904.

[87] Harmandaris, V. A.; Kremer, K. *Soft Matter*, **2009**, *5*(20), 3920–3926.

[88] Harmandaris, V. A.; Adhikari, N. P.; van der Vegt, N. F. A.; Kremer, K.; Mann, B. A.; Voelkl, R.; Weiss, H.; Liew, C. C. *Macromolecules*, **2007**, *40*, 7026–7035.

[89] Depa, P. K.; Maranas, J. K. *J. Chem. Phys.*, **2005**, *123*(9), 094901.

[90] Depa, P. K.; Maranas, J. K. *J. Chem. Phys.*, **2007**, *126*(5), 054903.

[91] Nielsen, S. O.; Lopez, C. F.; Srinivas, G.; Klein, M. L. *J. Chem. Phys.*, **2003**, *119*(14), 7043–7049.

[92] Voter, A. F. *Phys. Rev. Lett.*, **1997**, *78*(20), 3908–3911.

[93] Voter, A. F. *J. Chem. Phys.*, **1997**, *106*(11), 4665–4677.

[94] Richter, D.; Monkenbusch, M.; Arbe, A.; Colmenero, J. *Adv. Polym. Sci.*, **2005**, *174*, 1–221.

[95] Noid, W. G.; Chu, J.-W.; Ayton, G. S.; Krishna, V.; Izvekov, S.; Voth, G. A.; Das, A.; Andersen, H. C. *J. Chem. Phys.*, **2008**, *128*(24), 244114.

[96] Paul, W.; Binder, K.; Heermann, D. W.; Kremer, K. *J. Chem. Phys.*, **1991**, *95*(10), 7726–7740.

[97] Doi, M.; Edwards, S. F. *The theory of polymer dynamics*. Clarendon Press, Oxford, 1986.

[98] Everaers, R.; Sukumaran, S. K.; Grest, G. S.; Svaneborg, C.; Sivasubramanian, A.; Kremer, K. *Science*, **2004**, *303*(5659), 823–826.

[99] Sukumaran, S. K.; Grest, G. S.; Kremer, K.; Everaers, R. *J. Polym. Sci. Part B: Polym. Phys.*, **2005**, *43*(8), 917–933.

[100] Kremer, K.; Sukumaran, S. K.; Everaers, R.; Grest, G. S. *Comp. Phys. Comm.*, **2005**, *169*, 75–81.

[101] Fritz, D.; Herbers, C. R.; Kremer, K.; van der Vegt, N. F. A. *Soft Matter*, **2009**, *5*, 4556–4563.

[102] Hahn, O.; Mooney, D. A.; Müller-Plathe, F.; Kremer, K. *J. Chem. Phys.*, **1999**, *111*, 6061–6068.

[103] Hess, B.; Kutzner, C.; van der Spoel, D.; Lindahl, E. *J. Chem. Theory Comput.*, **2008**, *4*, 435–447.

[104] Auhl, R.; Everaers, R.; Grest, G. S.; Kremer, K.; Plimpton, S. J. *J. Chem. Phys.*, **2003**, *119*, 12718–12728.